

UNCLASSIFIED

AD NUMBER
AD844459
NEW LIMITATION CHANGE
TO Approved for public release, distribution unlimited
FROM Distribution authorized to U.S. Gov't. agencies and their contractors; Critical Technology; JUN 1968. Other requests shall be referred to Hydrodynamics Lab., Naval Ship Research and Development Center, Washington, DC.
AUTHORITY
USNRDC ltr, 1 Apr 1969

THIS PAGE IS UNCLASSIFIED

MASSACHUSETTS INSTITUTE OF TECHNOLOGY
Department of Naval Architecture and Marine Engineering

Report No. 68-12

VORTEX INTERACTIONS IN A PROPELLER WAKE

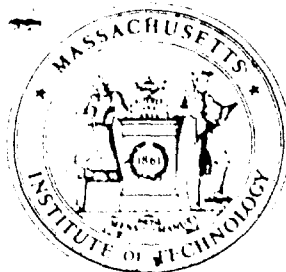
by

Damon E. Cummings

June 1968

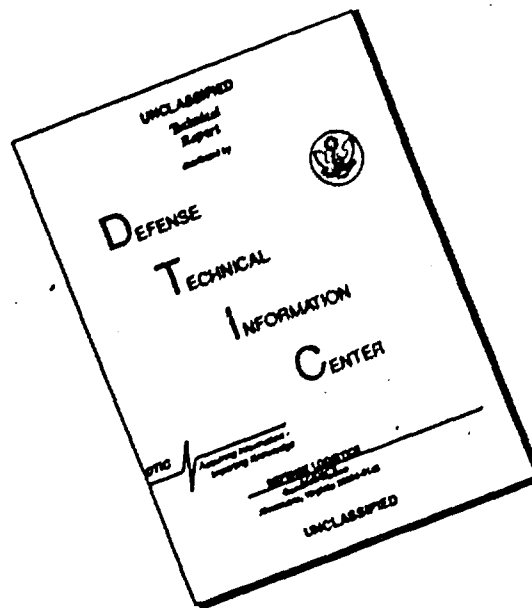
This research was carried out under the Naval Ship Systems Command General Hydromechanics Research Program SR 009 01 01, Administered by the Naval Ship Research and Development Center. Prepared under the Office of Naval Research Contract.

Nonr-1841(63).
M.I.T., D.S.R.-78422



This document is subject to special export controls and each transmittal to foreign governments or foreign national may be made only with proper approval of the Head, Hydrodynamics, Laboratory, Naval Ship Research and Development Center, Washington, D.C. 20007

DISCLAIMER NOTICE



THIS DOCUMENT IS BEST QUALITY AVAILABLE. THE COPY FURNISHED TO DTIC CONTAINED A SIGNIFICANT NUMBER OF PAGES WHICH DO NOT REPRODUCE LEGIBLY.

MASSACHUSETTS INSTITUTE OF TECHNOLOGY
Department of Naval Architecture and Marine Engineering

Report No. 68-12

VORTEX INTERACTIONS IN A PROPELLER WAKE

by

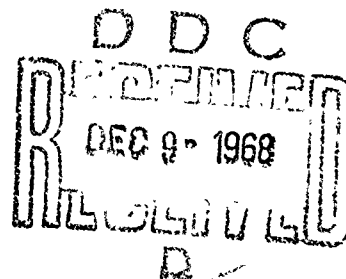
Damon E. Cummings

June 1968

This research was carried out under the Naval Ship Systems Command General Hydromechanics Research Program SR 009 01 01, Administered by the Naval Ship Research and Development Center. Prepared under the Office of Naval Research Contract.

Nonr-1841(63)
M.I.T., D.S.R.-78422

This document is subject to special export controls and each transmittal to foreign governments or foreign national may be made only with prior approval of the Head, Hydrodynamics Laboratory, Naval Ship Research and Development Center, Washington, D. C. 20007



ACKNOWLEDGEMENTS

The author wishes to express his appreciation to Professor Justin E. Kerwin, project supervisor; and to Professors Sheila E. Widnall and Patrick Leehey for their advice and assistance on this project. Particular thanks is due to Professors Widnall and Jerome Milgram for the use of computer programs which they have developed.

Mr. Leon Leob and John Burlison did the photography included in this report. Mr. Robert Ashworth was of great assistance in the experimental work.

The Civil Engineering Systems Laboratory was used for most of the computer work, and great cooperation was received from Miss Betty White of this laboratory. The facilities of the M.I.T. Computation Center were resorted to in emergencies.

Mr. Thomas McMahon was of great assistance in getting this project started since he did the preliminary investigations on this subject at this institute and was extremely cooperative in offering suggestions during the work.

TABLE OF CONTENTS

TITLE PAGE	i
ABSTRACT	ii
ACKNOWLEDGEMENTS	iii
TABLE OF CONTENTS	iv
LIST OF FIGURES	v
NOMENCLATURE	vi
INTRODUCTION	1
CHAPTER I	4
CHAPTER II	29
CHAPTER III	38
CHAPTER IV	45
CHAPTER V	57
CHAPTER VI	68
REFERENCES	69
APPENDIX	71

LIST OF FIGURES

1.1 Coordinate system	8
1.2 Wake rollup geometry	10
1.3 Method 1 results	12
1.4 Method 1 results	13
1.5 Method 2 results	16
1.6 Method 2 results	17
1.7 Method 3 results	21
1.8 Method 3 results	22
1.9 Method 4 results	27
1.10 Method 4 results	27A
3.1 Flow graph for tip vortex calculations and rollup	39
3.2 Results from strip theory foil with sink in tip vortex	40
3.3 Tip vortex pressure versus circulation	41
3.4 Downwash on a lifting line	44
3.5 Tip vortex pressure versus thickness of boundary layer	44A
4.1 Boundary layer thickness versus angle of attack for a rudder model	48
4.2 Calculated trajectory of vortex sheet and tip vortex core	54
4.3 Photograph of tip vortex core on a rudder model for comparison with 4.2	55
4.4 A top view of the rudder model used	56
4.5 A top view of the rudder model operating	57
4.6 Results for the rudder model	58
4.7 Calculated spanwise trajectory	58A
5.1 Propeller vortex rollup	63

5.2 Induced axial and tangential velocities on a moderately loaded propeller	66
5.3 Induced axial and tangential velocities on a heavily loaded propeller	67
5.4 Notation for induced velocity due to a trailing vortex from a propeller blade	68
5.5 Approach flow velocity diagram	69
5.6 Velocity diagram at a lifting line	70
5.7 Flow chart for propeller calculations	71
5.8 Compariso of results with experiment	72
A1 Flow chart for Method 1	78
A2 Computer program for Method 1	79
A3 Flow chart for Methods 2,3,and 4	81
A4 Method 4 computer program	79
A5 Sample output from Method 4	84
A6 Computer program for a lifting line foil	83
A7 Sample output from method of chapter 3	84
A8 Input form for propeller design	86
A9 Computer program for propeller	87
A10 Subroutines for propeller program	89
A11 Boundary layer programs	91

NOMENCLATURE

a	tip vortex core radius
A	area of vortex sheet
α	angle of attack
c	chord of foil
C_d	drag coefficient
C_f	skin friction coefficient
C_p	pressure coefficient
C_l	lift coefficient
D_i	induced drag
E_{in}	energy in vortex core
E_o	energy surrounding vortex core
E_t	total energy in vortex system
G, Γ, K	circulation
Γ_o	circulation at midspan
Γ_c	core circulation
γ	circulation density of vortex sheet
F	force on cross section of core
H	ratio of displacement to momentum thickness in a boundary layer
\vec{T}	vector element of vortex
p	pressure
r	radial coordinate in (x, r, θ) system
R	propeller radius
R_h	hub radius
ρ	density of fluid, dummy r coordinate in propeller calculations
\vec{s}	vector from control point to vortex element
s	span

- S_n point N on lifting line midway between vortices
 t time
 u velocity in x direction
 v velocity in y direction in (x,y,z) system
 velocity in r direction in (x,r, θ) direction
 w velocity in z direction in (x,y,z) system
 velocity in direction in (x,r, θ) system
 U_o free stream velocity
 \bar{u}_x x component of disturbance due to a unit vortex
 \bar{u}_r radial component of disturbance due to a unit vortex
 \bar{u}_t tangential component of the disturbance due to a unit vortex
 U_v velocity induced by vorticity at point x
 \bar{V} velocity vector
 V_o relative flow past a blade section, neglecting disturbance velocities
 V^* relative flow past a blade
 Ω angular velocity of propeller
 $\bar{\omega}$ volume density of vorticity distribution
 η dummy coordinate for foil
 ξ dummy x coordinate for propeller
 x axial component of (x,y,z) system or (x,r, θ) system.
 y y component of (x,y,z) system, along span of foil or blade
 z other component of (x,y,z) system
 Y_m y coordinate of midspan
 W weighting factor for changing vortex spacing
 ϕ velocity potential

INTRODUCTION

The subject of this report is the interaction kinematics and dynamics of the trailing vortex sheets in the wake of a propeller. The effects considered to be of primary interest are tip vortex cavitation, the downwash on the blade surface, and the resultant change in the assumed loading and field point velocities and pressures due to the configuration of the field of trailing vorticity. It was apparent early in this work that two important phenomena were taking place in propeller wakes which were not accounted for in the classical propeller design models. The trailing vortex sheets were not remaining on helicoidal sheets but were rolling up around a core containing the vorticity shed from the tip region and the velocity field at the propeller plane as a result was not that predicted by theory. In this highly rotational tip region, several factors should probably be taken into account that are normally considered negligible in potential flow theory as applied to lifting surfaces. There may be strong streamwise pressure gradients due to either diffusion of vorticity or to absorption of the sheet vorticity into the core. These considerations are especially important if the phenomenon of tip vortex cavitation is to be understood.

In Chapter I the classical vortex sheet rollup problem from a wing with elliptical loading is considered in a manner similar to that of Westwater (1). The problem is approached by a discrete vortex method modified by analytic calculations near the ends of the sheet where a square root singularity exists in the vorticity distribution. It is found that a strip theory model is adequate for the induced velocity calculations saving a great deal of computer time. The argument is made that an infinite vorticity, or equivalently a finite line vortex cannot exist in a real fluid and the tip vorticity is spread out over a finite thickness.

In Chapter II a model of the tip vortex core is examined with the intention of calculating pressures in the core and the effect of axial velocity gradients in the core on the velocity field outside the core. This analysis is based on the balance of pressure forces due to vorticity inside and surrounding the core and the resultant inward and axial velocities.

Chapter III is an application of the results of Chapters I and II to the case of an elliptically loaded lifting line. The pressures in the tip vortex and kinematics of the sheet motion are calculated. The velocities induced at the lifting line are calculated, and conclusions drawn as to how this would alter the assumed load distribution.

Chapter IV is an application of the theory developed earlier to a wing. The actual load, tip vortex pressures,

and vortex sheet kinematics are calculated and compared with experimental results.

Chapter V concerns the application of the vortex sheet kinematics and tip vortex core dynamics to the helicoidal geometry of propellers.

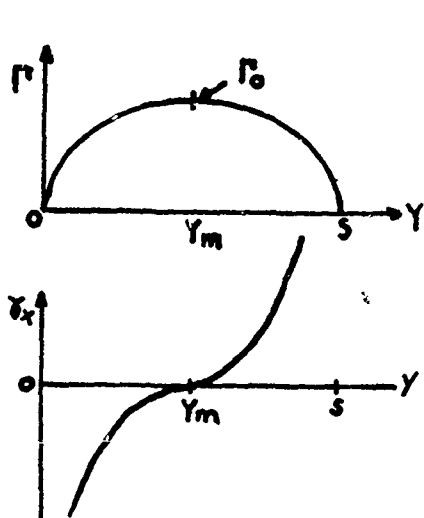
CHAPTER I

The instability of a vortex sheet shed from the trailing edge of a wing has been the subject of much contemplation and calculation since the beginnings of airfoil theory. Nevertheless for most design applications the trailing vortex sheet is assumed to lie in a flat plane extending to infinity downstream. Prandtl, Westwater and Kaden (2,1,3) among others worked on the problem of vortex sheet rollup with some success. The problem has not received much attention in recent years because the velocities induced on the surface of a wing are not greatly changed when the sheet is considered to be rolled up instead of straight. The rollup takes place far enough behind the wing to be ignored in aircraft applications in general. In the case of heavily loaded marine propellers, however, the effect may not be negligible. The trailing vortex sheet does not proceed directly downstream but, as seen from a propeller blade, rotates downstream on helicoidal surfaces. If the tangential velocities due to rotation of the propeller are large compared to the forward velocity of the ship, the sheets may pass very close to the following blades. The present author has reexamined the wing problem by several numerical techniques using a discrete vortex representation for the distribution of vorticity in the trailing vortex sheet.

The first method chosen was to select an elliptical loading on a lifting line and divide the trailing vortex

sheet into N discrete vortices at equal spacing along the wing. The elliptical loading is chosen because this gives a constant downwash along the span. Thus any rollup is due to the instability of the flat sheet model rather than to differences in velocities normal to the sheet along the span.

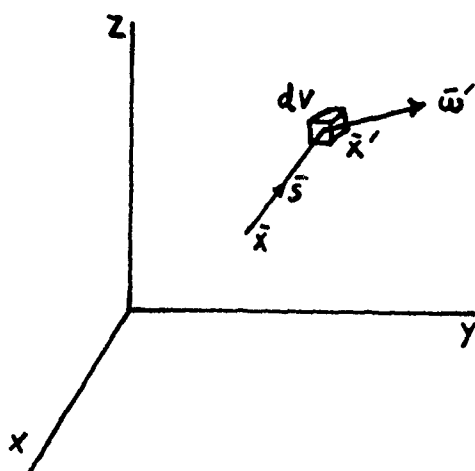
The wing loading and trailing vorticity distribution appear below.



$$\Gamma(Y) = \Gamma_0 \sqrt{1 - \frac{(Y_m - Y)^2}{Y_m^2}}$$

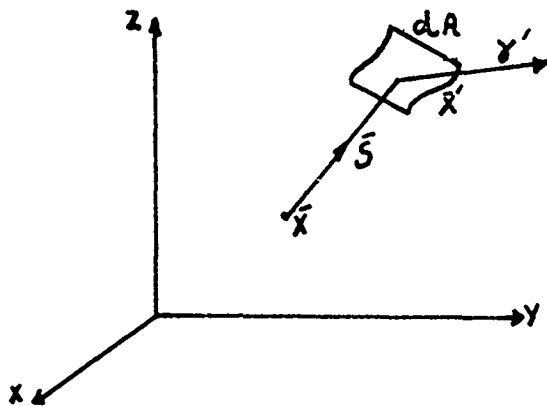
$$\gamma_x = \frac{d\Gamma(Y)}{dY}$$

The velocity induced on the sheet by the trailing vorticity is deduced by the law of Biot-Savart (4)



$$\vec{U}_v(\vec{x}) = \frac{-1}{4\pi} \int \frac{\vec{s} \times \vec{\omega}'}{|\vec{s}|^3} dv(\vec{x}')$$

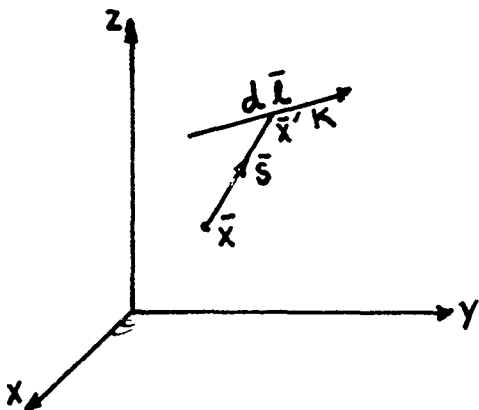
In the case of a sheet vortex:



$$U_v(\vec{x}) = \frac{-1}{4\pi} \int \frac{\vec{s} \times \vec{r}'(\vec{x}') dA(\vec{x}')}{|\vec{s}|^3}$$

If the control point x is within the sheet the Cauchy principal value of the integral is intended.

If the sheet is shrunk to a line vortex:



$$U_v(\vec{x}) = \frac{-K}{4\pi} \int \frac{\vec{s} \times d\vec{l}(\vec{x}')}{|\vec{s}|^3}$$

The procedure here is to represent the sheet vortex by a series of discrete line vortices. Since we are interested in the motion of the sheet, the Cauchy principal value restriction must be accounted for. This is done by always making calculations midway between vortices. (5)

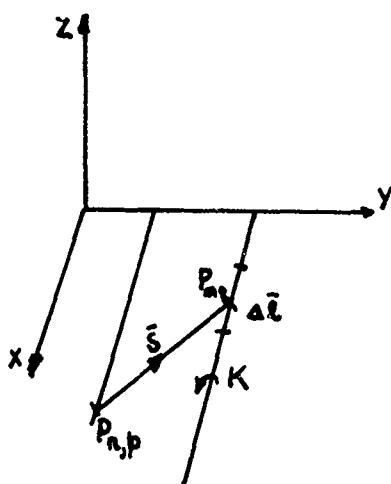
Method One

The foregoing leads to the most straightforward, but also most time consuming method for finding the actual stable configuration for the trailing vortex sheet from a lifting line with elliptical loading. The sheet is assumed

to start out straight downstream from the trailing edge and, as a first estimate for this position, is assumed to remain a flat sheet to infinity downstream. The sheet is divided into discrete vortices at an even spacing on the lifting line. (FIG. 1.1)

They are also divided lengthwise into sections of length Δx . The strength of the trailing vortex at position N is the difference in bound circulation between space position S1 and S2 since a vortex may not end in a fluid.

We thus start the calculation with a flat grid of vortices and downstream positions. The velocity induced by the vorticity of the rest of the sheet is then computed at each vortex at each discrete position downstream as follows:



$$\Delta \bar{l}_x = \bar{x}_{m,q} - \bar{x}_{m,q+1}$$

$$\Delta \bar{l}_y = \bar{y}_{m,q} - \bar{y}_{m,q+1}$$

$$\Delta \bar{l}_z = \bar{z}_{m,q} - \bar{z}_{m,q+1}$$

$$S_x = \bar{x}_{n,p} - \bar{x}_{m,q}$$

$$S_y = \bar{y}_{n,p} - \bar{y}_{m,q}$$

$$S_z = \bar{z}_{n,p} - \bar{z}_{m,q}$$

$$|S|^2 = S_x^2 + S_y^2 + S_z^2$$

The velocity at position $P(n,p)$ due to a vortex element at $P(m,p)$, has the value:

$$V_x = \frac{\Gamma_m}{4\pi S^3} [\Delta l_y S_z - \Delta l_z S_y]$$

$$V_y = \frac{\Gamma_m}{4\pi S^3} [\Delta l_z S_x - \Delta l_x S_z]$$

$$V_z = \frac{\Gamma_m}{4\pi S^3} [\Delta l_x S_y - \Delta l_y S_x]$$

$$\bar{V} = \frac{\Gamma_m}{4\pi S^3} \Delta \bar{l} \times \Delta \bar{S}$$

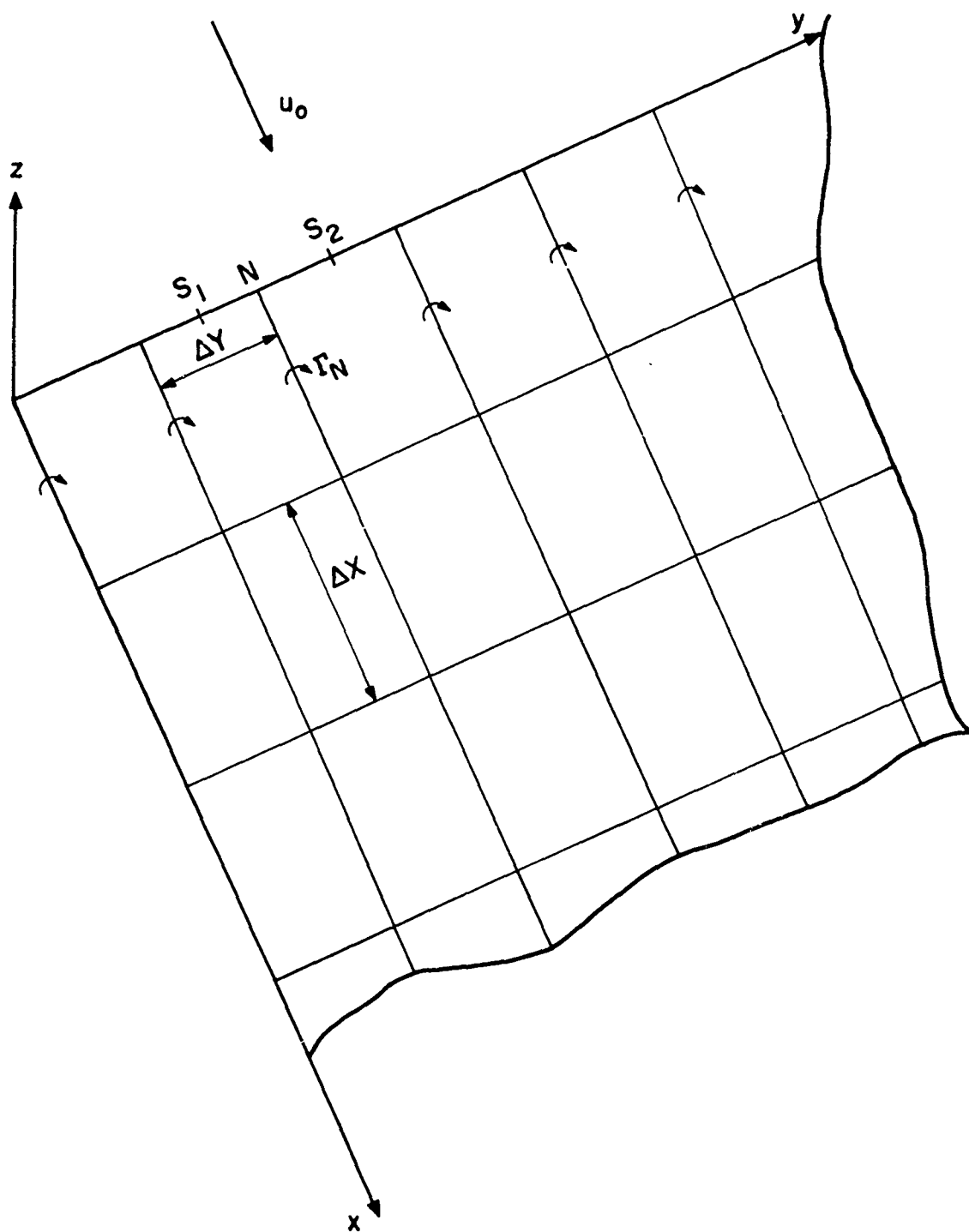


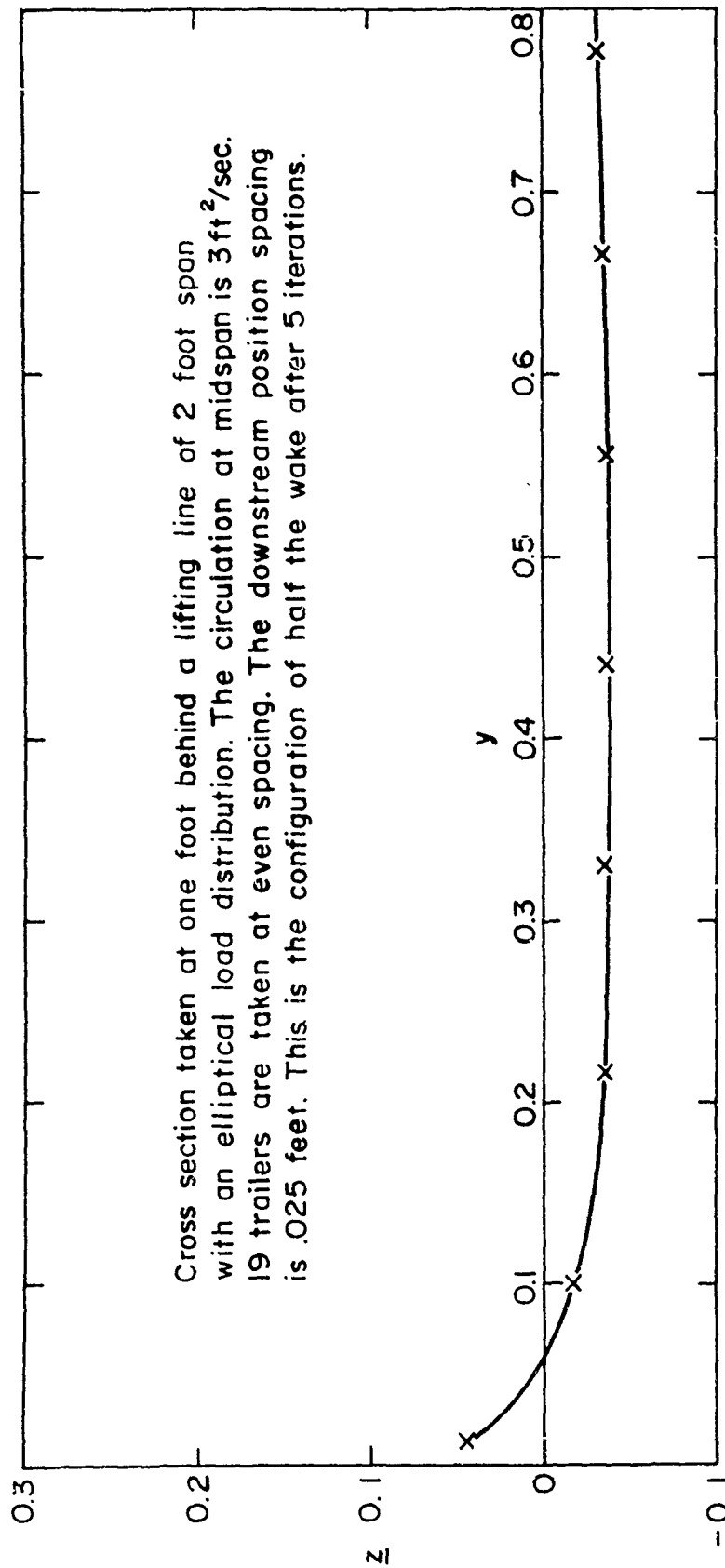
FIGURE 1.1

For each position the velocity due to each element is calculated and summed to obtain the resultant induced velocity at each point on the sheet due to the rest of the sheet. A matrix of induced velocities is formed due to the present assumed position of the sheet. The streamlines containing the vortex lines are then found, starting at the trailing edge with a straight line cross section and assuming that:

$$\bar{x}_{n,p} = \bar{x}_{n,p-1} + \bar{v}_{n,p-1} \Delta t$$

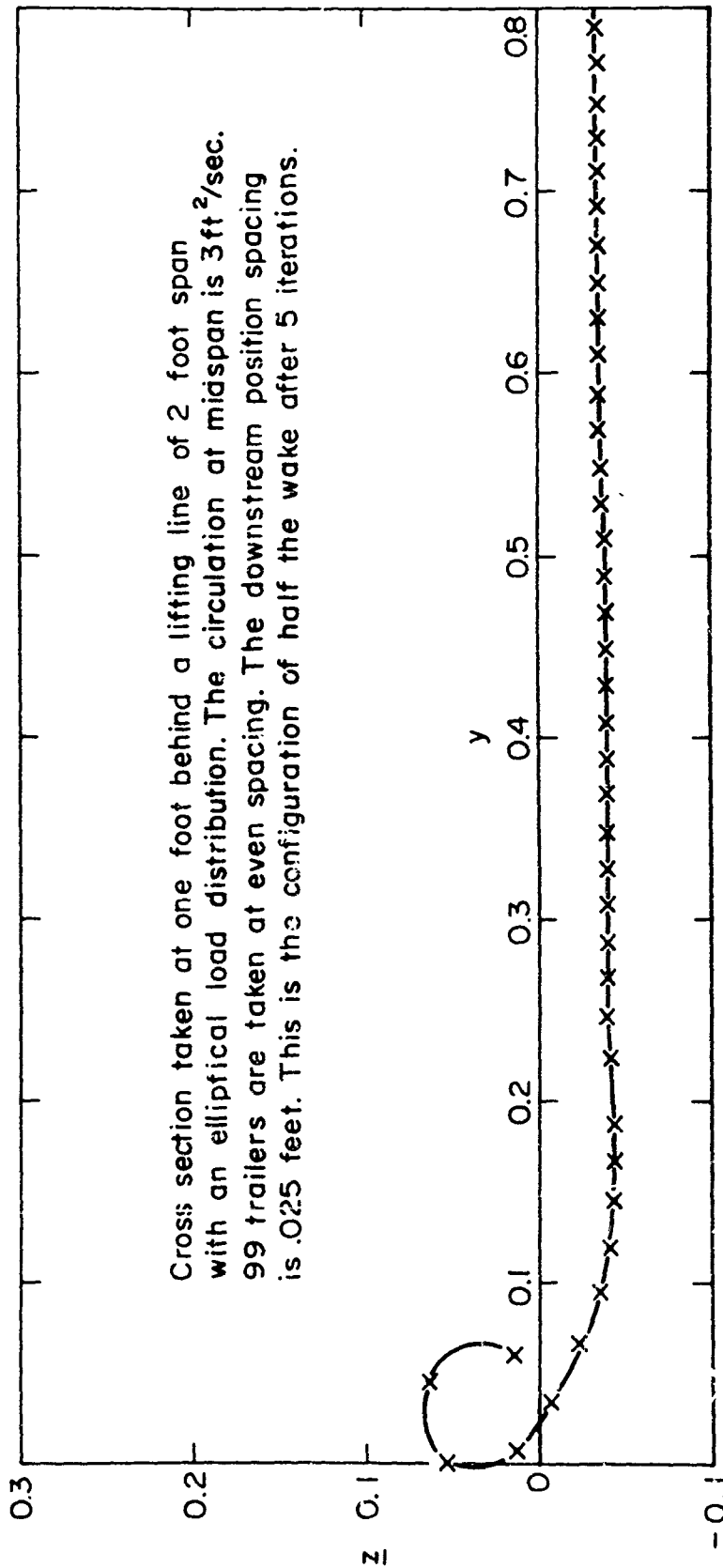
A new sheet is thus formed by integrating the streamlines back. If the flat plane wake were stable the downwash would remain constant at the trailing edge and increase to twice this value at cross sections far downstream. The sheet would, therefore, remain straight in cross section but slope with decreasing curvature downstream. Due, however, to truncation errors in the numerical methods and to roundoff error in the machine, the calculated downwash is never exactly constant across a cross section. The sheet will therefore not remain exactly flat. If it is indeed unstable in the flat configuration and stable in the rolled up position, as claimed by Kaden, it should proceed to the rolled up position post haste. After several iterations the sheet should be rolled up into whatever stable position it finds most comfortable. The drawing in Figure(1.2) shows the results of doing such a calculation on a wing of twenty foot span with an elliptical loading. For this sample calculation 31 vortices were used

and the calculation was carried far enough downstream to be rolled up although the spacing is too wide to distinguish details of the roll up mechanism in the tip region. Two further plots are shown in Figures (1.3) and (1.4). These assume a wing of two foot span with an elliptical load distribution. The magnitude of the circulation at the midspan is three feet squared per second. The first plot is of results using only nineteen trailing vortices. It is obvious that one foot downstream the sheet is no longer flat, but the effect is far more marked in the second plot for which 99 trailers were used. It is obvious that the choice of vortex spacing has an effect on the ultimate shape computed in the tip region, although the motion of the sheet in general away from the tip may be similar in the two cases. In fact, the smaller the spacing is chosen, the more dramatic the results at the tip. Since the kinematics and dynamics of the fluid in the tip region are of major importance, especially if cavitation is to be accurately anticipated, this ambiguity in detailed results must be resolved. This problem, will however be deferred for the moment, to consider the more mundane question of calculation time. The two calculations for 99 and 19 vortices consume respectively 20 and 12 minutes of computer time on a 360 Model 65. This fact dooms further examination along this path to financial disaster. No practical propeller design method could ever be successful with so expensive a calculation at its base, considering the inevitable added



METHOD 1

FIGURE 1.3



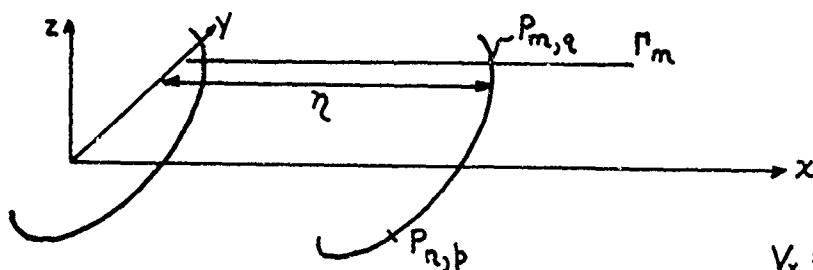
METHOD 1

FIGURE 1.4

calculation required to apply a method to the helicoidal geometry of propeller wakes.

Method Two

A more efficient means of calculating the trailing vortex paths was sought to decrease the number of computations required. Since the effect of one element of a vortex on the velocity at a control point is proportional to the inverse of its distance to the control point squared, it would seem that the major effect is that of the nearby elements. A slight inaccuracy in the locations of the vortex elements far from the point in question may not cause a significant error in the final result. A strip theory model was, therefore, used assuming that the shape of the sheet cross section at each downstream position was constant from that section upstream to the foil and downstream to infinity. This greatly simplifies the calculations since the trailers may be considered straight lines parallel to the x axis at each position and the induced velocity may be calculated analytically.



$$a^2 = (y_n - y_m)^2 + (z_n - z_m)^2$$

$$|\vec{V}| \text{ at } n,p \text{ due to } \Gamma_m = \frac{\Gamma_m}{4\pi a} \left[1 - \frac{\eta}{\sqrt{a^2 + \eta^2}} \right]$$

$$V_x = 0$$

$$V_z = |\vec{V}| \frac{y_n - y_m}{a}$$

$$V_y = |\vec{V}| \frac{z_n - z_m}{a}$$

The procedure is to start out at the trailing edge with the sheet straight in cross section as before and calculate the induced velocities on the sheet. The vortex locations at the next station downstream are then found from:

$$\bar{X}_{p+1} = \bar{X}_p + \bar{V} \Delta t$$

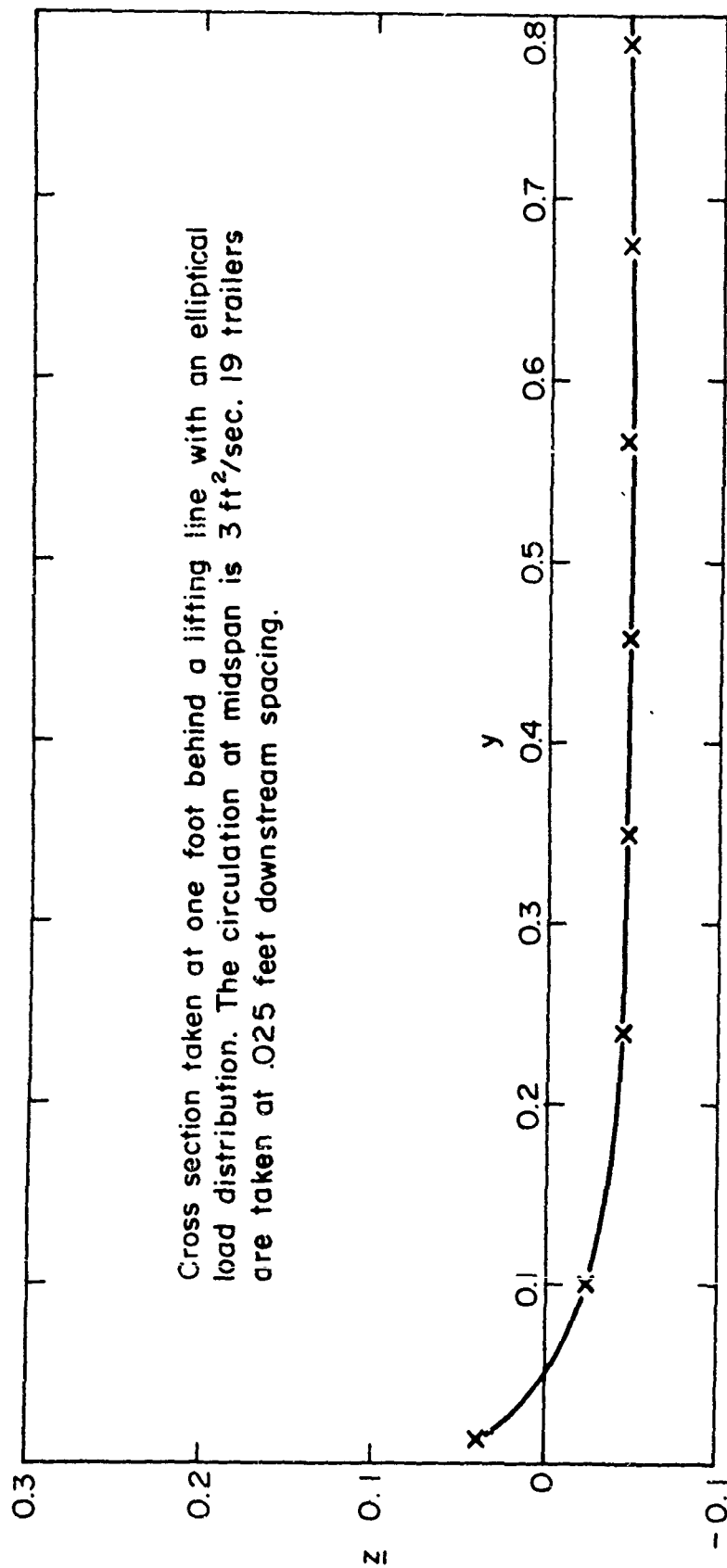
where Δt is the spacing in the downstream direction divided by the wing velocity U_0 . this procedure eliminates the need for iteration and storing large arrays of positions and induced velocities and gives results approaching those of the first method. See Figures (1.5) and (1.6)

Method Three

The obvious fallacy in the methods discussed so far is that a discrete vortex model of the elliptical loading may not give a constant downwash except in the case of vanishing spacing. The singularity in trailing vortex strength is represented rather poorly with such a model. If the model is such that the tip vortex immediately moves out of the plane of the rest of the sheet, the rollup will proceed immediately. See below.

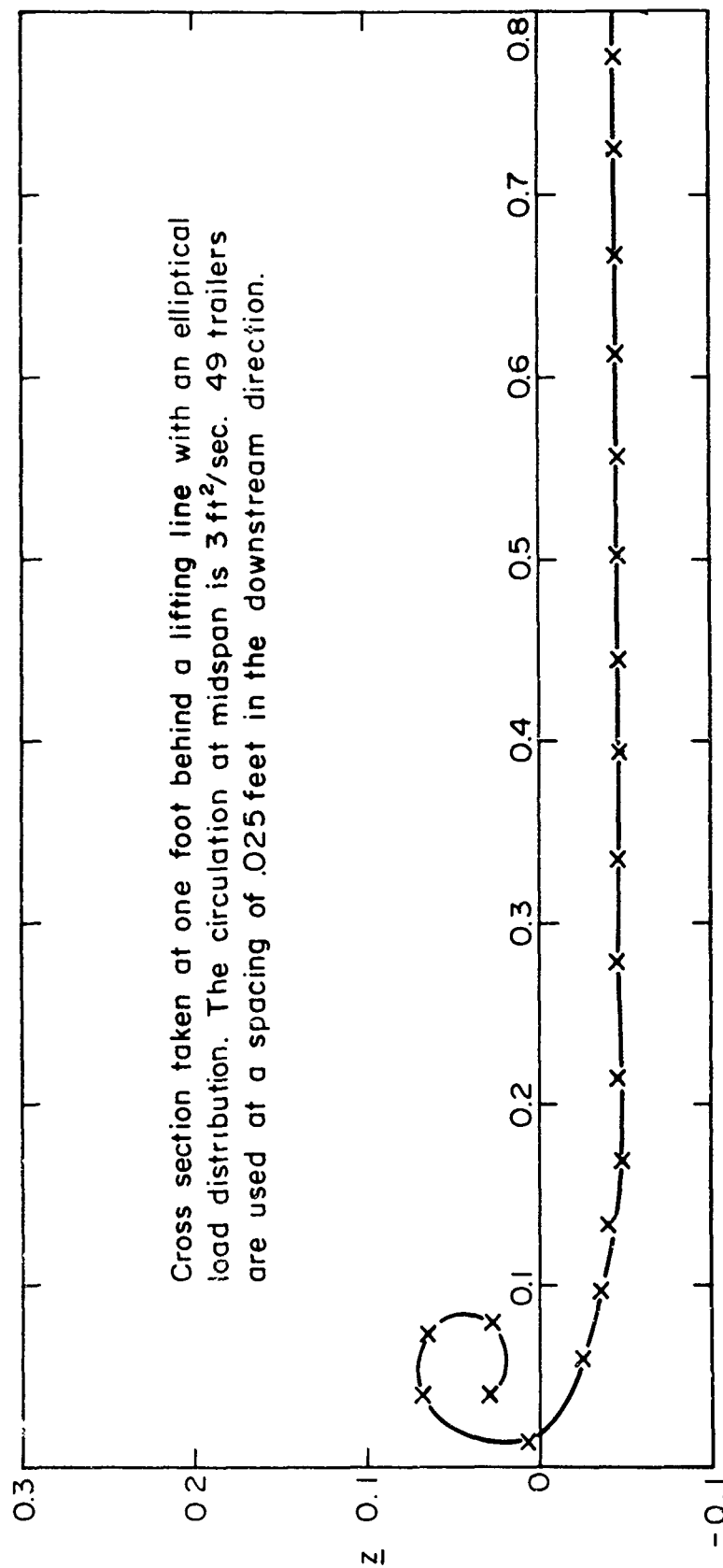


If, however, this area at the end of the wing is represented in a more mathematically satisfying manner by evaluating the downwash at the tip due to the singularity analytically, the sheet still rolls up. This argument is necessary only in an ideal fluid since in a real fluid the



METHOD 2
TEST OF STRIP THEORY
COMPARISON WITH METHOD 1

FIGURE 1.5

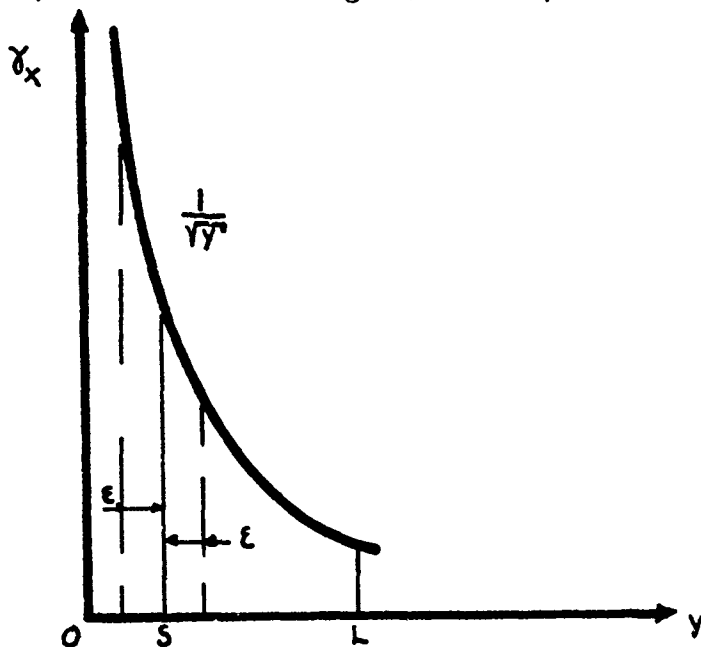


METHOD 2
TEST OF STRIP THEORY
COMPARISON WITH METHOD 1

FIGURE 1.6

vorticity may not remain infinite for any finite length of time. A line vortex may not maintain a zero core thickness but will diffuse over a finite area. Nevertheless the ideal fluid argument is worth pursuing both for the sake of consistency and to see if it invalidates the previous results.

First, an expression is needed for the downwash at the tip due to a loading in the tip area of form: $1/\sqrt{y}$



The velocity induced at a point s near the tip by such a loading between $y=0$ and $y=L$ can be calculated from the law of Biot-Savart.

$$|\bar{v}| = K \times \lim_{\substack{\epsilon \rightarrow 0 \\ s \rightarrow 0}} \left[\int_0^{s-\epsilon} \frac{dy}{\sqrt{y}(s-y)} + \int_{s+\epsilon}^L \frac{dy}{\sqrt{y}(s-y)} \right]$$

$$\text{let } \xi = x^{1/2}$$

$$|\bar{v}| = K \times \lim \left[\int_0^{\sqrt{s}-\epsilon} \frac{2\xi d\xi}{(s-\xi^2)} + \int_{\sqrt{s}+\epsilon}^{\sqrt{L}} \frac{2\xi d\xi}{(s-\xi^2)} \right]$$

$$= K \times \lim \left[-\frac{1}{\sqrt{s}} \log \frac{2\sqrt{s}-\epsilon}{\epsilon} + 0 + \frac{1}{\sqrt{s}} \log \frac{\sqrt{L}-\sqrt{s}}{\sqrt{L}+\sqrt{s}} - \frac{1}{\sqrt{s}} \log \frac{\epsilon}{2\sqrt{s}+\epsilon} \right]$$

$$\text{as } \epsilon \rightarrow 0$$

$$= \frac{K}{\sqrt{s}} \log \frac{\sqrt{L}-\sqrt{s}}{\sqrt{L}+\sqrt{s}}$$

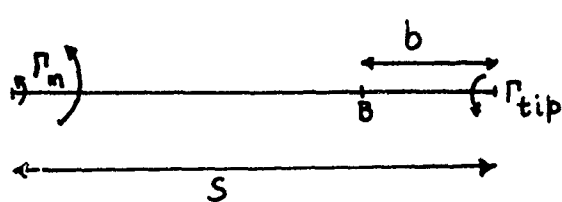
$$\text{as } s \rightarrow 0$$

$$= \frac{-K}{\sqrt{s}} \times 2 \left[\left(\frac{s}{L} \right)^{1/2} - \left(\frac{s}{L} \right)^{3/2} \frac{1}{3} + \dots \right]$$

$$= \frac{-2K}{\sqrt{L}}$$

The point of this discussion is that there is a finite downwash due to the inverse square root singularity in the trailing vorticity distribution even when the tip is approached. To represent this effect with a discrete vortex model it is necessary to consider the last vortex out to experience a downwash due to the singularity in the vorticity distribution in the last interval. This problem

should be taken account of in the computation of the motion of the sheet. The method used was to introduce a control point just inside the tip vortex. The strength of the tip vortex is weighted so that the proper velocity is calculated at this point B.



$\Gamma_m \rightarrow \text{next vortex in}$

$$\frac{w \Gamma_{tip}}{b} = \frac{\Gamma_{tip} b}{S-b}$$

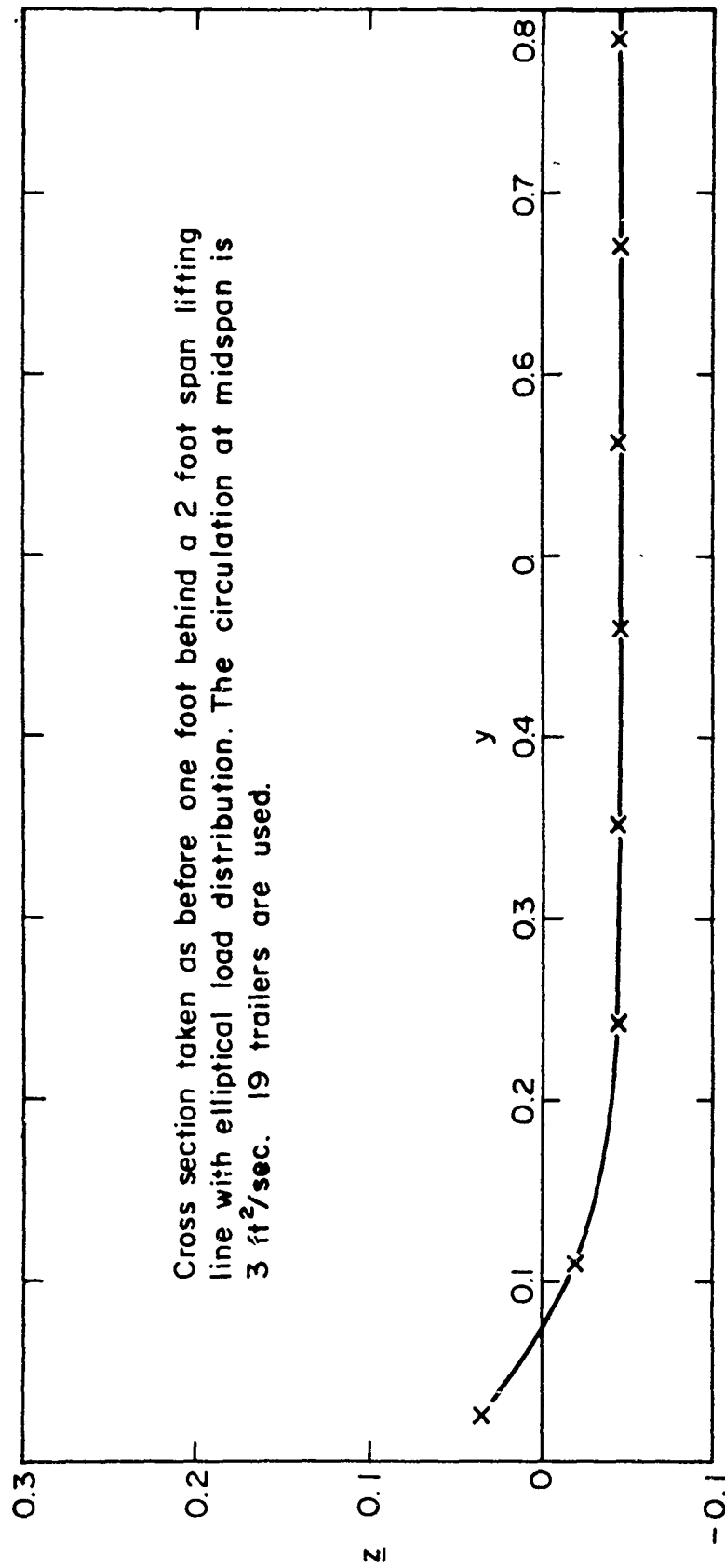
$$\Gamma = \Gamma_{tip} \times w = \Gamma_{tip} \times \frac{b}{S-b}$$

The velocities and positions of this point B are calculated at each control point rather than those of the tip vortex. The tip vortex position is obtained by extrapolating the position of the next vortex in through point B.

If this value is used in the induced velocity calculations according to the strip theory of Method two, the triggering is less sudden but the final rollup configuration is the same. See Figures (1.7) and (1.8)

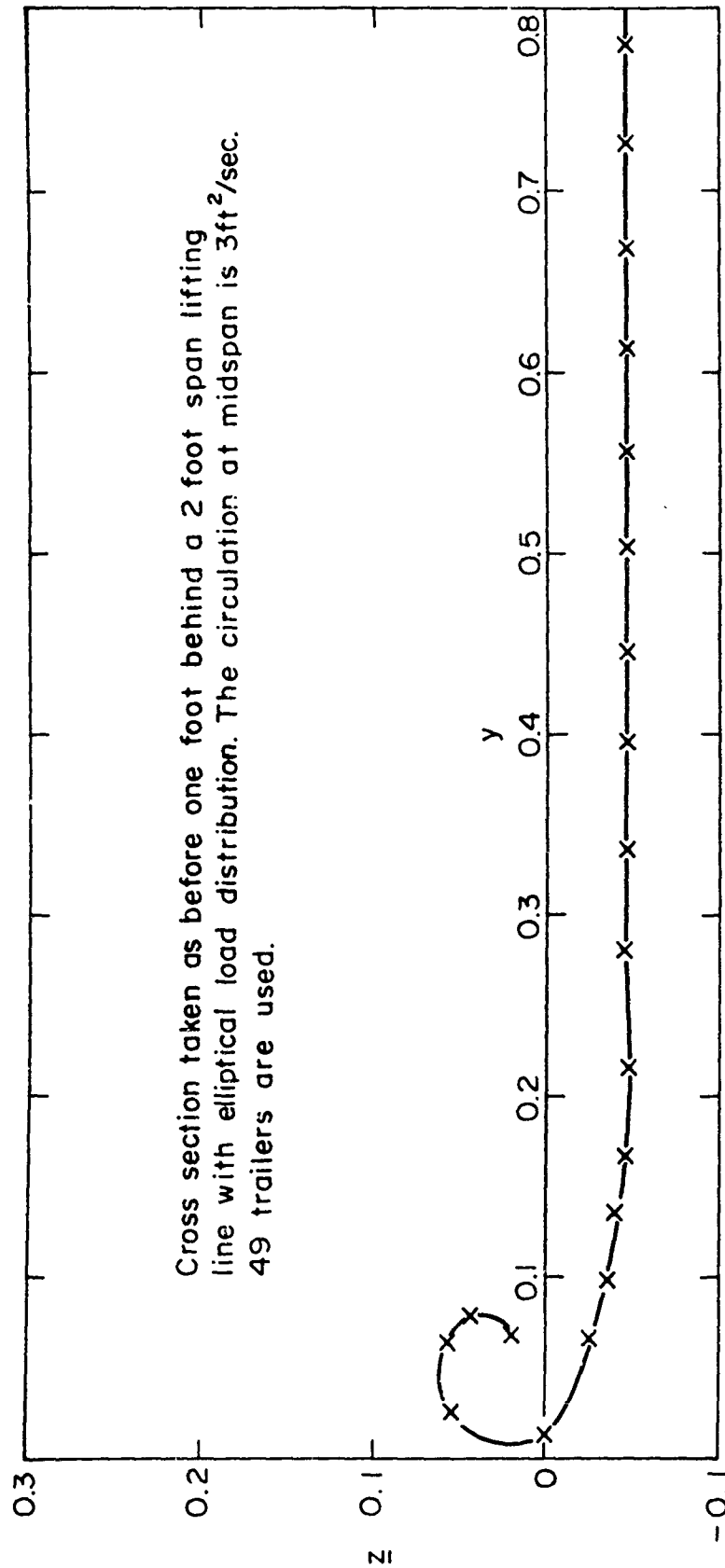
Method Four

The problem of ambiguous results in the wing tip region must now be considered. Since the results depend on the



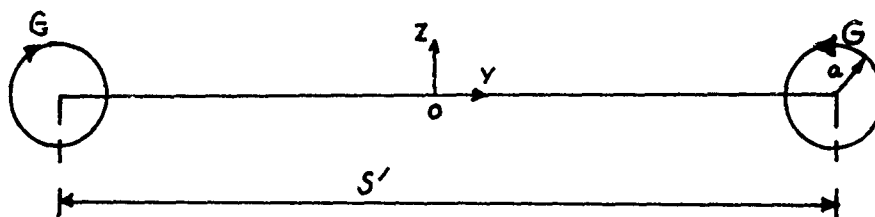
METHOD 3
ATTEMPT TO PREVENT ROLLUP BY APPROXIMATING
CAUCHY PRINCIPAL VALUE AT THE TIP
COMPARISON WITH METHOD 1

FIGURE 1.7



METHOD 3
 ATTEMPT TO PREVENT ROLLUP BY APPROXIMATING
 CAUCHY PRINCIPAL VALUE AT THE TIP
 COMPARISON WITH METHOD 1
 FIGURE 1.8

vortex spacing selected, there must be a length characteristic of the flow which would give a scale for the spacing selection. There is no ambiguity in the results if a real foil is towed in a real fluid. Since the problems occur at the tip of the wing, it is suspected that the length scale sought has some relation to the configuration of the flow in a real fluid in the tip region. The most obvious approach to this problem is to define a size for the viscous core at the tip. The usual means of doing this is by equating the total kinetic energy per foot downstream in the ultimate rolled up wake to the induced drag on the foil. Assuming that the final configuration is two Rankine vortices of strength G , the kinetic energy may be calculated as follows. The vortices are assumed to be s feet apart and to have core radius a . (6)



The velocity potential of the flow outside the core is given by:

$$\varphi = \frac{G}{2\pi} \left[\tan^{-1} \frac{z}{y-s'} - \tan^{-1} \frac{z}{y+s'} \right]$$

The kinetic energy outside the cores is given by:

$$E_0 = \frac{\rho}{2} \oint \varphi \frac{\partial \varphi}{\partial n} ds = \frac{\rho G^2}{2\pi} \log \left[\frac{s' + \sqrt{s'^2 + a^2}}{s' - \sqrt{s'^2 + a^2}} \frac{-a}{+a} \right]$$

The kinetic energy inside the cores is:

$$E_{in} = \frac{\rho}{2} \int_0^a \left(\frac{G}{2\pi a} \right)^2 \frac{r^2}{a^2} 2\pi r dr = \frac{\rho G^2}{8\pi}$$

This gives a total kinetic energy per foot or induced drag of:

$$E_T = \frac{\rho G^2}{8\pi} \left[1 + 4 \log \left(\frac{s' + \sqrt{s'^2 + a^2} - a}{s' - \sqrt{s'^2 + a^2} + a} \right) \right] = D_i$$

since a is presumed much smaller than the span:

$$D_i = \frac{\rho G^2}{8\pi} \left[1 + 4 \log \left(\frac{2s' - a}{a} \right) \right]$$

if the loading is elliptical:

$$a = .197 S \quad C_d = \frac{C_L^2}{\pi a}$$

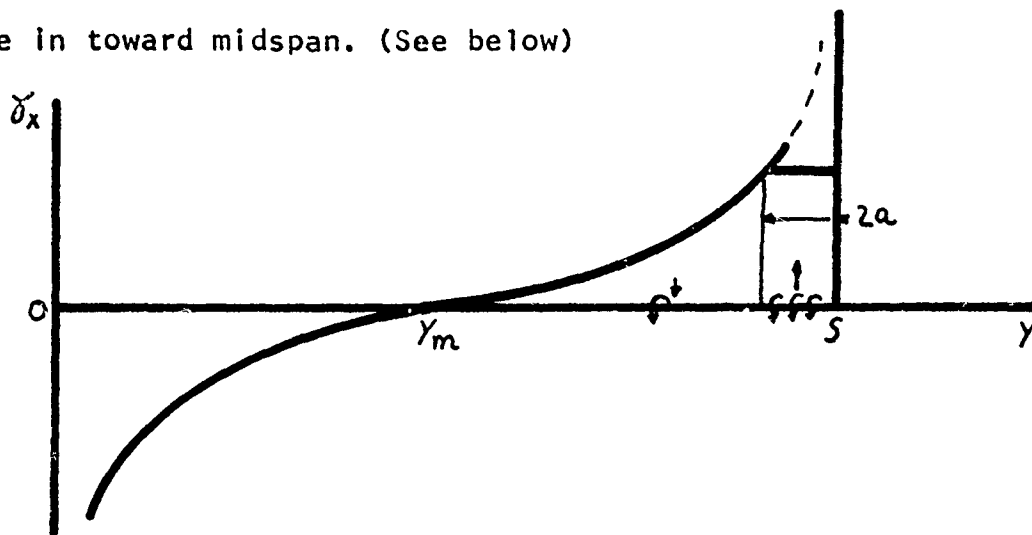
This gives a measure of the core size. However there are two major objections to this procedure. First the area close to the wing is of major practical importance and the total circulation certainly may not be considered absorbed into the core immediately on departure from the trailing edge.

Second, in a model which assumes small perturbation velocities in the downstream direction any concentration of vorticity from elsewhere in the sheet in the core is impossible. The vortices must move with the fluid and if there is no sink at the core center, there can be no net flow into the core region. By observing the paths of the vortices in the models considered so far, it is obvious that this is true. There is no concentration of vorticity in the core region but rather a rollup of large diameter about it. This fact leads to the third objection which is that in real flows a concentration in the core region is possible and , in fact , likely by allowing axial changes in velocity and pressure in the core. This introduces a sink or source at the core center in the two-dimensional models and invalidates the energy argument. The method used for this analysis must look more closely at the formation of the core near the wing. It was suggested by McCormick (7) that the important dimension was the boundary layer thickness.

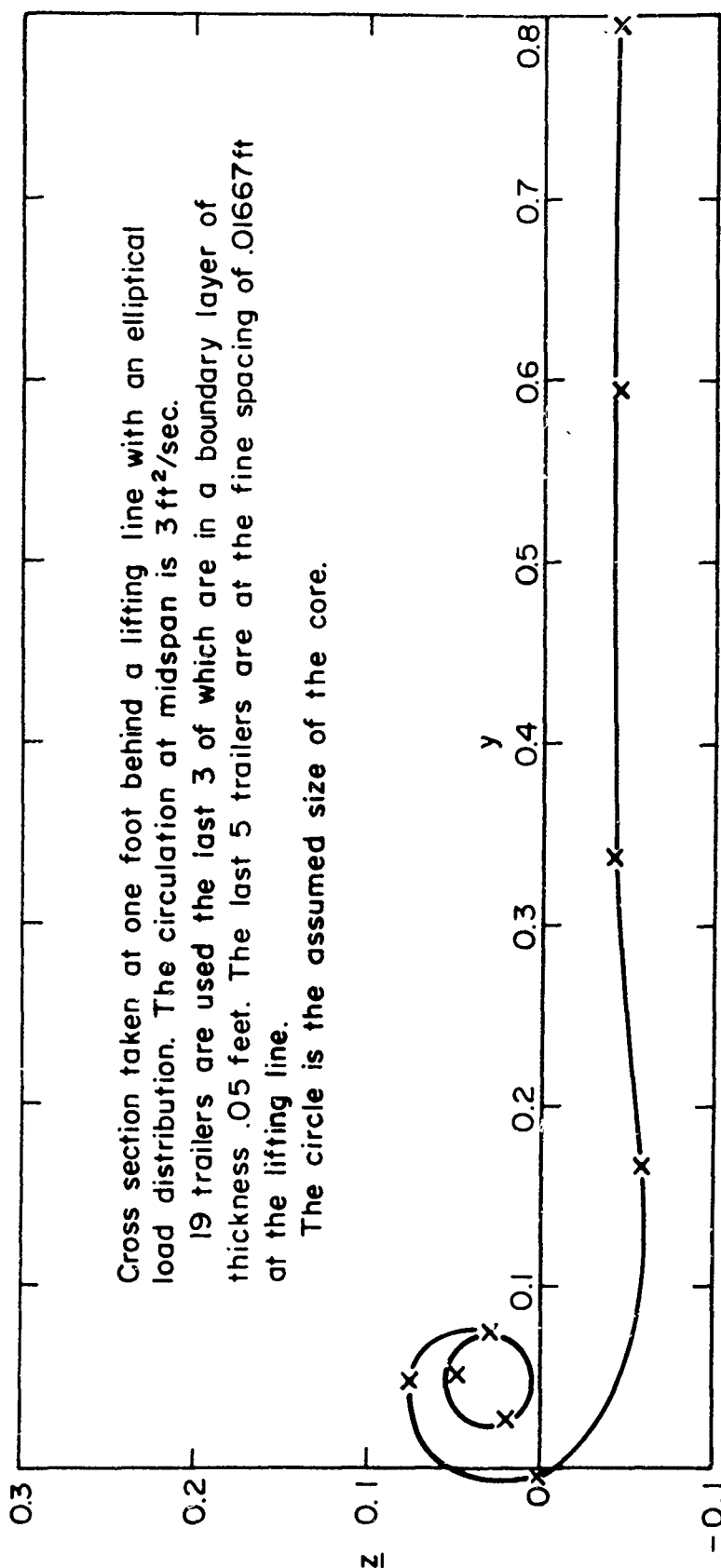
As was mentioned above, the deliberations about the principal value of the induced velocity integral at the tip when the slope of the bound circulation strength is infinite are somewhat beside the point in a real fluid. Such a strong vorticity as would be expected at the tip of a wing with elliptical loading must be spread out over a finite area in a real fluid. If this vorticity is being shed from a wing tip , it must be spread out over the boundary layer thickness of the fluid on the under (pressure) surface of

the wing when this fluid reaches the wing tip. If there is separation of the flow around the tip, this area would, of course, be greater. The tip vortex is, therefore, not a line vortex but has a finite core and the velocities due to it are finite everywhere. The core region describes a solid body rotation about its center.

The infinite value of vorticity at the tip has now disappeared, and the core vorticity is symmetrical about the center of the core. The velocity induced at the center of the core by the core itself is therefore zero. The rest of the sheet induces an upward velocity at the core center. The rollup phenomena is now easily visualized. The end of the sheet starts up while the rest of the sheet bends down. The core then pulls the sheet out and the sheet pulls the core in toward midspan. (See below)

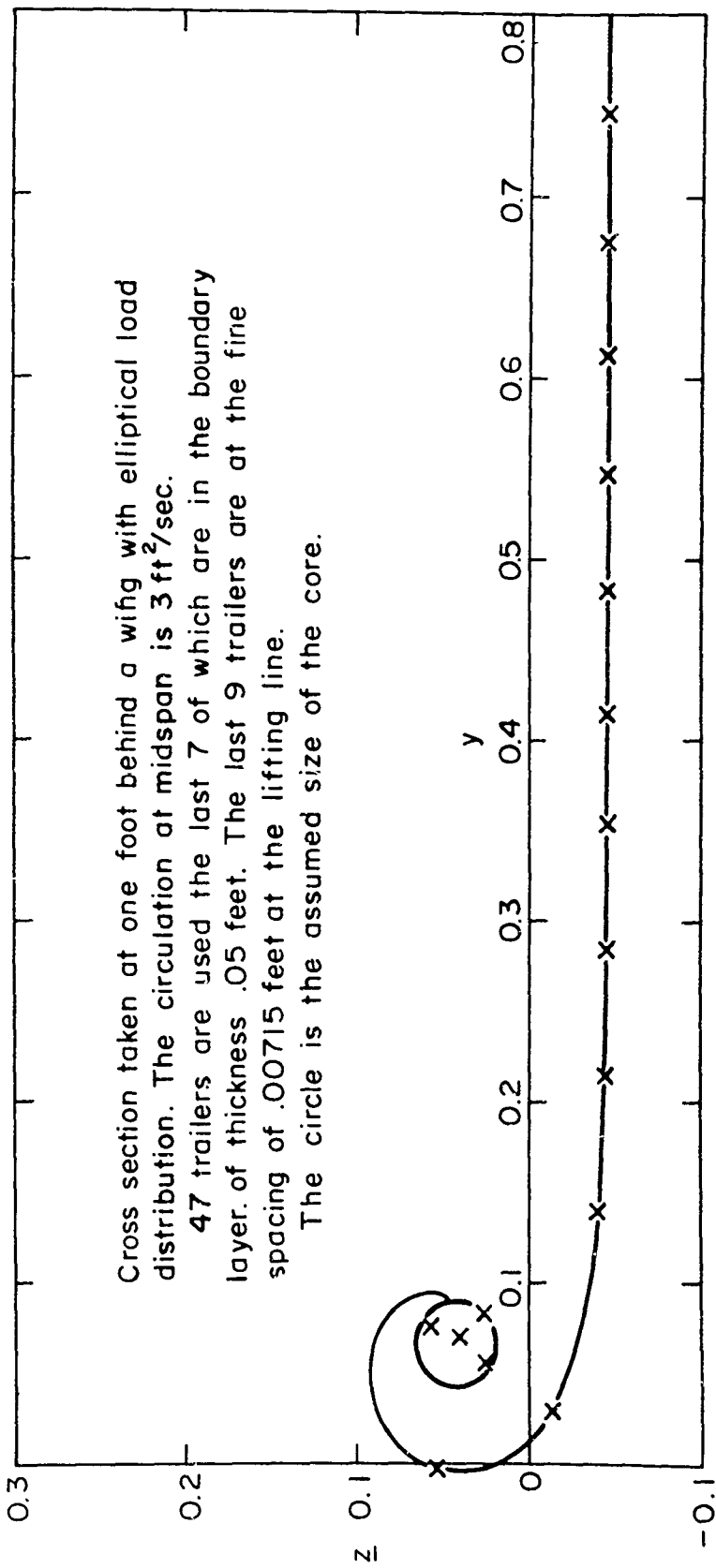


Since this model is the one that the author feels represents physical reality best, it will be used in the remainder of the paper. Results using this method are similar to those of the other systems (See Figure 1.9), but for further investigations into the dynamics of the tip



METHOD 4

FIGURE 1.9



METHOD 4
FIGURE 1.10

vortex core region this model seemed most appropriate.

The vortex spacing at the tip is chosen small enough so that several vortices are included in the tip. The strength of the tip vortex is then evenly divided between these vortices that lie within a boundary layer thickness of the tip. The rollup kinematics show little dependence on the choice of boundary layer thickness. This question does become more important when the dynamics of the core region are being considered. The minimum pressure at the center of the rotating region is for instance dependent on the core diameter selected. The success of this model in eliminating the previous difficulties with ambiguous results due to various choices of spacing may be observed by comparing figures (1.9) and (1.10).

CHAPTER II

The preceding analysis , as may be seen from the results of Chapter I, does not lead to a concentration of vorticity in the core region, although it does give a rollup of the vortex sheet. As a matter of fact , it is impossible for any concentration of vorticity to occur in a model which assumes the streamwise velocity to be constant. The only mechanism which can produce a concentration of vorticity, which implies a concentration of fluid since the vortices move with the fluid, is a sink at the core in the two dimensional strip theory model, which corresponds to an increase in the axial velocity in the three dimensional problem. Batchelor in (8) investigated the diffusion of a line vortex and the axial velocities and core pressure gradients associated therewith. His analysis is , however , limited to the region far downstream from the wing where all vorticity is considered concentrated in the core region and there is no additional vorticity entering the core from the sheet. His model is , therefore , one with a deacceleration of the axial velocities due to an increase of pressure downstream. The pressure rises downstream due to the viscous deacceleration of tangential velocities in the core region and the resultant decrease in centrifugal forces. The core therefore expands and weakens downstream in the far downstream region. Professor Sheila Widnall and Thomas McMahon conducted a preliminary investigation of the tip vortex rollup problem using Batchelor's model. (9)

Batchelor begins his analysis with the assumption that the motion is axisymmetric and the following equations of motion are valid in axisymmetric incompressible flow:

$$-1- u \frac{du}{dx} + v \frac{du}{dr} = -\frac{1}{\rho} \frac{dp}{dx} + \nu \nabla^2 u$$

$$-2- u \frac{dv}{dx} + v \frac{dv}{dr} - \frac{w^2}{r} = -\frac{1}{\rho} \frac{dp}{dr} + \nu [\nabla^2 v - \frac{v}{r^2}]$$

$$-3- u \frac{dw}{dx} + v \frac{dw}{dr} + \frac{vw}{r} = \nu [\nabla^2 w - \frac{w}{r^2}]$$

where:

$$-4- \nabla^2 = \frac{d^2}{dx^2} + \frac{d^2}{dr^2} + \frac{1}{r} \frac{d}{dr}$$

The assumption is made that axial gradients are small compared to radial gradients. Thus:

$$\frac{d}{dx} \ll \frac{d}{dr}$$

$$v \ll u$$

These assumptions are valid for the tip vortex dynamics considered in this report. The radial velocity is never more than two percent of the axial velocity and axial changes in velocity are small compared to radial changes. Thus equations -1- through -4- become:

$$-5- u \frac{du}{dx} + v \frac{du}{dr} = -\frac{1}{\rho} \frac{dp}{dx} + \nu \left[\frac{d^2 u}{dr^2} + \frac{1}{r} \frac{du}{dr} \right]$$

$$-6- \frac{1}{\rho} \frac{dp}{dr} = \frac{w^2}{r}$$

$$-7- u \frac{dw}{dx} + v \frac{dw}{dr} + \frac{vw}{r} = \nu \left[\frac{d^2 w}{dr^2} + \frac{1}{r} \frac{dw}{dr} - \frac{w}{r} \right]$$

$$-8- \nabla^2 = \frac{d^2}{dr^2} + \frac{1}{r} \frac{d}{dr}$$

The integral form of equation -6- is:

$$-9- \quad p = p_{\infty} - \rho \int_r^{\infty} \frac{w^2}{r} dr$$

In the region far downstream, Batchelor finds a solution for this system of equations of form:

$$-10- \quad w = \frac{\Gamma}{2\pi r} \left[1 - e^{-\frac{U_0 r^2}{4\nu x}} \right]$$

If the core radius a is defined as the radius where the tangential velocity w is a maximum, this core radius may be solved for:

$$-11- \quad a^2 = \frac{4\nu x}{U_0} (1.258)$$

This assumes that the core had zero radius (was a point vortex) at $x=0$. The change of core radius with distance downstream is:

$$-12- \quad \frac{da}{dx} = \frac{a}{2x}$$

The magnitude of this quantity is important in determining the importance of viscous effects in the core region near the wing. In the problems dealt with here .02 feet may be taken as a typical value for the core radius near the wing as derived from the boundary layer thickness. U_0 is typically 25 feet per second and the kinematic viscosity of water is about ten to the minus five feet squared per second. These values give for the downstream distance x which is a measure of how long it takes a point vortex to

diffuse to a core radius a:

$$-13- \quad x \approx \frac{25 \times 0.0004}{4 \times 10^{-5} \times 1.26} = 198 \text{ ft.}$$

In other words, the vortex would have to start as a point vortex 198 feet upstream to have diffused to a core radius of .02 feet at the trailing edge. At this value of x:

$$-14- \quad \frac{da}{dx} = \frac{.02}{400} \approx .00005 \text{ ft/ft.}$$

Therefore, it is concluded that in water the core radius does not change fast enough due to viscosity to have any significant effect on results in the region close to the wing.

Near the wing, however, the model is considerably altered. It is possible to have vorticity from the sheet enter the core, thus increasing the circulation and lowering the core pressure downstream. This gives rise to an increasing axial velocity in the core region and an inward component of velocity at the core surface.

The mechanics of the analysis proceed as follows. The wing is divided up into trailers as before and the last few are considered to be in the boundary layer and of constant strength. The boundary layer is assumed to be identical with the core thickness and the vorticity is assumed to be diffused over the surface of the core. The model is therefore, at each downstream section, a Rankine vortex with a group of trailing vortices outside it.

Initially at the wing when the sheet is straight, the minimum pressure in the core is easily calculated assuming axial symmetry and a small effect of the sheet on the core.

$$\begin{aligned}
 \text{for } r < a \quad p(r) &= p_{\infty} - \int_r^{\infty} \frac{w^2}{r} dr \\
 &= \frac{\rho \Gamma_c^2}{4 \pi^2 a^4} \int_r^a r dr - \frac{\rho \Gamma_c^2}{4 \pi^2} \int_a^{\infty} \frac{dr}{r^3} + p_{\infty} \\
 &= p_{\infty} - \frac{\rho \Gamma_c^2}{8 \pi^2 a^4} [a^2 - r^2] - \frac{\rho \Gamma_c^2}{8 \pi^2 a^2}
 \end{aligned}$$

$$\text{at } r=0 \quad p(0) = p_{\infty} - \frac{\rho \Gamma_c^2}{4 \pi^2 a^2}$$

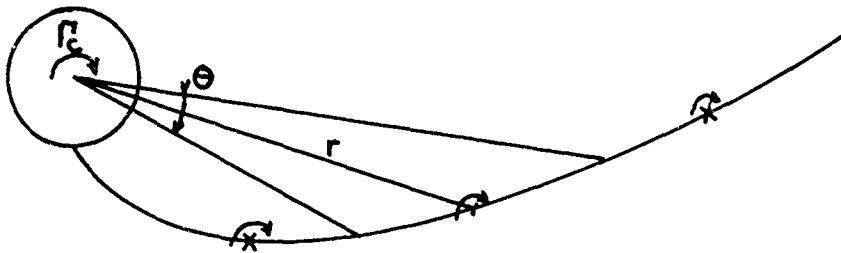
The pressure force on the upstream end of the core is:

$$\begin{aligned}
 F_{up} &= \int_0^a 2 \pi r p(r) dr \\
 &= \pi a^2 \left[p_{\infty} - \frac{\rho \Gamma_c^2}{8 \pi^2 a^2} \right] - \int_0^a \frac{2 \pi r \rho \Gamma_c^2}{8 \pi^2 a^4} [a^2 - r^2] dr \\
 &= \pi a^2 p_{\infty} - \frac{3}{16} \frac{\rho \Gamma_c^2}{\pi}
 \end{aligned}$$

Further downstream two effects act to decrease the core pressures and forces. The rollup of the vortex sheet increases the circulation surrounding the core and any flow into the core brings in circulation from the sheet. The first effect, that of the sheet rollup, is small due to the fact that the sheet vorticity is small compared to that in the core and the $1/R^3$ term in the pressure integral (above). This effect is approximated, however, in the following way

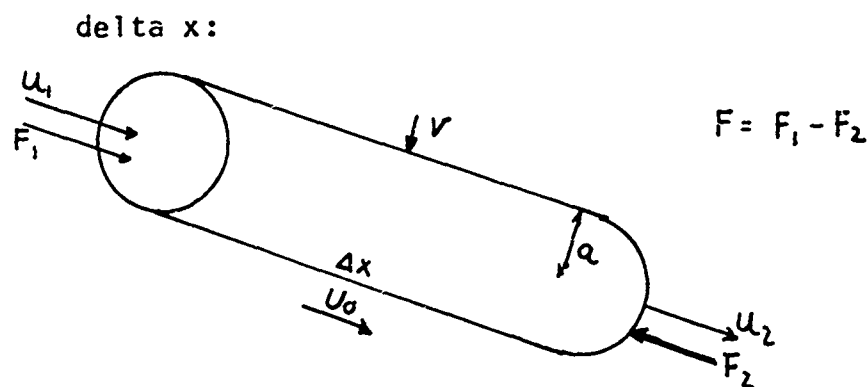
both for the sake of completeness and to trigger the concentration phenomenon.

The analysis assumes axial symmetry and , therefore , the outside vorticity must be considered to be evenly distributed about the axis. This is approximated by calculating the angle subtended by each section of the sheet on the core and considering the effective strength of that vortex on the core pressure is this angle divided by two pi. times its real strength. Its radius from the core center R is considered to be that of the discrete vortex.



This model is , of course , crude but the effect is in any case small compared to the concentration effects in the core region itself.

The major effect is that of the increasing core circulation due to absorption of the trailing vortex sheet into the core. This may be represented as follows. A length Δx of the core is considered with a pressure force F acting on it in the axial direction. A radial velocity V is assumed at first to be zero. Using the momentum equation in the x direction over a control volume of radius a and length



$$\text{X momentum out/sec.} = \rho \pi a^2 U_2^2$$

$$\text{X momentum in/sec.} = \rho \pi a^2 U_1^2 + 2\pi a \rho V U_0 \Delta x$$

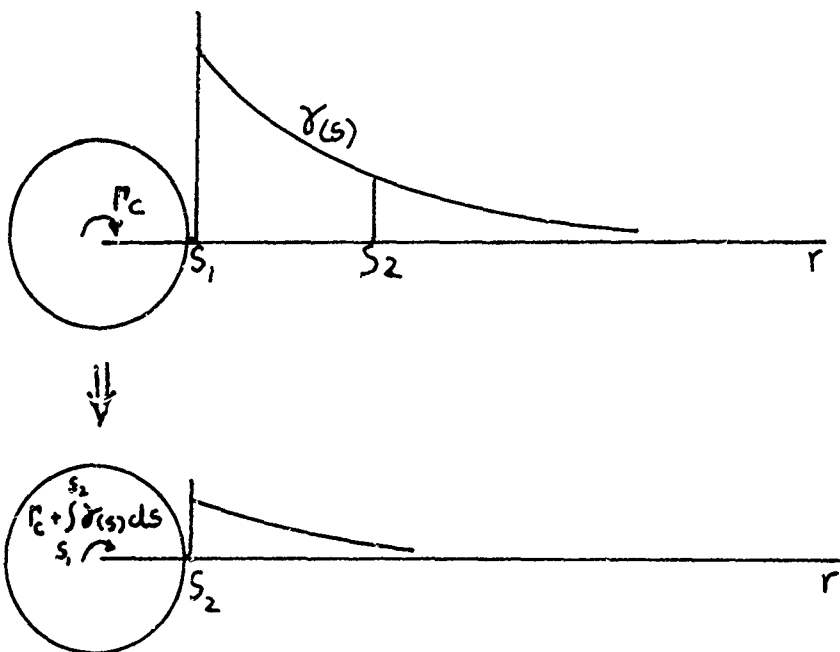
$$F = \pi \rho a [a U_2^2 - a U_1^2 - 2 \Delta x V U_0]$$

$$\text{from continuity} \quad U_2 = U_1 + \{2V/a\} \Delta x$$

$$\therefore V = \frac{a}{4\Delta x} \left[U_0 - 2U_1 + \sqrt{(U_0 - 2U_1)^2 + \frac{4F}{\rho \pi^2 a^2}} \right]$$

The original F is calculated from the small rollup effect described in the previous pages. The resulting radial velocity V means that a sink of strength $2 aV$ per unit length is pulling fluid, and sheet vorticity with it in toward the core. The resulting increase in core strength is calculated by assuming that all sheet vorticity within a radius difference of $V \Delta t$ is added to the core strength and subtracted from the sheet strength. (The stretching effect is neglected.)

This gives a decreased pressure on the downstream end and a resultant increase of axial velocity and sink strength. The calculation is repeated until the radial velocity converges to a limit. The new vortex positions may now be calculated and the process moved to the next downstream position.



It is entirely possible that the tangential velocity in the core is not proportional to the distance from the core center. However, it may be assumed that the tangential velocity is a smooth function of radius from core center to core radius. If, for example, a parabolic velocity profile is assumed, the pressure at core center is only changed 6.3 percent. The Rankine vortex is therefore assumed to be a reasonable approximation for the purpose of calculating minimum pressures. It is also assumed that the axial

velocity is uniform across the core crosssection and equal to U_0 outside the core. The more rigorous method for selecting these initial axial velocities would be through calculating the head at each radius and completing the energy balance. However, this fluid in the core has passed through the boundary layer on the wing and has lost an indeterminate amount of energy. For want of a better approximation the axial velocity is, therefore, assumed uniform.

CHAPTER III

The purpose here is to apply the theory of the previous chapter to a lifting line load and try to use it to calculate the resultant core pressures and the motion of the sheet. It is apparent that the minimum pressure coefficient is dependent on core diameter, load and the load distribution over the span, and the amount of rollup that has taken place.

To evaluate these effects, a lifting line with a span of two feet was loaded with various elliptical loads and boundary layer thicknesses. The motions of the trailing vortex sheets are calculated and the pressures in the core region estimated. The greatest attention was given to the wake near the trailing edge of the foil since this has the most effect on the foil itself.

The program operates in a manner similar to that of method four in Chapter I. The only modification necessary is a line sink at the core center and axial and radial velocities are calculated in the core region. The minimum pressure is calculated at the core center at each downstream position. A flow diagram for this program is shown in Figure (3.1). Runs were made at a variety of different boundary layer thickness, maximum circulations, and downstream spacings to determine the effect of these parameters on the minimum pressure.

In Figure (3.2) the minimum pressure, y coordinate of the core center, axial velocity in the core, and radial

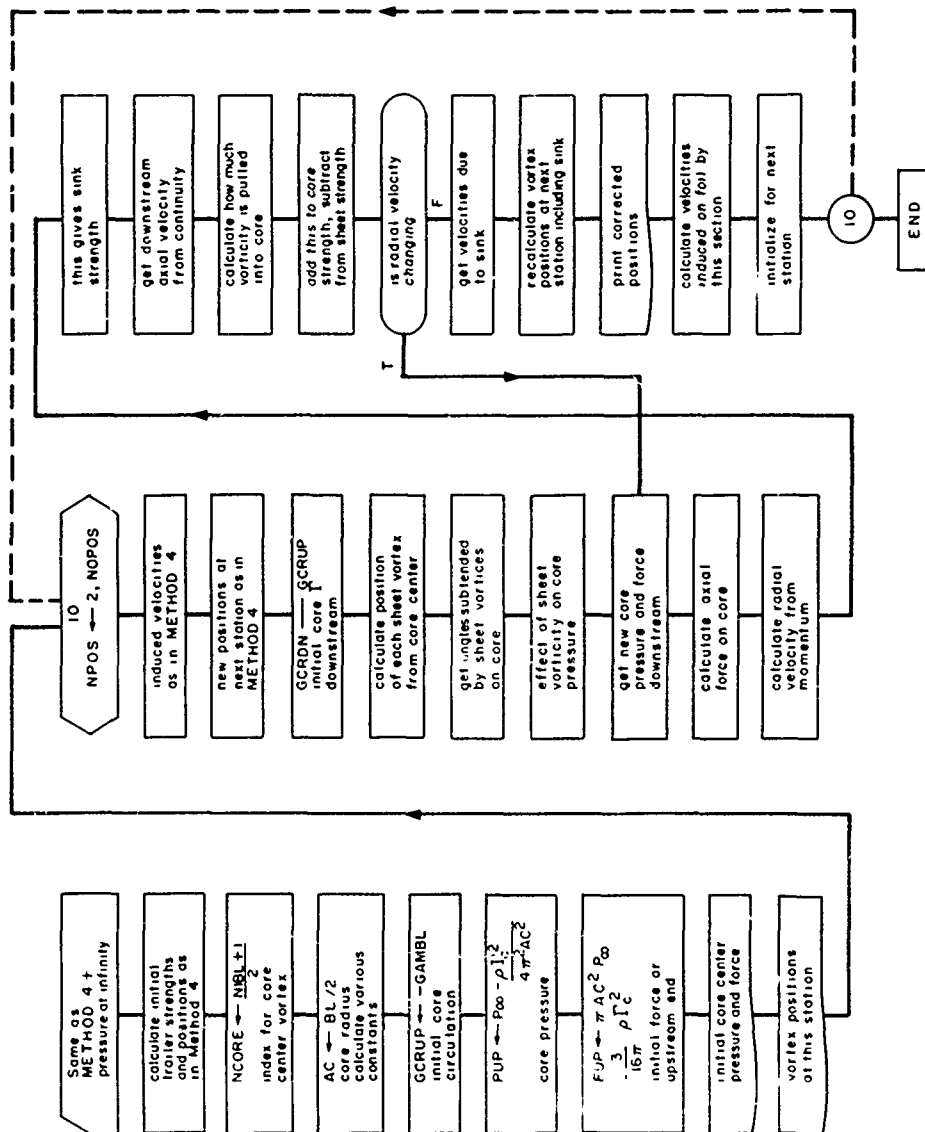


FIG.3.1 LOGIC FLOW GRAPH FOR VORTEX SHEET AND TIP VORTEX CALCULATIONS WITH A SINK AT THE CORE CENTER. A STRAIGHT LIFTING LINE WITH ELLIPTICAL LOAD DISTRIBUTION IS ASSUMED.

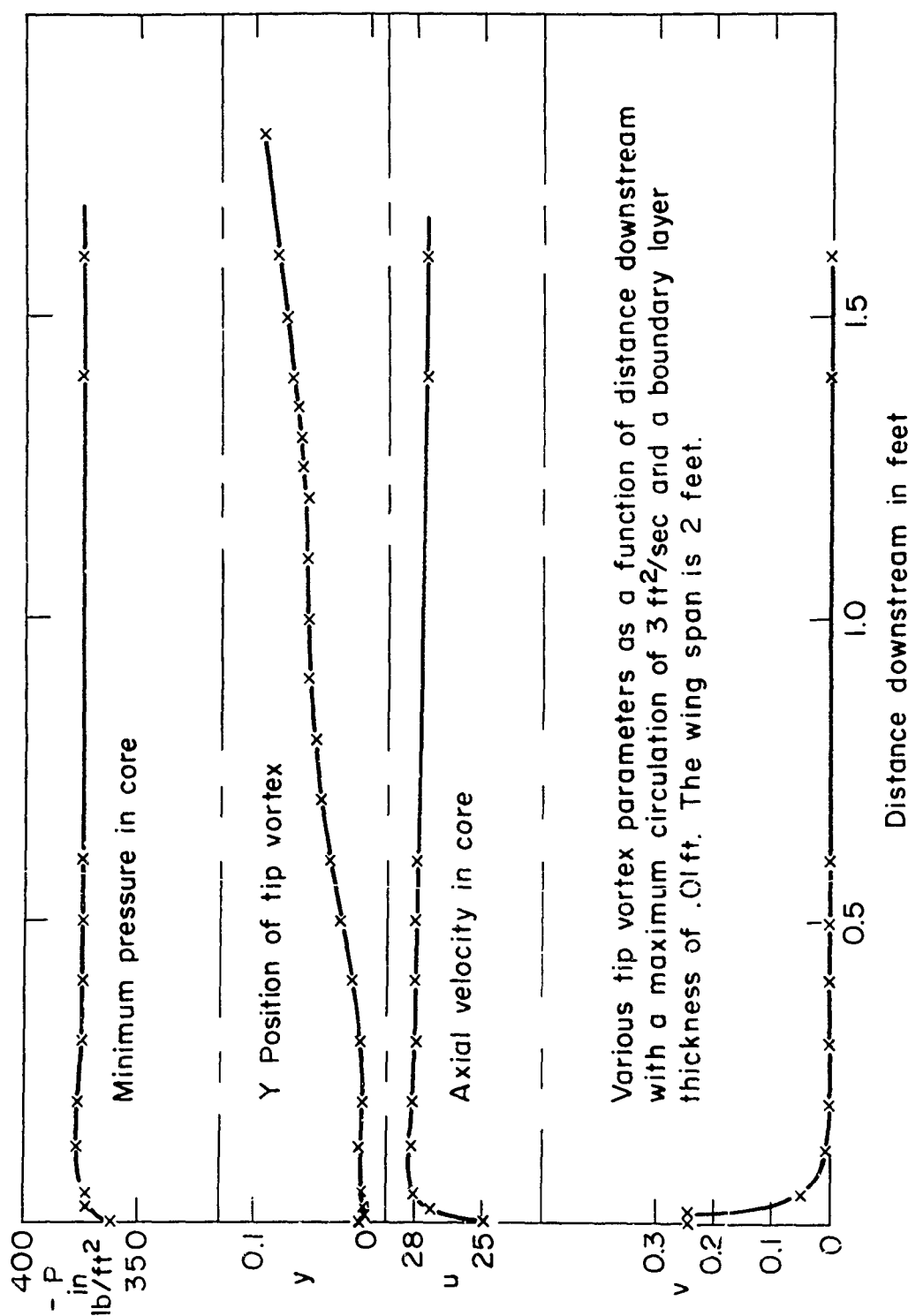


FIGURE 3.2

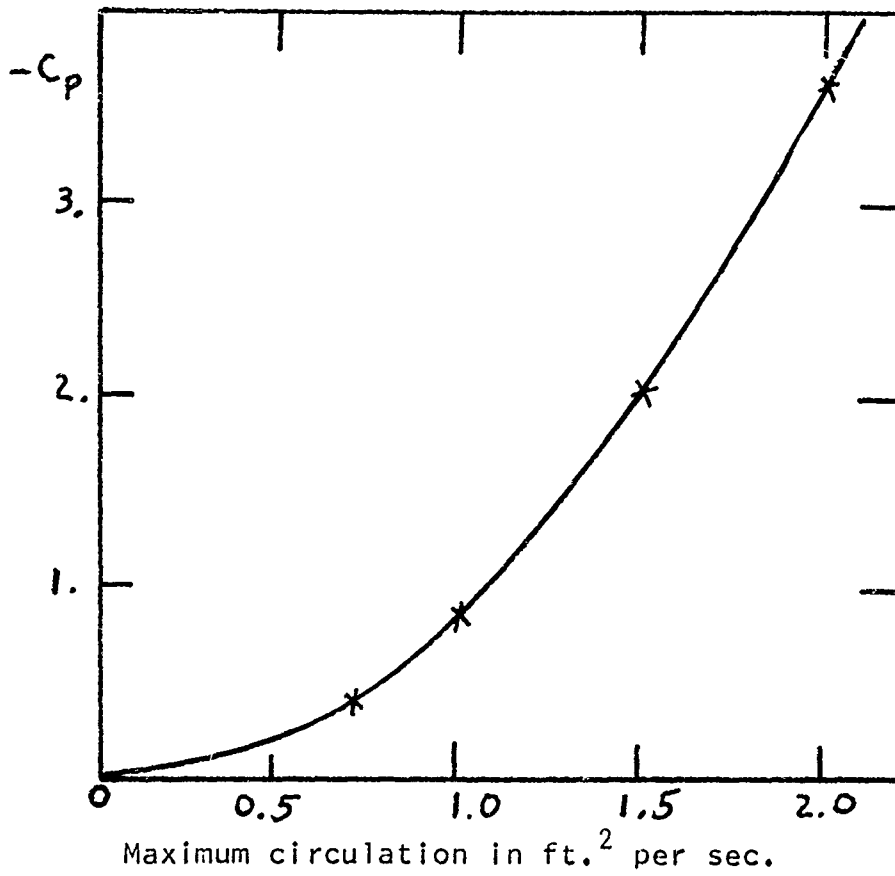


Figure 3.3 Minimum pressure coefficient in the tip vortex core for various maximum circulations. These results are calculated for an elliptically loaded lifting line with 1.67 foot span. The boundary layer thickness is assumed to be .001 feet.

velocity at the core boundary are plotted for various distances downstream for a maximum circulation of 3 feet squared per second and a boundary layer thickness of .01 feet. The results show that there is an immediate radial flow into the core close behind the trailing edge with a corresponding drop in the pressure. This is why tip vortices are sometimes observed to cavitate a short distance behind the foil rather than exactly at the foil. It is apparent that for the minimum pressure calculations the spacing in the downstream direction must be taken quite fine near the foil to obtain the details near the foil. If only the kinematics of the sheet are required, the spacing may be much coarser. In Figure (3.3) the minimum pressure is plotted versus maximum circulation for a boundary layer thickness of 0.001 feet, a thickness that corresponds to a laminar flow on the pressure side of the rudder model of Chapter IV. The minimum pressure is strongly dependent on the maximum circulation especially at very small boundary layer thicknesses as would seem reasonable according to equation -9- of Chapter II. The vertical component of induced velocity was plotted for a maximum circulation of 1.86 feet squared per second on a lifting line of 1.67 feet span. See Fig. (3.4). It is clear that the downwash from this trailing vortex sheet is anything but constant although the load is elliptical. The induced velocity is in fact positive at the tip. This clarifies some discrepancies between propeller design theory and practice, assuming that

the results are analogous for propeller blades. A blade designed for elliptical load distribution would in fact be much more highly loaded in the tip region than anticipated due to this upwash. The tip vortex would be correspondingly stronger and the minimum pressure in the core would be lower. Propeller designers have tended to reduce their design load drastically in the tip region to prevent tip vortex cavitation. These results indicate that the load is inevitably greater than predicted in the tip region if lightly or moderately loaded propeller theory is used. The boundary thickness must be known accurately if the minimum pressure is to be predicted with any confidence. The dependence of minimum pressure on boundary layer thickness is indicated in Figure (3.5)

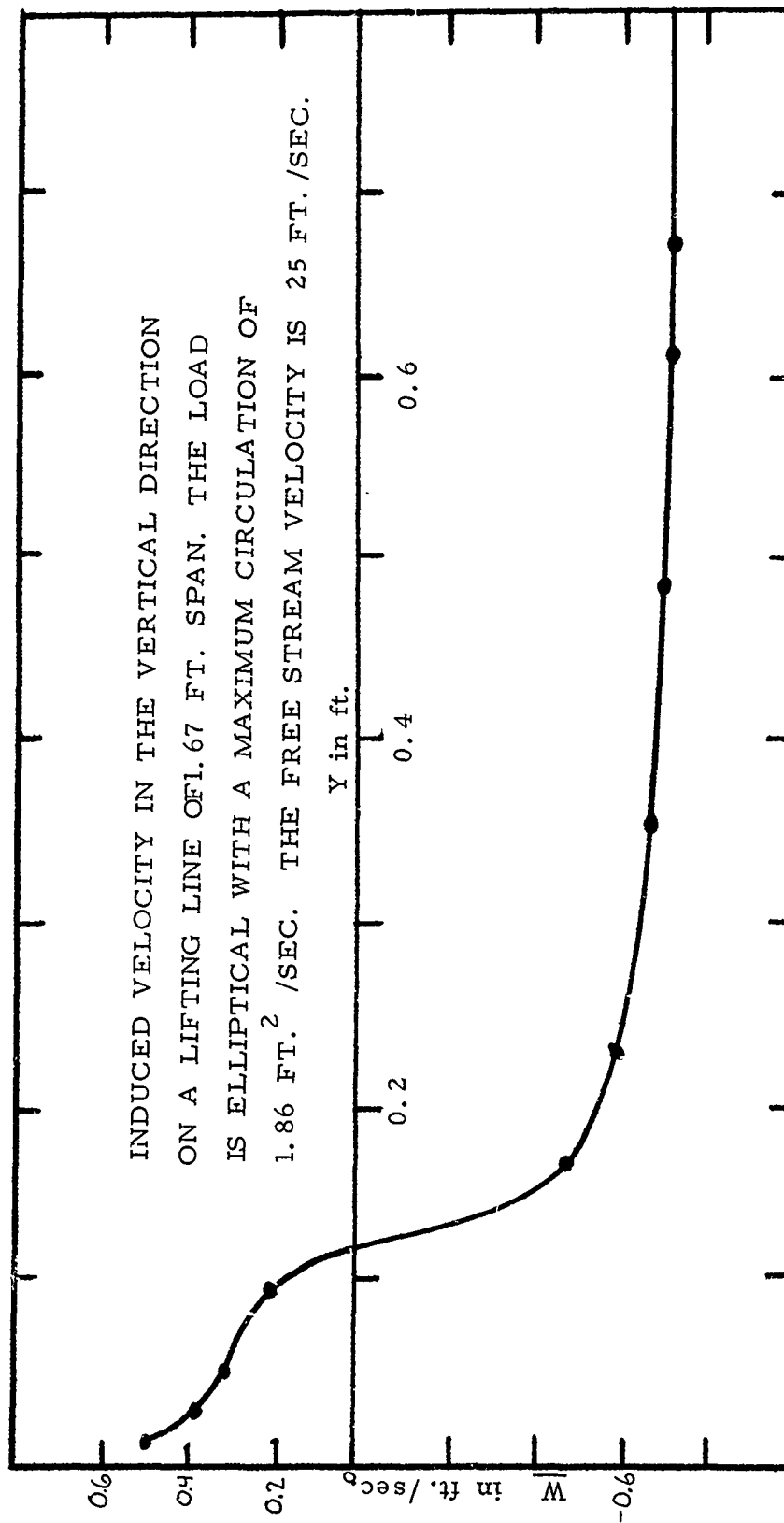
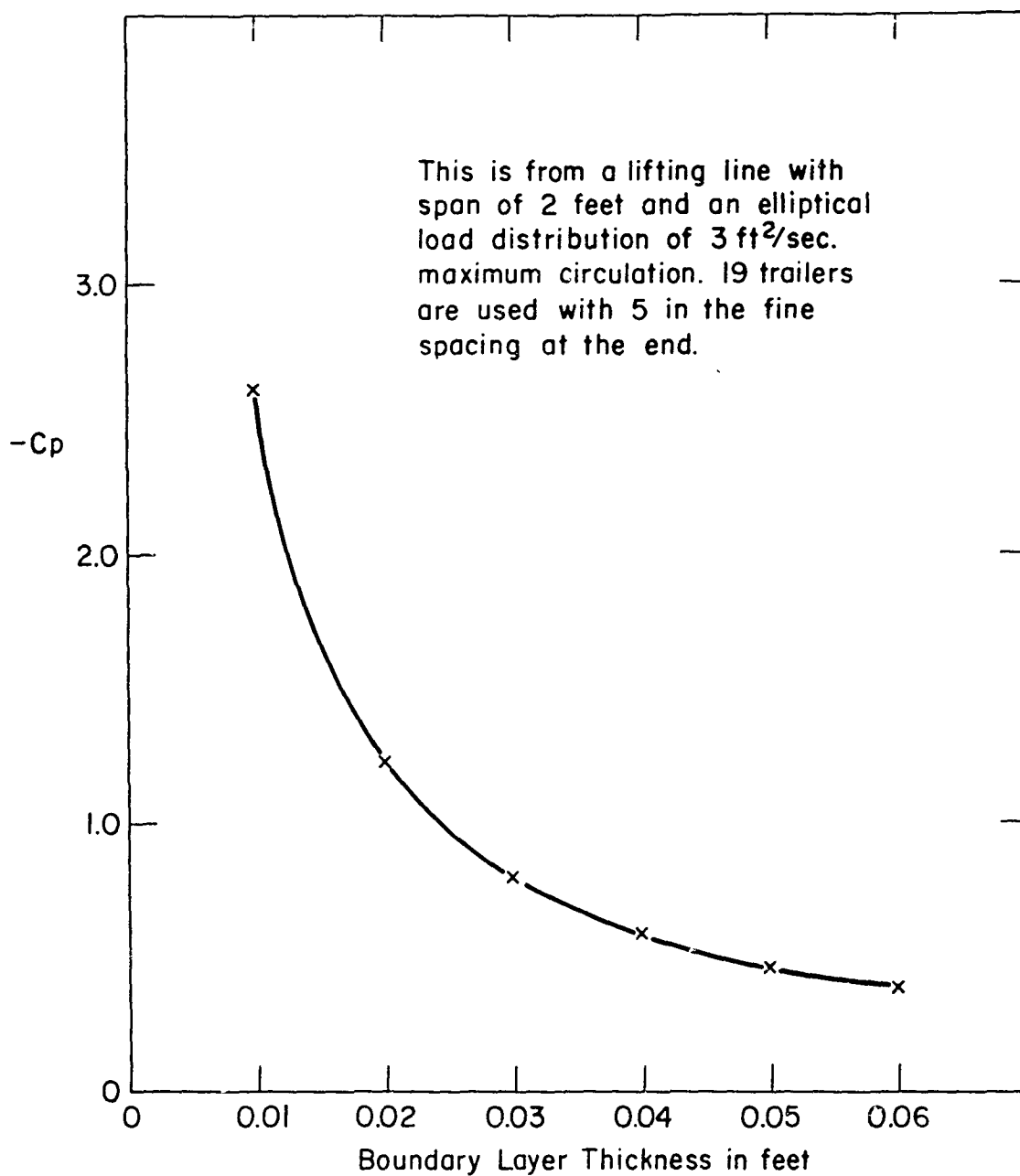


FIG. 3.4 EFFECT OF ROLLUP ON DOWNWASH



MINIMUM PRESSURE COEFFICIENT
AS A FUNCTION OF BOUNDARY
LAYER THICKNESS AT TRAILING
EDGE OF TIP, PRESSURE SIDE
FIGURE 3.5

CHAPTER IV

The results of Chapter III offer the possibility of experimental verification. The minimum pressure coefficient may be determined by observing the point where cavitation begins in the tip vortex core in a moving stream of water of known pressure and velocity. The calculations of the preceding chapter provide a method for determining the minimum pressure coefficient in the vortex core. When this pressure coefficient becomes equal to the cavitation index of the flow, a vapor core should be observed in the tip vortex. The foil selected for these tests was a bronze rudder model with the following characteristics:

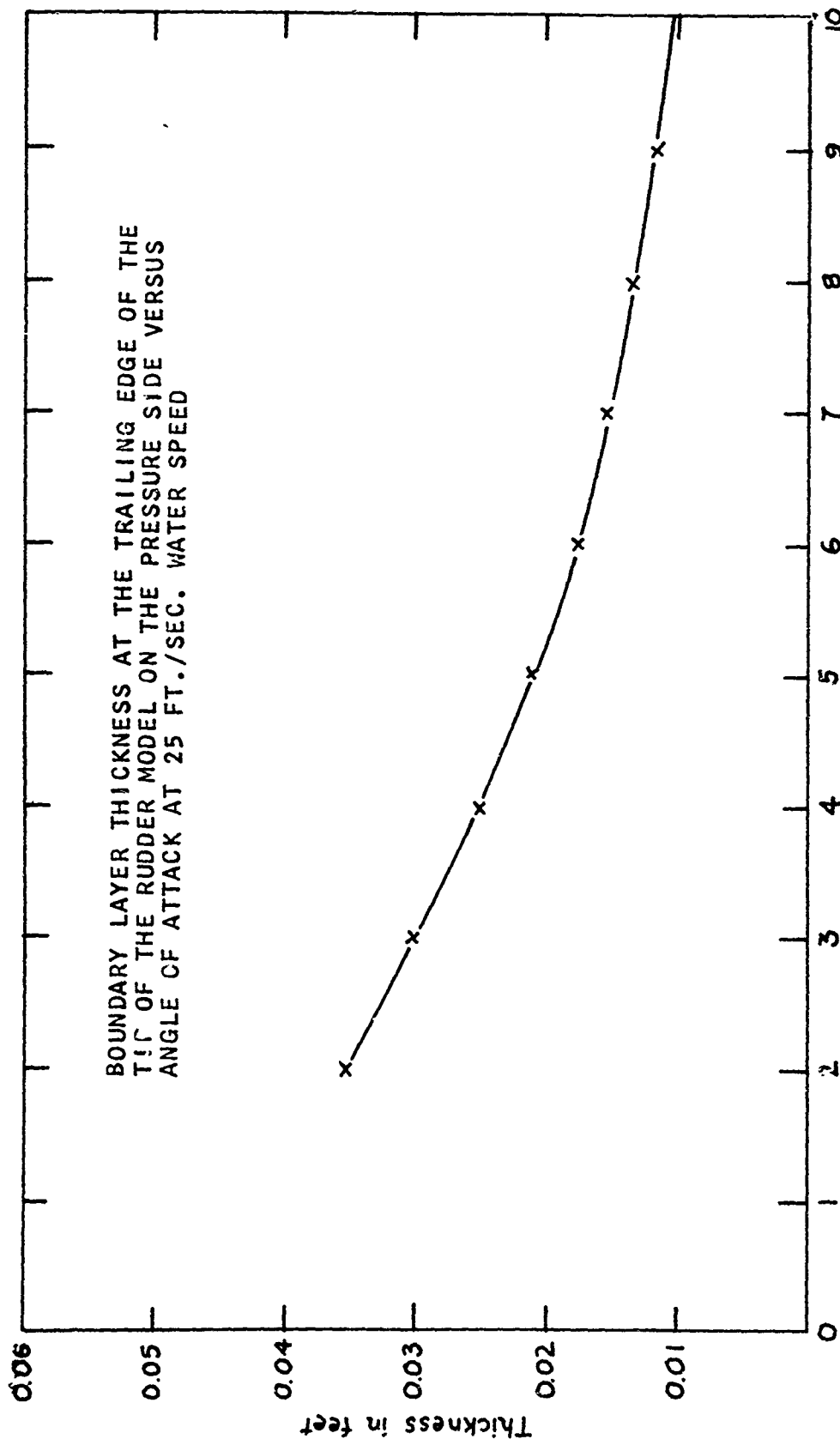
span	10"
root chord	8.925"
tip chord	5.360"
sweep of 1/4 chord	11 degrees aft
geometric aspect ratio	1.40
taper ratio	.60
section type	NACA 66
thickness to chord ratio	root .2, tip .1

The boundary layer thickness is of course a critical parameter in the calculation of minimum pressures in the vortex core as shown in Fig. (3.5). To make an accurate estimate of boundary layer thicknesses, it is necessary to know the pressure distribution on the pressure side of the foil. This is calculated for various angles of attack using

the published characteristics for this two dimensional section from Abbott and Doenhoff (). Of course the interest here is only in the flow aft of the stagnation point. The high pressures forward of the stagnation point may be disregarded since this fluid passes to the other side of the wing. For the integration of the boundary layer equations back from the stagnation point to obtain the displacement thickness I am indebted to Professor Jerome Milgram (11) who has programmed the methods of Truckenbrodt(12) and Spence(13). In both of these methods Ludwig and Tillmann's (13) equation for the wall shear stress is used:

$$C_F = .246 R_\theta^{-.268} 10^{-.678 H}$$

It is assumed that the boundary layer is turbulent in these calculations. This assumption is reasonable for ship propellers but leads to difficulty in the experimental work with this rudder model. It was necessary to add strips of plastic aluminum to the pressure side of the foil to produce a turbulent condition on the model. Cross flow effects were not taken into account and this may cause the calculated boundary layer thickness to be greater than the true thickness. Sample results are shown in Figure (4.1). Truckenbrodt's method does not converge properly in an adverse pressure gradient and therefore only the method developed by Spence is used in the low angle of attack range. It is felt by Professor Milgram that the difficulty in the application of Truckenbrodt's method lies in his



Angle of attack in degrees
FIGURE 4.1

numerical handling of the equations at high values of H (the ratio of displacement thickness to momentum thickness) rather than an inherent fault of the method. In the range of values of angle of attack above 5 degrees, the two methods agree nicely. It is felt that these methods give a better estimate of the boundary layer thickness than that used by McCormick (7), which does not take the pressure gradients due to the potential flow around the foil into account.

The computer program described in Chapter IV is used to calculate the motions of the sheet and minimum pressure coefficient in the vortex cores. The loading is assumed to be elliptical so that the downwash is constant across the span. For a span of 1.67 feet (twice the real span due to the image effect of the tunnel wall) and a chord at midsection of .745 feet, the circulation at midsection is computed as follows for angle of attack α :

$$C_L \approx \frac{\rho U_0 \Gamma}{\frac{1}{2} \rho U_0^2 C} \approx \frac{2\pi\alpha}{1+2C/s} = 3.32\alpha$$

With a tunnel water velocity of 25 feet per second:

$$\Gamma = .517 \alpha$$

where α is in degrees. The downwash may also be computed assuming that the sheet remains flat:

$$w = U_0 \frac{C_L C}{\pi s}$$

The lift coefficient for this low aspect foil was checked using a lifting surface computer program developed by S. Widnall(15). This program gives a slightly lower lift coefficient at each angle of attack.

$$C_L = 2.57 \alpha$$

The results both from the program and experimental are plotted in figure (4.6). The points represented by small circles on this plot were measured by observing the pressure at which cavitation first appeared in the tip vortex core. The pressure in the cavity was then assumed to be vapor pressure. Some error may be expected due to this assumption. The cavity pressure may well be higher due to air content in the water. The consistency of the results as the tunnel remained under vacuum for several hours, however, indicates that this effect was not major. The initial runs were made with a tip rounded with plastic putty. The initial job was rough and the maximum span was about at the three quarter chord point rather than at the trailing edge. This caused the tip vortex to form forward of the leading edge and to separate around the tip. The Reynolds number of the flow around this model was about 10^5 and some difficulty was encountered in obtaining turbulent flow in the favorable pressure gradient on the pressure side of the foil. The tip was rebuilt with putty and the foil was carefully smoothed with steel wool. See Fig. (4.5). Turbulence stimulation was provided by a spanwise strip of putty along one side of the foil at the point of maximum thickness. The results obtained

with this foil are also plotted in Figure (4.6). It is evident that when the smooth side is the pressure side the foil cavitates much more readily at low angles of attack than when the turbulence stimulation is on the pressure side. Transition to turbulent flow is indicated by the results for the smooth pressure side at high angles of attack. The critical cavitation numbers for the two cases then approach each other. These results compare favorably with those of McCormick(7) although the hysteresis effect that he observed was not apparent in these tests. The critical cavitation number was the same when the critical point was approached from low pressures or from high pressures. The results indicate that the foil cavitates at slightly higher pressures than anticipated by theory. This may be explained by the fact that the lift in the tip region is higher than predicted by theory as discussed in Chapter III. The laminar flow boundary layer thickness is calculated without taking account of the pressure gradient along the blade. Since this report is concerned with marine propellers, which operate in a highly turbulent flow normally, the laminar results are interesting only in a purely academic sense. If, however, the reader is tempted to apply these results to cases where the flow is truly laminar it would be advisable to program a laminar boundary layer thickness calculation for a variable pressure gradient in the outer flow.

The trajectory of the tip vortex was plotted (Fig. 4.2) for the rudder model at an eight degree angle of attack. Its position at one foot downstream from the trailing edge is .135 feet above the center of the sheet. This agrees with the photograph (Fig.4.3) of the rudder operating in these conditions in the Propeller Tunnel. (The angle of attack is negative in the photograph so that lift is down and the tip vortex is the lower curve.) It was observed during these tests that the tip vortex moved in the free stream direction, in other words along the axis of the tunnel, shortly after leaving the trailing edge while the rest of the trailing vortex sheet curved downward as predicted by airfoil theory. This agrees with the calculations of this paper (see Fig. 4.2) and is explained by the fact that, if most of the trailing vorticity is concentrated in the core, there is nothing to induce a perturbation velocity on the tip vortex but its image, which is far away. The downwash due to the image vortex, assuming that it is 1.67 feet away and that the circulation at midspan is 3 feet squared per second is less than one degree. Therefore the tip vortex moves in the freestream direction as soon as it has absorbed most of the rest of the vorticity. The spanwise trajectory of the tip vortex is shown in the photograph of Figure (4.5). The eight degree angle of attack with 25 feet per second water speed condition was maintained for this photograph. Again the tip vortex curves sharply in the vicinity of the foil and then

proceeds nearly straight downstream. The calculated spanwise trajectory is shown for comparison in Figure (4.7).

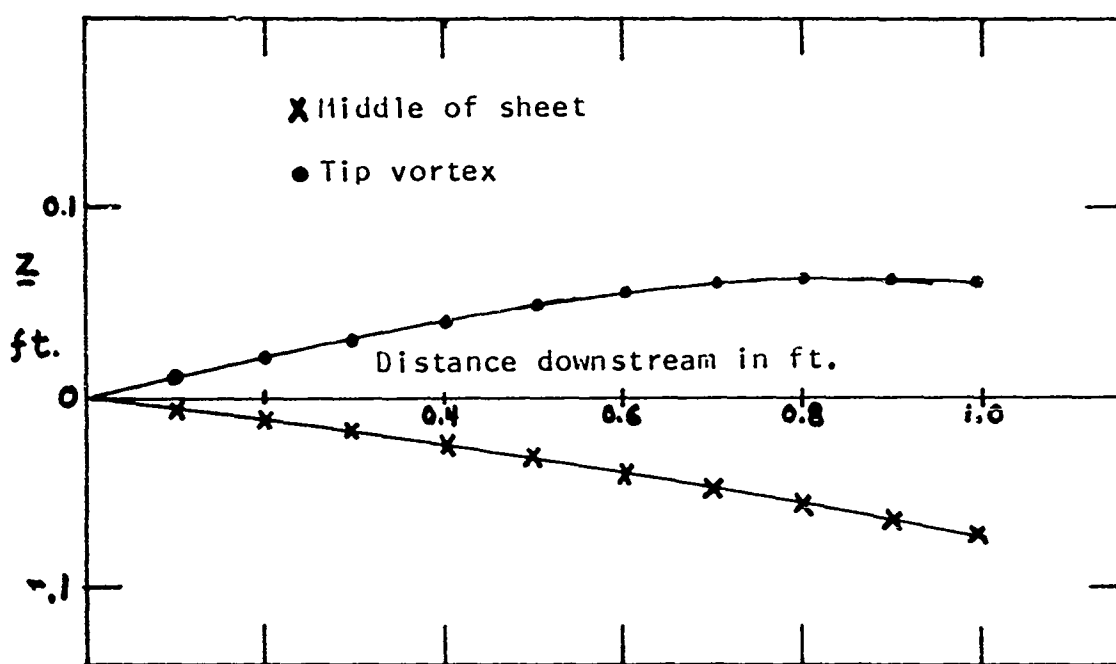
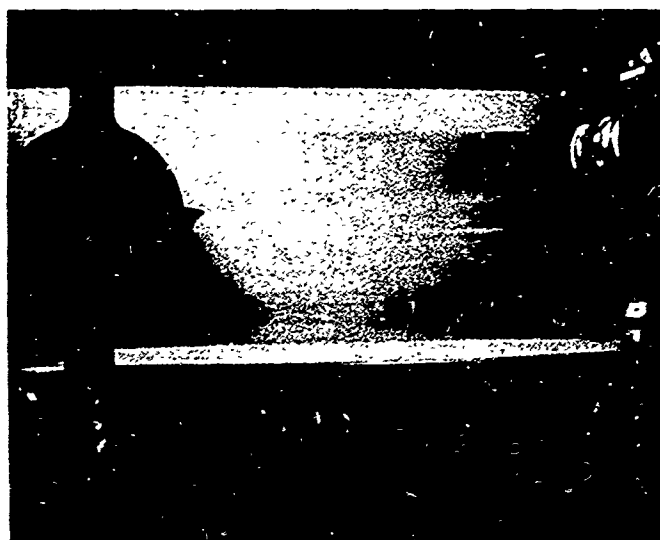


FIG. 4.2 Calculated trajectory of the tip vortex core and the wake at midspan for the rudder model at 8 degrees angle of attack and 25 ft./sec. water speed.



1 foot

FIG. 4.3 A photograph of the rudder model operating at 8 degrees angle of attack and 25 ft./sec. water speed. The lower streak is the tip vortex. The upper streak is the rest of the wake.

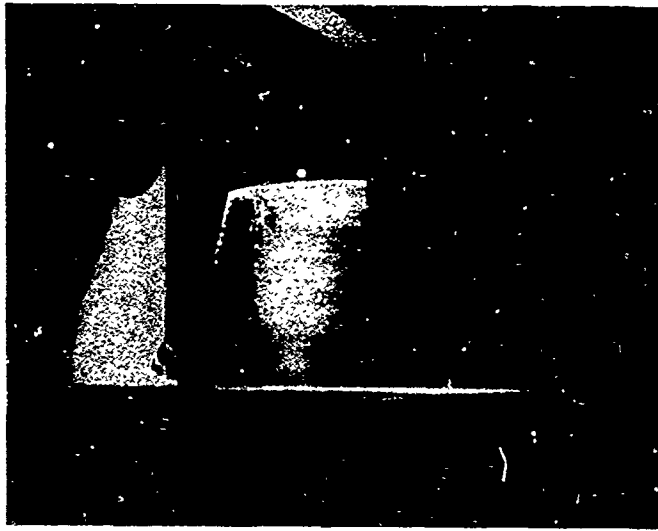


FIG. 4.4 A top view of the rudder model showing turbulence stimulating strips.

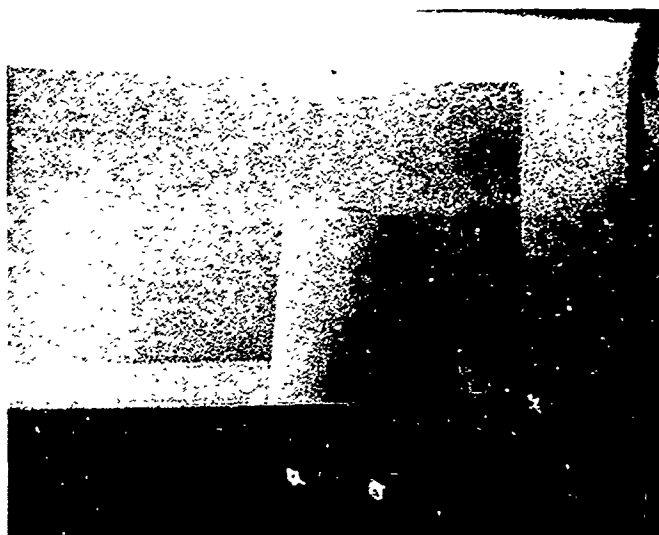


FIG. 4.5 A top view of the rudder model operating
at 8 degrees angle of attack and 25 ft./sec.
water speed.

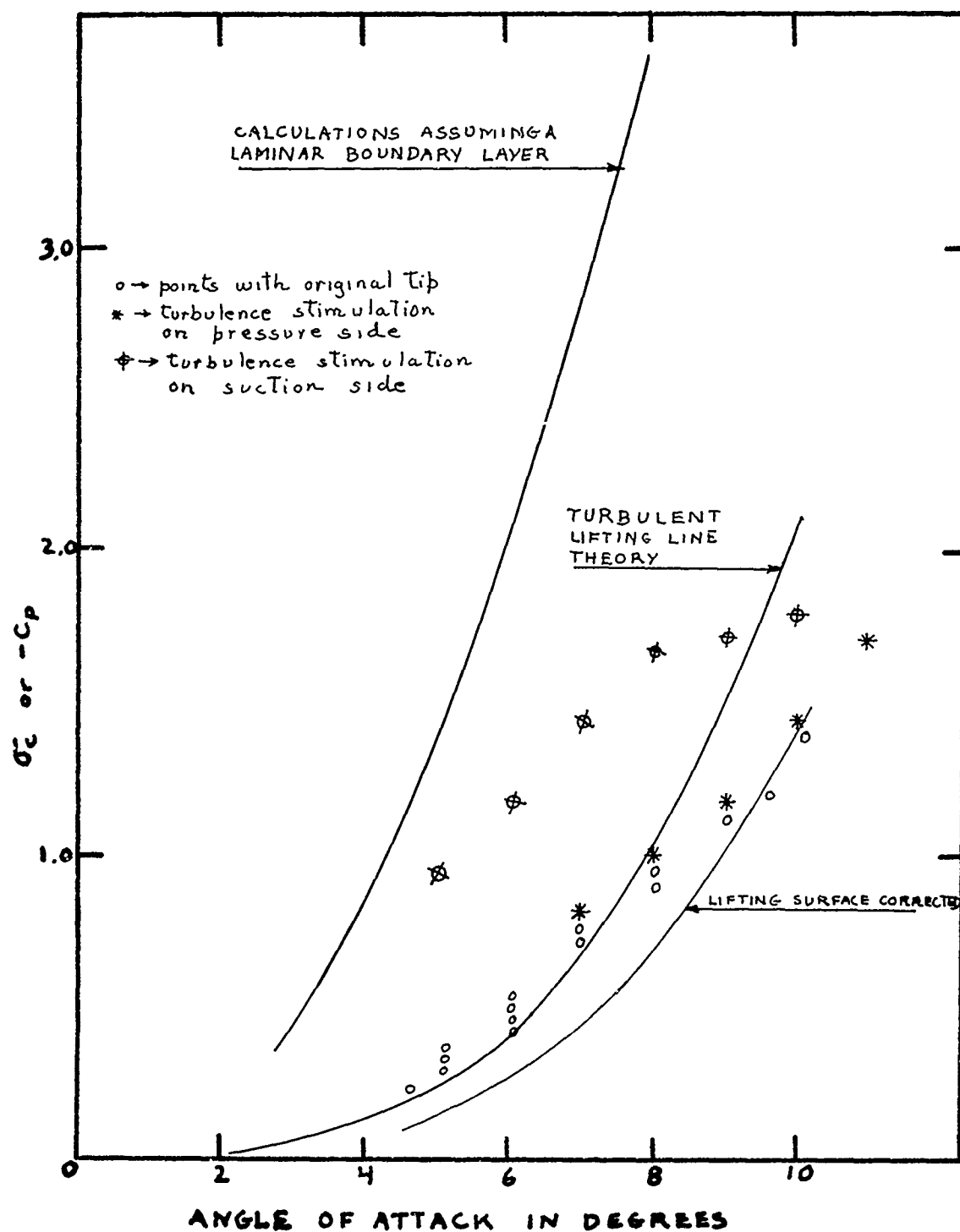


FIG. 4.6 Minimum pressure coefficient for the rudder model at tip vortex cavitation inception

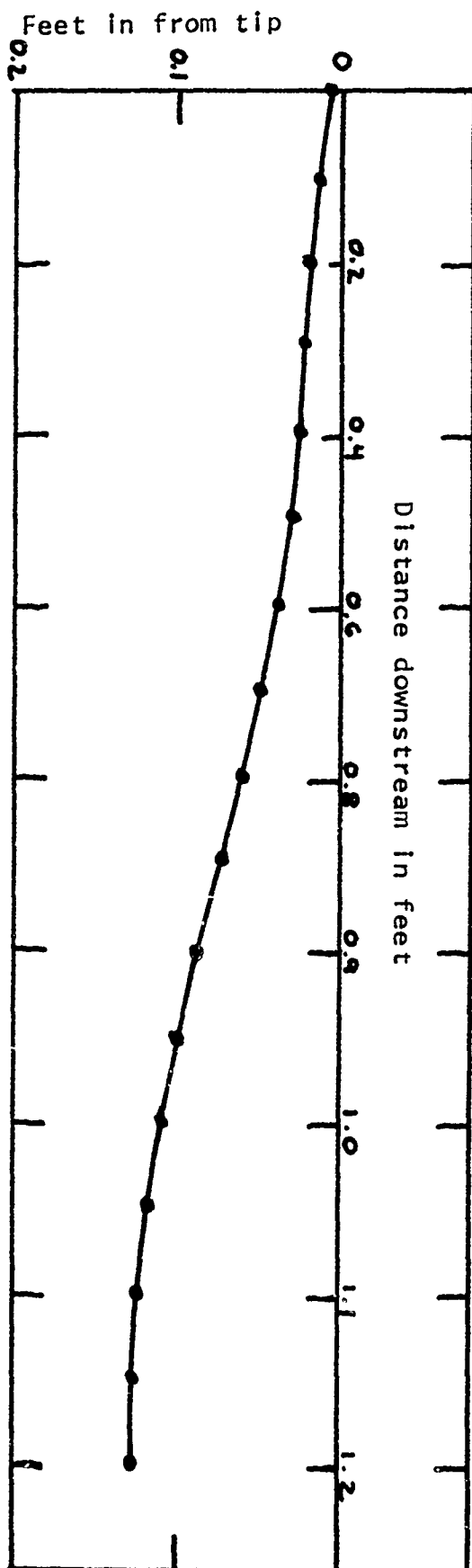


FIG. 4.7 Spanwise calculated trajectory of the tip vortex core for the rudder model at 8 degrees angle of attack and 25 ft./sec. water speed. The ordinate is distance from the tip. This calculation is for comparison to the photograph in Fig. 4.5.

CHAPTER V

If the wake configuration, induced velocities, and minimum pressures due to a lifting line wing can be calculated as in Chapter IV, there is no reason why the lifting line model of a propeller can not be handled in the same manner. The propeller is more difficult only in the sense that its geometry is cylindrical rather than flat and the discrete trailing vortex filaments will follow more or less helical paths rather than straight lines downstream as seen by an observer on a blade. If the trailing vortices had no effect on themselves, the axial velocity would be the forward velocity of the ship or the tunnel water speed in a propeller testing tunnel. The wake of the ship is neglected although modifications to include this are in the planning stage. The tangential velocity would be Ωr where Ω is the rotational speed of the propeller and r is the distance out from the shaft center. These axial and tangential velocities are augmented by the velocities induced by the trailing vortices from the blade under consideration and also to those shed from all other blades. It is also entirely possible that in the case of a heavily loaded propeller the radial induced velocities are important, especially in the determination of the roll up kinematics. The vortices shed from each of K blades, which are assumed to be similar, are assumed to travel in similar trajectories, so that only the position of one vortex sheet must be calculated.

The strip theory model is employed as in the wing model at downstream stations. The r and θ or equivalently Y and Z coordinates of the intersection of each trailer with the plane perpendicular to the X axis at x is calculated from positions at $x - \Delta x$ as before.

The only difference between this computation and that for the wing is that each trailing vortex is now assumed to travel in a helical trajectory rather than in a straight line downstream. The induced velocity at the vortices is only weakly dependent on the pitch angle of the helix and this is assumed to be constant for each vortex and of magnitude determined by moderately loaded lifting line propeller theory(16). The equations for the velocity induced at a point x, r, θ by a helical vortex of unit strength starting at ξ, ρ, ϕ are: (16)

$$\bar{u}_\theta = \frac{1}{4\pi R} \int_{\phi'=\phi}^{\infty} \frac{[\rho^2 - \rho r \cos(\phi' - \theta)] d\phi'}{[(x - \xi')^2 + r^2 + \rho^2 - 2r\rho \cos \phi']^{3/2}}$$

$$\bar{u}_r = \frac{1}{4\pi R} \int_{\phi'=\phi}^{\infty} \frac{[\pi(\rho) (r - \rho \cos(\phi' - \theta)) + (x - \xi') \rho \sin(\phi' - \theta)] d\phi'}{[(x - \xi')^2 + r^2 + \rho^2 - 2r\rho \cos \phi']^{3/2}}$$

$$\bar{u}_x = \frac{1}{4\pi R} \int_{\phi'=\phi}^{\infty} \frac{[\pi(\rho) \rho \sin(\phi' - \theta) + (x - \xi') \rho \cos(\phi' - \theta)] d\phi'}{[(x - \xi')^2 + r^2 + \rho^2 - 2r\rho \cos \phi']^{3/2}}$$

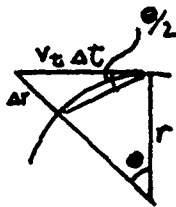
The basic difference between the propeller calculations and those for the foil is that these equations must be integrated to obtain the induced velocities at each vortex due to all the others rather than the comparatively simple equations for the velocity due to a straight line vortex. This is more a difficulty in computer time cost than mathematics. The method used was a five point Gauss integration performed over five intervals from 0 to 4380 degrees downstream.(16). The integrations are performed as if the trailer began at the downstream plane in question and extended from this plane to infinity downstream. This simplifies the calculations considerably since all integrations are performed over the same interval. The results are then multiplied by the factor analogous to that for the strip theory foil model on page 14 of Chapter 1:

$$1 + \frac{X}{\sqrt{X^2 + \Delta r^2}}$$

to retrieve the effect of the portion of the cause vortex extending from the plane being considered back upstream to the propeller plane. The geometry may perhaps best be visualized by reference to Figures (5.4), (5.5), and (5.6). The velocity induced by all the other blades on the sheet in question is calculated at the beginning of the program and assumed constant thereafter. A flow diagram for the calculation is shown in Figure (5.7).

The integration of the velocities at point X to obtain the new vortex positions at plane $X + \Delta X$ leads to difficulty in the propeller problem. The tangential velocities in a

propeller wake (as seen from a blade) are often four times the axial velocity. The integration of the Y,Z components of this tangential velocity can lead to a spiraling divergence from the correct radius. This effect is corrected by introducing the second order term in the numerical integration as a radial velocity as follows:



Δr is the error made in Δt sec. by using a first order numerical integration.

$$\begin{aligned} \Delta r^2 &= (V_t \Delta t)^2 + (2r \sin \frac{\theta}{2})^2 - 2V_t \Delta t \cdot 2r \sin \frac{\theta}{2} \cos \frac{\theta}{2} \\ \tan \theta &= V_t \Delta t / r, \text{ let this} = \eta \quad \left| \begin{aligned} \sin^2 \frac{\theta}{2} &= \frac{\theta^2}{4} - \frac{1}{3} \frac{\theta^4}{16} \dots = \frac{\eta^2}{4} - \frac{\eta^4}{6} \dots \\ \sin \theta &= \theta - \frac{\theta^3}{6} \dots = \eta - \frac{\eta^3}{3} - \frac{\eta^5}{6} \dots \\ \theta^2 &= (\eta^2 + \frac{2}{3} \eta^4) + \frac{1}{9} \eta^6 \dots \\ \theta^3 &= \eta^3 - \frac{1}{3} \eta^5 \dots \end{aligned} \right. \\ \theta^2 &= (\eta^2 + \frac{2}{3} \eta^4) + \frac{1}{9} \eta^6 \dots \\ \theta^3 &= \eta^3 - \frac{1}{3} \eta^5 \dots \end{aligned}$$

$$\Delta r^2 = r^2 \eta^2 + 4r^2 \left[\frac{\eta^2}{4} - \frac{2\eta^2}{12} \right] - 2\eta r^2 \left[\eta - \frac{\eta^3}{3} \right]$$

$$= r^2 \eta^2 + r^2 \eta^2 - \frac{2}{3} r^2 \eta^4 - 2r^2 \eta^2 + r^2 \eta^4$$

$$\therefore \Delta r = (1/\sqrt{3}) r \eta^2$$

$$\text{let } \Delta r = \Delta t [-V_{rs}]$$

$$V_{rs} = -\frac{1}{\sqrt{3}} V_t^2 \frac{\Delta t}{r}$$

Using this method, a calculation was made on a 20 foot diameter propeller with a elliptical loading along the span. The results of this calculation are shown in Fig. (5.1).

The calculated position of a trailing vortex sheet from a 10 foot radius 4 bladed propeller.

The hub radius is 2 feet

The loading is elliptical ($G=0.1\sin$)

The rotational velocity is 10 rad./sec.

The boundary layer thickness is assumed to be .05 ft.

The circles represent vortex positions. 19 are used with 5 in the fine spacing at the end and three in the core. Only the center of the core is plotted.

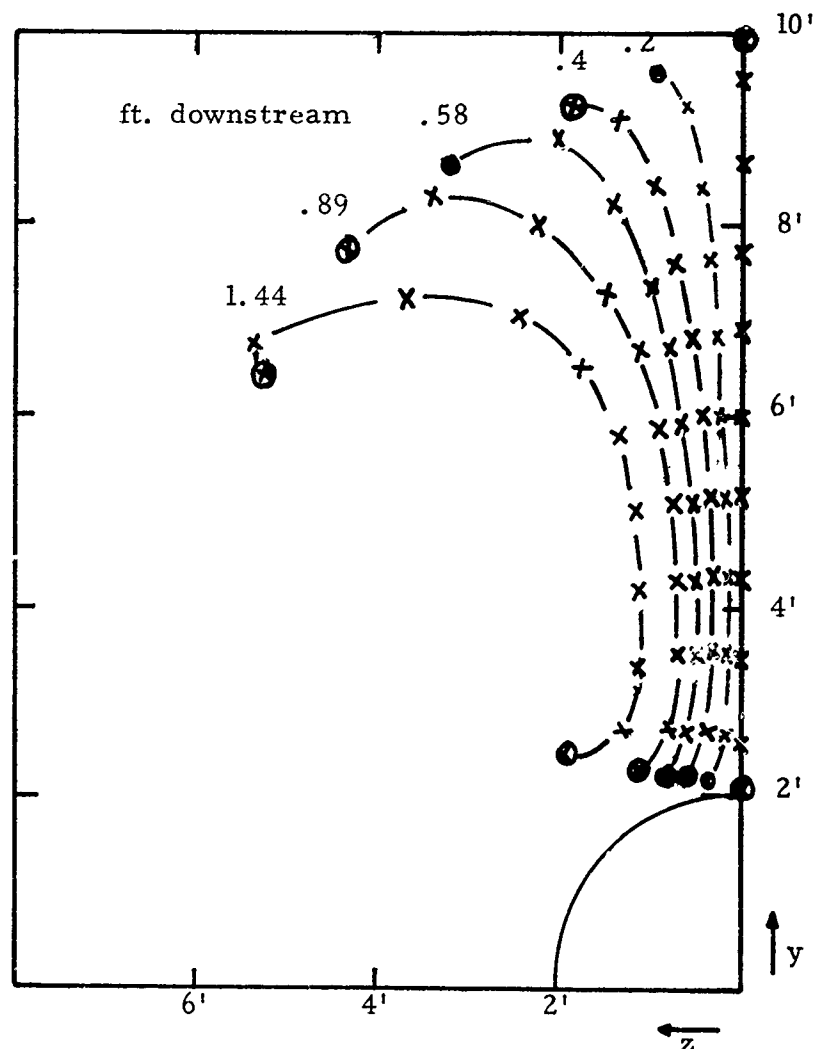


FIG. 5.1 PROPELLER VORTEX ROLLUP

The loading for this propeller was extreme ($G=.1\sin\Theta$) and the rollup is dramatic. The induced velocities for this propeller were calculated on the blade by calculating the velocity induced by each element of each vortex of the sheet being calculated on control points on each blade. The velocities induced by this sheet at a given radius on each blade are then summed to find the effect of all the sheets on a single blade. In Figures (5.2) and (5.3) the velocities induced by a blade with reasonable loading and those due to this extreme loading are plotted for comparison with the results from moderately loaded propeller theory as developed by Kerwin(16). It is observed that again this method gives a heavier loading at the tip than expected due to the fact that the downwash is negative at the tip, increasing the angle of attack. The results at the hub are doubtful since the effect of the hub itself is neglected. Work is in progress on a scheme to include the hub as a line sink. Since the propeller used as an example here is a purely hypothetical one, a purely hypothetical boundary layer thickness of .05 feet was assumed.

A check was made to compare the contraction of the tip vortex trajectory calculated by this method to the experimental results of Abraham (18). The results of this comparison are shown in Figure (5.8). Abraham photographed the tip vortex (which was visible due to tip vortex cavitation) and plotted its radial position as a function of distance downstream. His calculations for wake contraction,

also shown in Figure (5.8), did not agree well with experimental results but the present calculations agree quite well with the experiment. The inclusion of rollup of the trailing vortex sheet is apparently important in making this calculation.

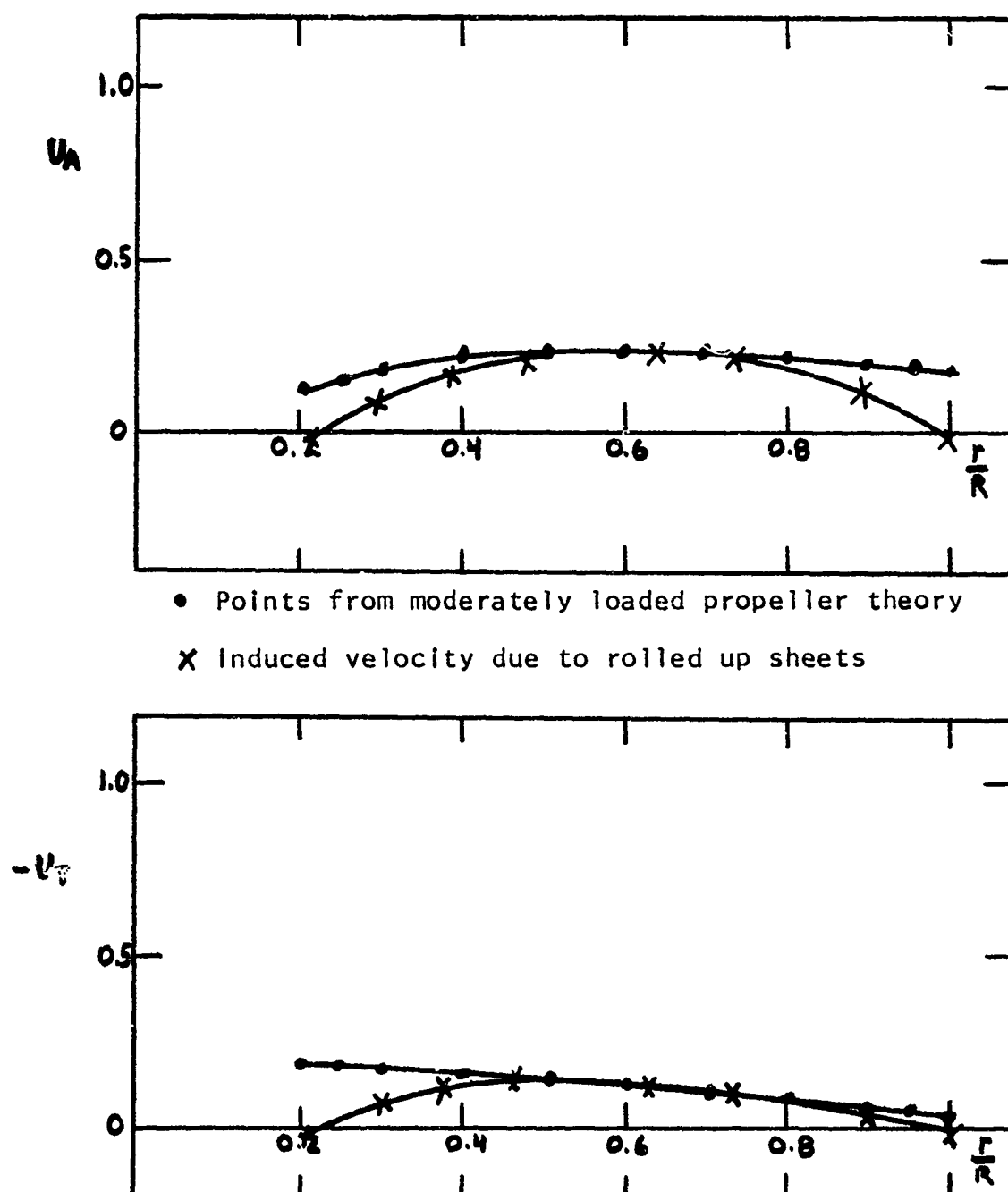


FIG. 5.2 A comparison of non dimensional axial and tangential velocities for a lightly loaded propeller using moderately loaded propeller theory and rolled up trailing vortex sheets.
 $G = 0.03 \sin \Theta$, Hub radius = $0.2R$

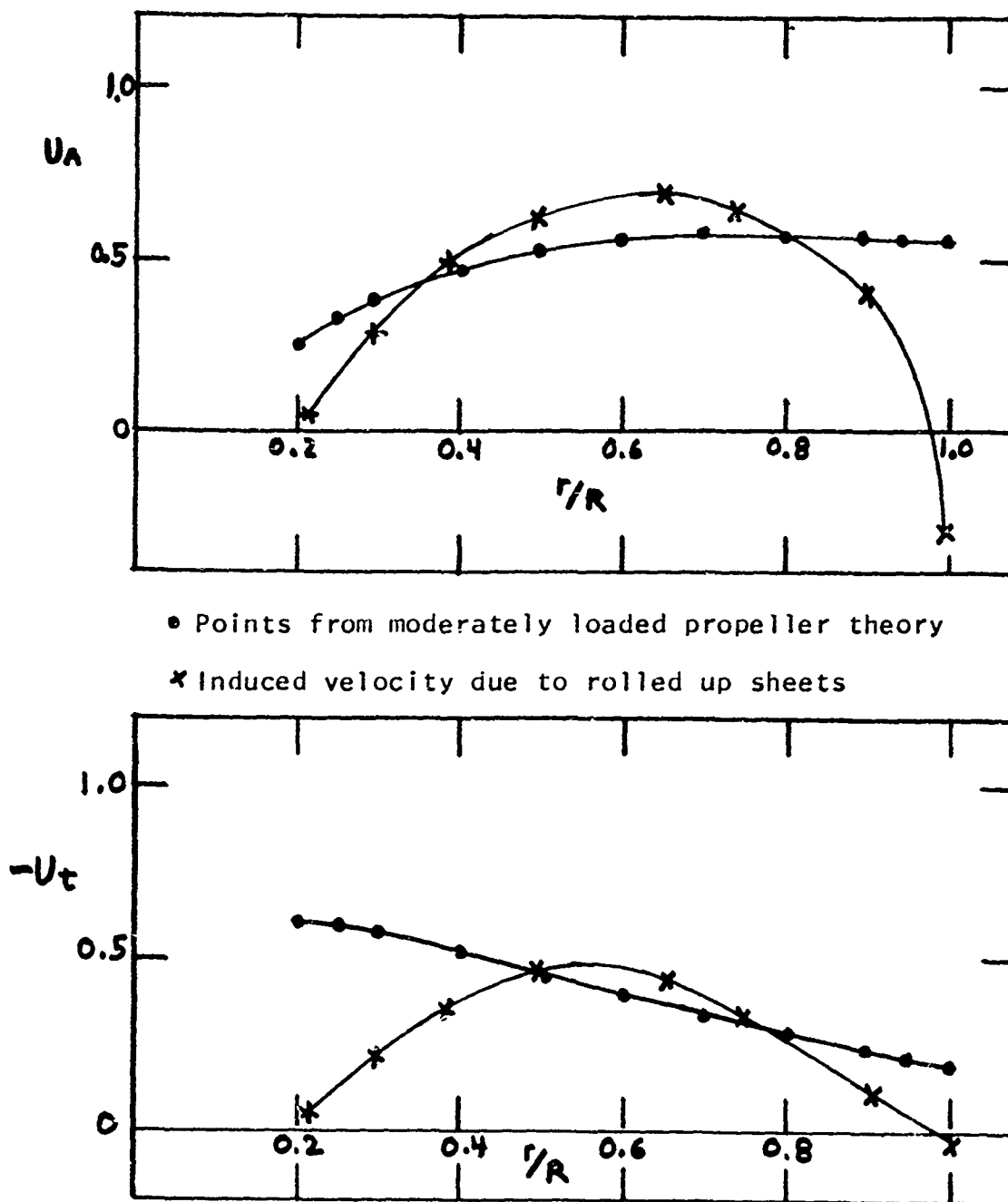
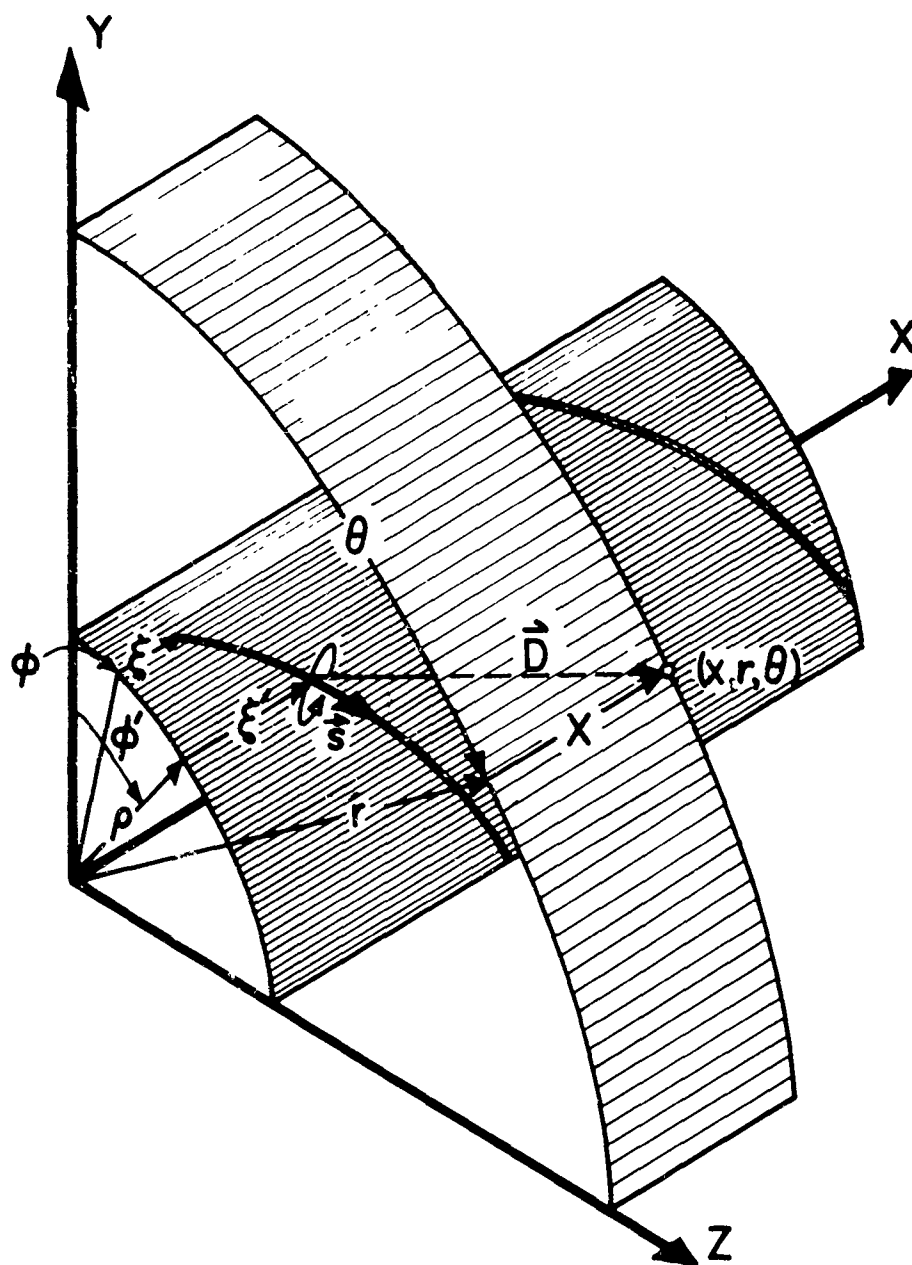
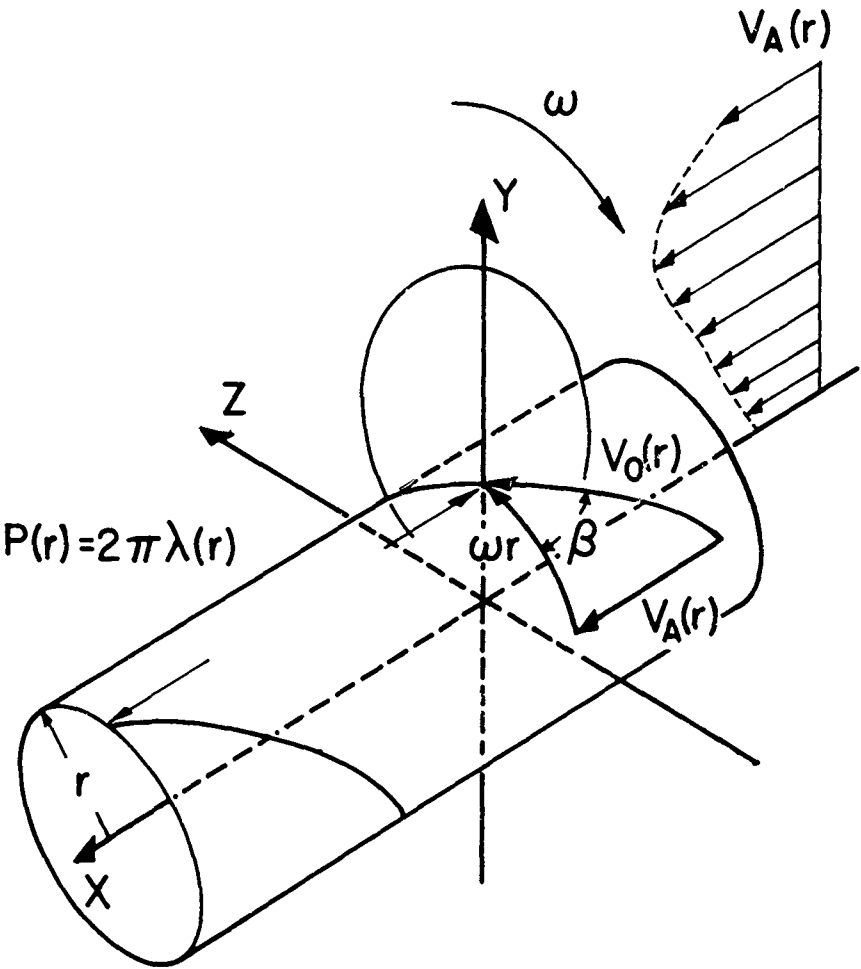


FIG. 5.3 A comparison of non dimensional axial and tangential velocities for a heavily loaded propeller using moderately loaded propeller theory and rolled up trailing vortex sheets.
 $G = 0.1 \sin \theta$, Hub radius $= 0.2 R$



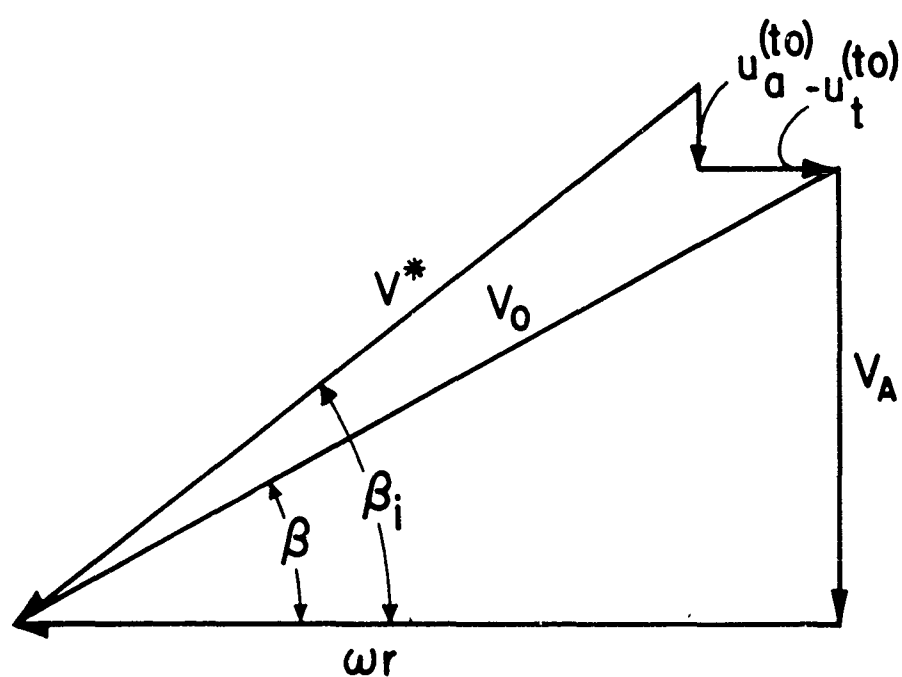
NOTATION FOR VELOCITY AT
 (x, r, θ) INDUCED BY AN ELEMENT
 OF A TRAILER AT (ξ', ρ, ϕ) . THE
 TRAILER ORIGINATES AT (ξ, ρ, ϕ) .

FIGURE 5.4



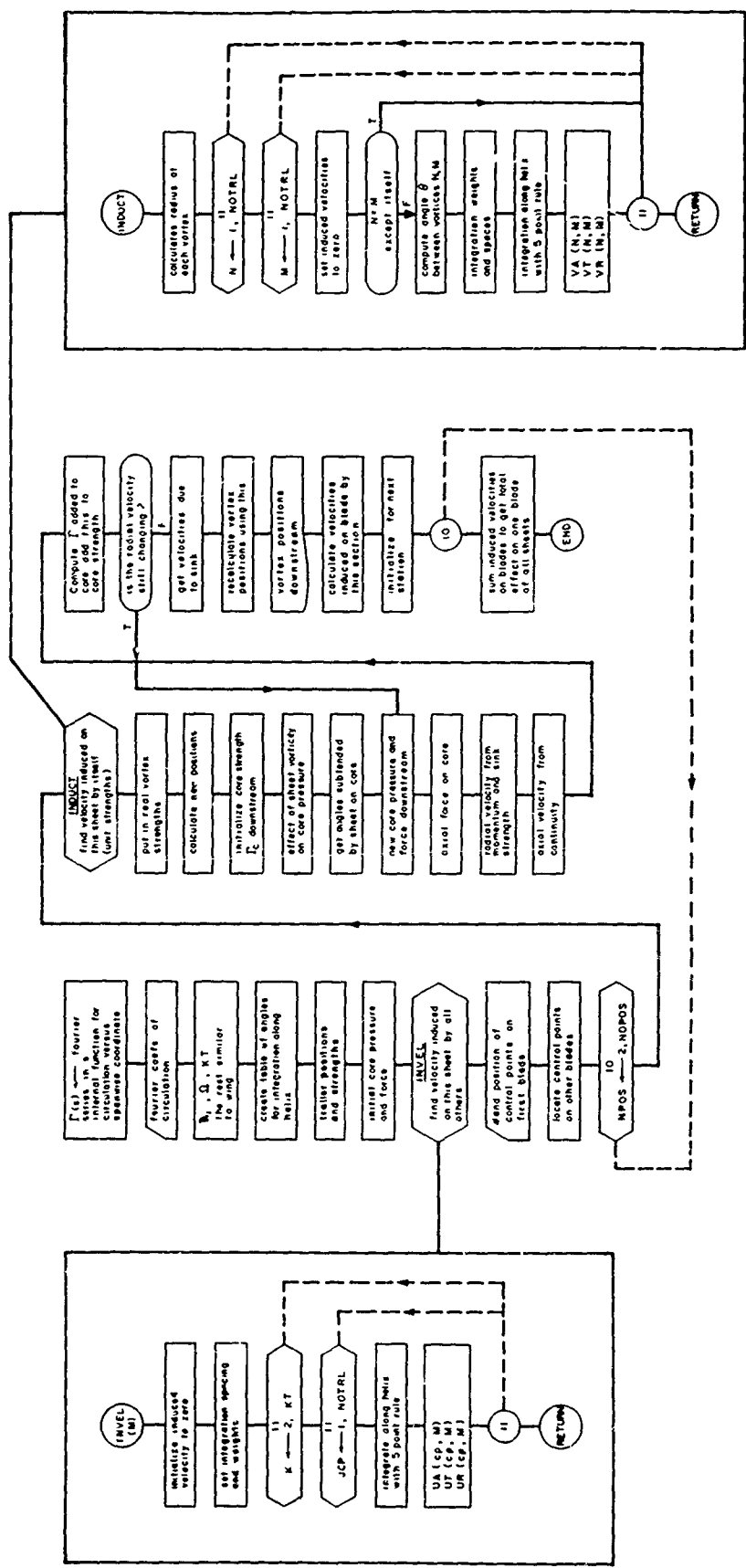
APPROACH FLOW VELOCITY
DIAGRAM

FIGURE 5.5



VELOCITY DIAGRAM AT A
LIFTING LINE

FIGURE 5.6



SUBROUTINE INVEL FINDS THE INDUCED VELOCITY AT EACH VORTEX ON THE SHEET DUE TO CAUSE VORTEX M ON THE OTHER SHEETS ASSUMING M IS OF UNIT STRENGTH.

MAIN PROGRAM CALCULATES THE MOTION AND CORE DYNAMICS OF THE TRAILING VORTEX SHEET FROM ONE BLADE. CALCULATES THE VELOCITIES INDUCED BY THIS SHEET ON ALL BLADES AND SUMS THESE TO FIND THE TOTAL VELOCITY INDUCED ON ONE BLADE.

SUBROUTINE INDUC FINDS THE INDUCED VELOCITY AT EACH VORTEX ON THE SHEET DUE TO ALL OTHERS ON THE SAME SHEET. IT ASSUMES UNIT STRENGTH OF ALL VORTICES.

FIG.5.7 LOGIC FLOW CHART FOR THE LIFTING LINE PROPELLER CALCULATIONS DESCRIBED IN CHAPTER 5.

CHARACTERISTICS OF MODEL PROPELLER TESTED BY ABRAHAM

SEE REF. (18)

Hub radius	.1 ft.	Water speed	13.35 ft./sec.
Propeller radius	.5 ft.	Revs./sec.	16.68
T_c	.301	4 Blades	

A comparison of the tip vortex radial contraction observed by Abraham, his calculated trajectory using Kerwin's field point velocity program, and results from the present program appear below:

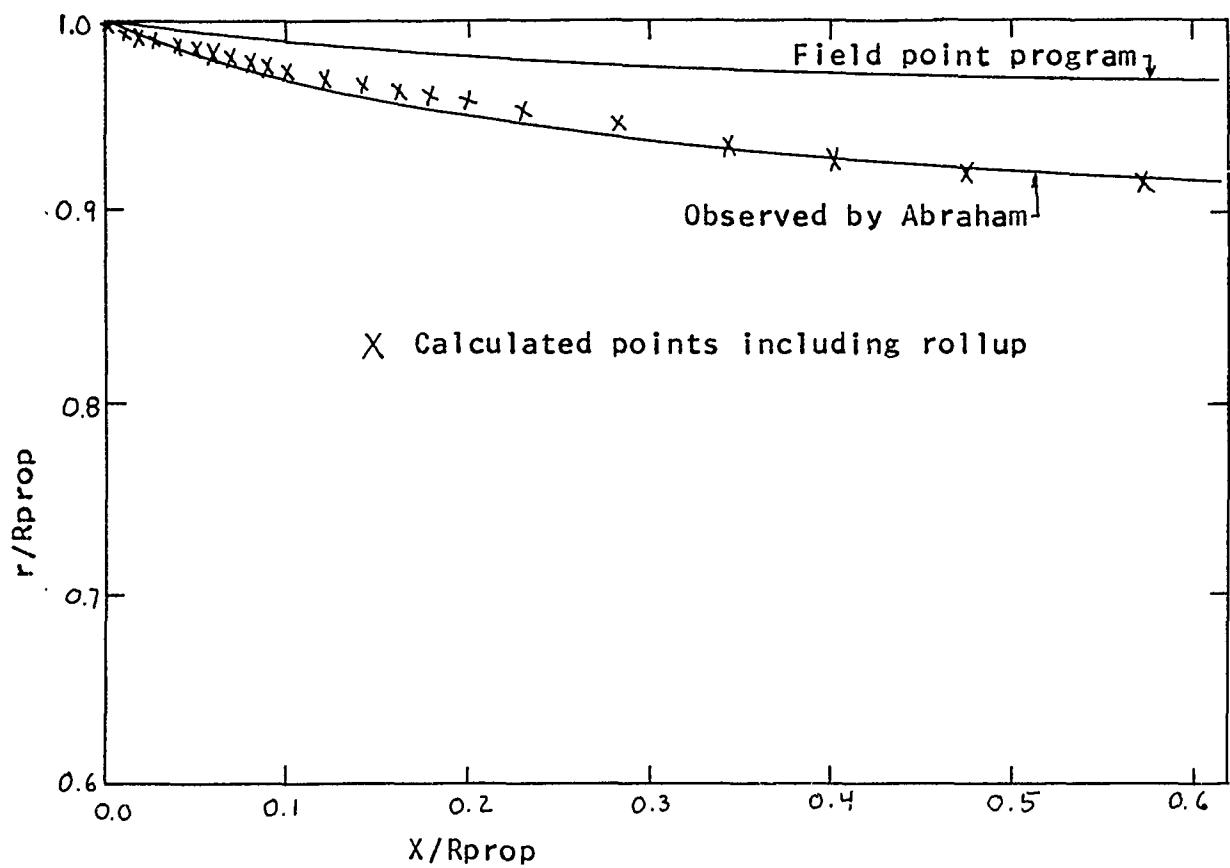


FIG. 5.8 A COMPARISON OF RESULTS FOR THE CONTRACTION OF A TIP VORTEX SHED FROM A MODEL PROPELLER

CHAPTER VI

CONCLUSIONS

It has been shown that the trailing vortex sheet problem may be solved numerically for an elliptically loaded foil and the singularity at the end of the vortex sheet in the potential flow problem may be dealt with by resorting to an inner solution employing boundary layer theory at the tip of the foil. The model, although crude, predicts both the minimum pressure in the tip vortex core and the motions of the sheet with reasonable accuracy. The use of a strip theory model shortens the computation time to the point where the method may be of practical use.

The lifting line propeller problem is solved for the downwash on the lifting line and the kinematics of the trailing vortex sheet as a direct application of the foil solution, a rotation of the coordinate system and the inclusion of the effect of other sheets from the rest of the blades being the only modifications necessary.

It is indicated that the velocities induced by the trailing vortex system on the blades, particularly at the tip, may be quite different from those predicted by moderately loaded propeller theory. This may lead to a load distribution on the blades which differs considerably from that predicted. Work is in progress on the inclusion of the lifting line model in the lifting surface propeller design method described by Kerwin (17).

REFERENCES

1. Westwater, F.L., "Rolling Up of the Surface of Discontinuity Behind an Airfoil of Finite Span", British ARC, R&M 1692, 1935
2. Prandtl, L., "Tragflugeltheorie", I Mitt., Gottingen Nachrichten, 1918, s. 451-477. See also Alexander, R.C., "Self Similar Hydrodynamics with Vortex Sheets" AD 620-323
3. Kaden. See Ref. (6)
4. Batchelor, G.K., "AN INTRODUCTION TO FLUID DYNAMICS", Cambridge University Press, 1967
5. Monacella, V.J., "On Ignoring the Singularity in the Numerical Evaluation of Cauchy Principal Value Integrals", David Taylor Model Basin Report 2356, Feb. 1967
6. Spreiter, J.R., and Sacks, A.H., "The Rolling Up of the Trailing Vortex Sheet and its Effect on Downwash Behind Wings", Journal of the Aeronautical Sciences, vol. 18, 1951, pp. 21-32. 72
7. McCormick, B.W. Jr., "On Cavitation Produced by a Vortex Trailing from a Lifting Surface", Journal of Basic Engineering, Sept. 1962, pp. 369
8. Batchelor, G.K., "Axial Flow in Trailing Line Vortices", Journal of Fluid Mech. (1964). vol. 20, part 3, pp. 645-658
9. McMahon, T.A. and Widnall, S.E., "Vortex Wake Rollup and Vorticity Concentration Behind an Airfoil", ASRL TR 143-1, June 1967
10. Abbott, I.H., and Von Doenhoff, A.E., "Theory of Wing Sections", Dover Publications Inc., New York, N.Y., 1959
11. Milgram, Jerome, "Aerodynamics of Sails, 7th Symposium on Naval Hydrodynamics, Aug. 1968
12. Truckenbrodt, E., "A Method of Quadrature for Calculation of the Laminar and Turbulent Boundary Layer in case of Plane and Rotationally Symmetrical Flow", NACA TM, 1379, May 1955
13. Spence, D.A., "The Development of Turbulent Boundary Layers", JAS, vol. 23 No 1
14. Ludwig and Tillmann, "Investigation of the Wall Shearing Stress in Turbulent Boundary Layers", NACA TM, 1285, 1950

15. Ashley, Landau, and Widnall, "New Directions in Lifting Surface Theory" AIAA Journal Jan. 1965

16. Kerwin, J.E., "Linearized Theory for Propellers in Steady Flow ", David Taylor Model Basin Report, July 1963

17. Kerwin, J.E., "A Design Theory for Subcavitating Propellers ", SNAME Transactions 1964

18. Abraham, M., "Theoretical and experimental correction of streamlines in the race of a marine propeller", SM Thesis, Department of Naval Architecture and Marine Engineering, MIT, 1965

APPENDIX

COMPUTER PROGRAMS

INTRODUCTION

The programs used in this work are listed in this appendix. They are written in the FORTRAN IV language with the exception of Professor Milgram's boundary layer programs which are written in the MAD language for the M.I.T. Time Sharing System. Flow charts are included for those programs which were not flow charted in the main text.

METHOD 1 COMPUTER PROGRAM

This program is the iterative solution for the position of the trailing vortex sheet. A flow chart is shown in Figure (A1). This program uses a tremendous amount of computer time unnecessarily and it is hoped that it will never be run again. A listing of the source program is shown in Figure (A2). Sample results are shown in Figure (1.2) of the main text.

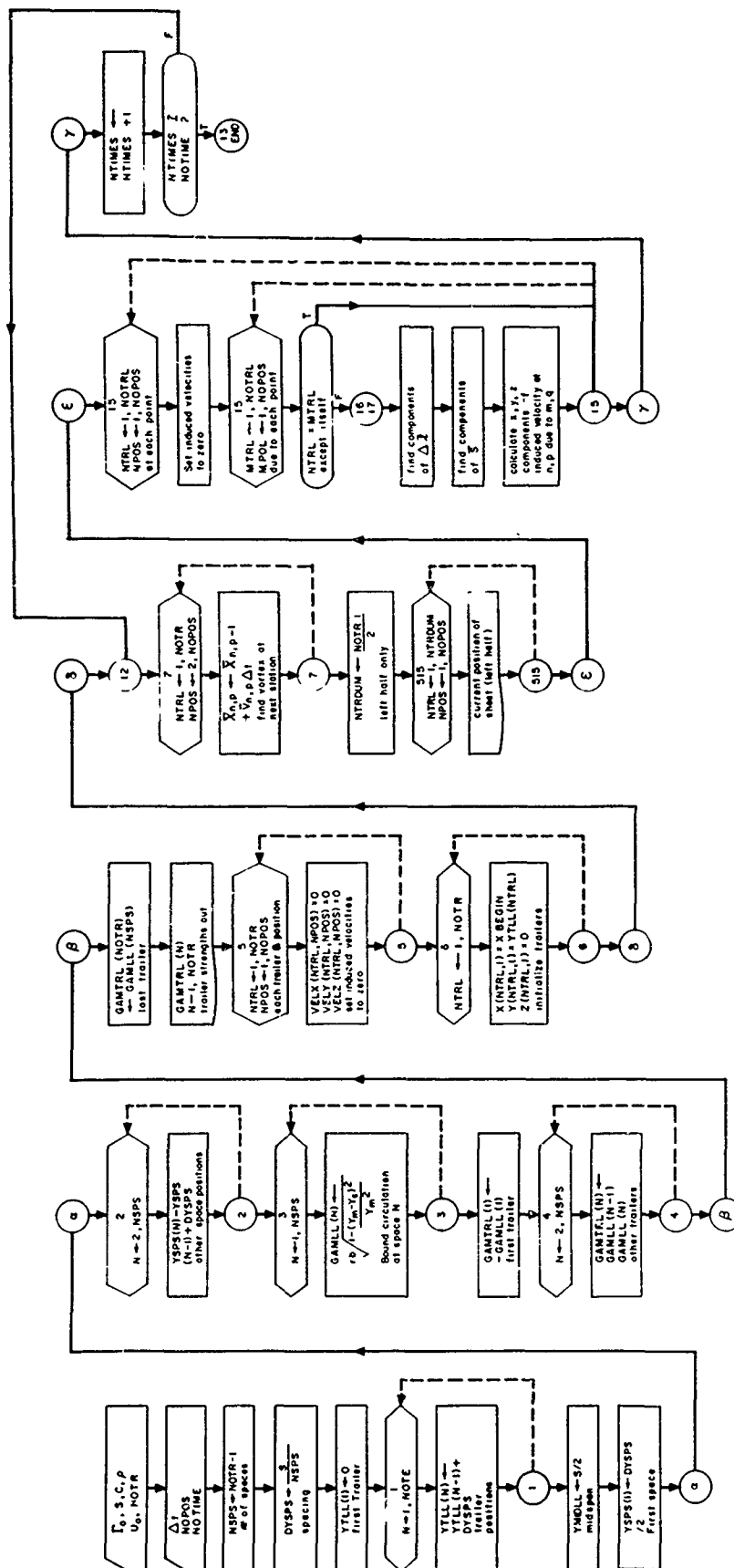
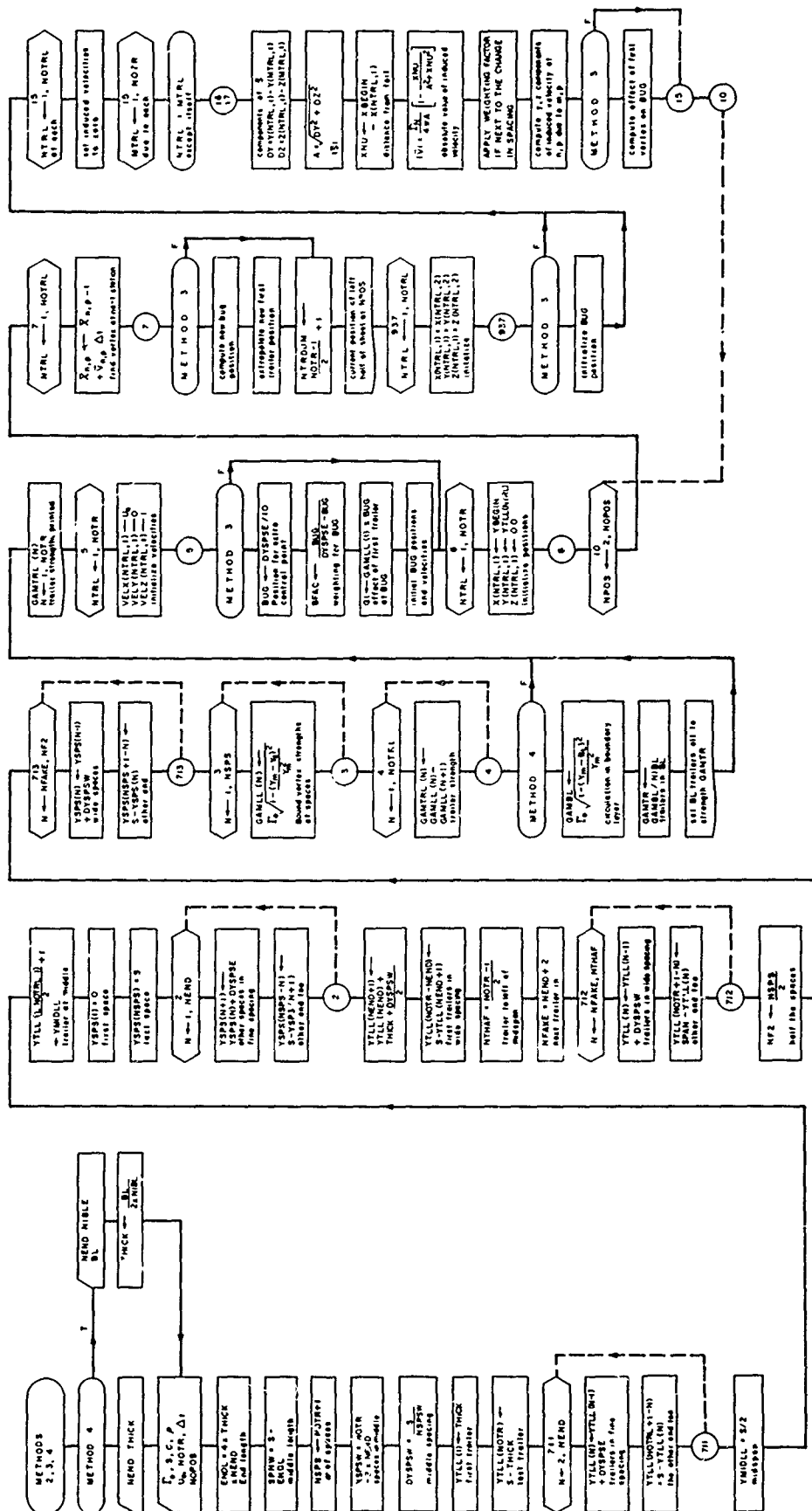


FIG. A1 LOGIC FLOW GRAPH FOR METHOD 1 OF CHAPTER 1. A STRAIGHT LIFTING LINE WITH ELLIPTICAL LOAD DISTRIBUTION IS ASSUMED

METHODS 2,3,4 COMPUTER PROGRAMS

These programs for strip theory models of the trailing vortex sheet from an elliptically loaded lifting line differ from each other only in minor details as indicated by the flow chart in Figure (A3). A listing of the Method 4 program is shown in Figure (A4). Sample results are given in Figure (A5).



FINAL COMPUTER PROGRAM FOR A LIFTING LINE FOIL

This program includes a sink at the tip vortex core center and calculates minimum pressures as well as motions of the sheet. At each interval downstream the velocity induced by each vortex element on selected control points on the blade is calculated for eventual inclusion in a lifting surface method. A flow chart was given in the main text (Fig. 3.1). A listing of the source program is given in Figure (A6) and sample output in (A7).

FIG.A6 SOURCE PROGRAM FOR A STRAIGHT FOIL. The load is assumed elliptic in form of strength Γ_0 . The motions and minimum pressures in the trailing vortex sheet are calculated including source type flow into the core. Induced velocities back on the foil are also calculated.

NOT REPRODUCIBLE

1	2	1	0.0375	1.00
2	3	2	0.0625	1.00
3	7	3	0.0625	1.00
4	7	4	0.0625	1.00
5	6	5	0.0625	1.00
6	2	6	0.0625	1.00
7	2	7	0.0625	1.00
8	2	8	0.0625	1.00
9	2	9	0.0625	1.00
10	2	10	0.0625	1.00
11	3	11	0.0625	1.00
12	2	12	0.0625	1.00
13	2	13	0.0625	1.00
14	2	14	0.0625	1.00
15	2	15	0.0625	1.00
16	2	16	0.0625	1.00
17	2	17	0.0625	1.00
18	2	18	0.0625	1.00
19	2	19	0.0625	1.00
20	2	20	0.0625	1.00
21	2	21	0.0625	1.00
22	2	22	0.0625	1.00

2 42	1.24700	0.0000
2 42	1.24700	0.0000
3 42	1.24699	0.0000
4 42	1.24698	0.0000
5 42	1.24697	0.0000
6 42	1.24696	0.0000
7 42	1.24695	0.0000
8 42	1.24694	0.0000
9 42	1.24693	0.0000
10 42	1.24692	0.0000
11 42	1.24691	0.0000
12 42	1.24690	0.0000
13 42	1.24689	0.0000
14 42	1.24688	0.0000
15 42	1.24687	0.0000
16 42	1.24686	0.0000
17 42	1.24685	0.0000
18 42	1.24684	0.0000
19 42	1.24683	0.0000
20 42	1.24682	0.0000
21 42	1.24681	0.0000
22 42	1.24680	0.0000
23 42	1.24679	0.0000
24 42	1.24678	0.0000
1 43	1.24678	0.0000
2 43	1.24679	0.0000
3 43	1.24680	0.0000
4 43	1.24681	0.0000
5 43	1.24682	0.0000
6 43	1.24683	0.0000
7 43	1.24684	0.0000
8 43	1.24685	0.0000
9 43	1.24686	0.0000
10 43	1.24687	0.0000
11 43	1.24688	0.0000
12 43	1.24689	0.0000
13 43	1.24690	0.0000
14 43	1.24691	0.0000
15 43	1.24692	0.0000
16 43	1.24693	0.0000
17 43	1.24694	0.0000
18 43	1.24695	0.0000
19 43	1.24696	0.0000
20 43	1.24697	0.0000
21 43	1.24698	0.0000
22 43	1.24699	0.0000
23 43	1.24700	0.0000
24 43	1.24700	0.0000
1 44	1.246999	0.0000
2 44	1.246999	0.0000
3 44	1.246999	0.0000
4 44	1.246999	0.0000
5 44	1.246999	0.0000
6 44	1.246999	0.0000
7 44	1.246999	0.0000
8 44	1.246999	0.0000
9 44	1.246999	0.0000
10 44	1.246999	0.0000
11 44	1.246999	0.0000
12 44	1.246999	0.0000
13 44	1.246999	0.0000
14 44	1.246999	0.0000
15 44	1.246999	0.0000
16 44	1.246999	0.0000
17 44	1.246999	0.0000
18 44	1.246999	0.0000
19 44	1.246999	0.0000
20 44	1.246999	0.0000
21 44	1.246999	0.0000
22 44	1.246999	0.0000
23 44	1.246999	0.0000
24 44	1.246999	0.0000

CA 指数	CA 指数	CA 指数	CA 指数	CA 指数
-0.19799	-0.19799	-0.19799	-0.19799	-0.19799
-0.19799	-0.19799	-0.19799	-0.19799	-0.19799
0.19799	0.19799	0.19799	0.19799	0.19799
0.19799	0.19799	0.19799	0.19799	0.19799

CONF PRESSURE=	-712.717295	FORCE UN	UPSTEIN EN=	-6.176161
1	0.0	0.00133	0.0	0.0
2	1	0.0	0.01000	0.0
3	1	0.0	0.00500	0.0
4	1	0.0	0.00133	0.0
5	1	0.0	0.01000	0.0
6	1	0.0	0.14676	0.0
7	1	0.0	0.35556	0.0
8	1	0.0	0.57617	0.0
9	1	0.0	0.78119	0.0
10	1	0.0	1.00000	0.0
1	2	0.05900	0.00133	0.01901
2	2	0.01000	0.01000	0.00500
3	2	0.01000	0.01000	0.00500
4	2	0.05000	0.01000	-0.01013
5	2	0.05000	0.01000	-0.01261
6	2	0.05000	0.00500	-0.01409
7	2	0.05000	0.35556	-0.00701
8	2	0.05000	0.57617	-0.00272
9	2	0.05000	0.78119	-0.00162
10	2	0.05000	1.00000	-0.00142
11	3	0.05000	1.21261	-0.00701
12	3	0.05000	1.00000	-0.00727
13	3	0.05000	1.00000	-0.00727
14	3	0.05000	1.00000	-0.00727
15	3	0.05000	1.00000	-0.00727
16	3	0.05000	1.00000	-0.00727
17	3	0.05000	1.00000	-0.00727
18	3	0.05000	1.00000	-0.00727
19	3	0.05000	1.00000	-0.00727
20	3	0.05000	1.00000	-0.00727

[illegible][illegible]

FIG.A5 SAMPLE OUTPUT FROM
METHOD 4

FIG.A7 SAMPLE OUTPUT FROM
AN ELLIPTICAL LOADING
USING THE LINE SINK OF
CHAPTER 3

NOT REPRODUCIBLE

LIFTING LINE PROPELLER PROGRAM

This is the final program for propeller design purposes. An input form is shown in Figure (A8) to simplify use. The Fourier series coefficient of the load distribution are the coefficients in the following series for the circulation on the lifting line.

$$G(\theta) = K \left[A \cos\left(\frac{\theta}{2}\right) + \sum_{n=1}^4 B_n \sin(n\theta) \right]$$

$$\theta = \frac{r - R_{hub}}{SPAN} * \pi$$

where

$$K = 2\pi R U_0$$

$$SPAN = R - R_{hub}$$

This allows the application of this method to other than elliptical load distributions. The rest of the input quantities are straightforward. A flow chart was given in the main text (Fig. 5.7). The main source program is listed in Figure (A9) and the two subroutines INVEL and INDUCT which integrate along helices for the effect of the other trailing vortex sheets and the other vortices on the sheet being considered respectively are shown in Figure (A10). The output is of the same form as for the foil problem.

LIFTING LINE PROPELLER TIP VORTEX MINIMUM PRESSURE AND INDUCED VELOCITY
CALCULATION INPUT FORM

FOURIER COEFS OF LOAD DISTRIBUTION (5 MAXIMUM)

1	2	3	4	5	6	7	8	9	10	11	12	13	14	15	16	17	18	19	20	21	22	23	24	25	26	27	28	29	30	31	32	33	34	35	36	37	38	39	40	41	42	43	44	45	46	47	48	49	50
---	---	---	---	---	---	---	---	---	----	----	----	----	----	----	----	----	----	----	----	----	----	----	----	----	----	----	----	----	----	----	----	----	----	----	----	----	----	----	----	----	----	----	----	----	----	----	----	----	----

ASSUMED ADVANCE COEF μ 1 20 ROTATIONAL VELOCITY IN RAD/SEC

1	2	3	4	5	6	7	8	9	10	11	12	13	14	15	16	17	18	19	20	21	22	23	24	25	26	27	28	29	30	31	32	33	34	35	36	37	38	39	40	41	42	43	44	45	46	47	48	49	50
---	---	---	---	---	---	---	---	---	----	----	----	----	----	----	----	----	----	----	----	----	----	----	----	----	----	----	----	----	----	----	----	----	----	----	----	----	----	----	----	----	----	----	----	----	----	----	----	----	----

NUMBER OF TRAILERS IN FINE SPACING (ODD NUMBER)

NUMBER OF TRAILERS IN BOUNDARY LAYER (ODD NUMBER)

BL THICKNESS

PRESSURE AT INFINITY (LEAVE BLANK NORMAL MODE)

1	2	3	4	5	6	7	8	9	10	11	12	13	14	15	16	17	18	19	20	21	22	23	24	25	26	27	28	29	30	31	32	33	34	35	36	37	38	39	40	41	42	43	44	45	46	47	48	49	50
---	---	---	---	---	---	---	---	---	----	----	----	----	----	----	----	----	----	----	----	----	----	----	----	----	----	----	----	----	----	----	----	----	----	----	----	----	----	----	----	----	----	----	----	----	----	----	----	----	----

FOLLOWING IN FEET

HUB RADIUS SPAN PROP RADIUS WATER DENSITY SHIP SPEED (FT./SEC)

1	2	3	4	5	6	7	8	9	10	11	12	13	14	15	16	17	18	19	20	21	22	23	24	25	26	27	28	29	30	31	32	33	34	35	36	37	38	39	40	41	42	43	44	45	46	47	48	49	50
---	---	---	---	---	---	---	---	---	----	----	----	----	----	----	----	----	----	----	----	----	----	----	----	----	----	----	----	----	----	----	----	----	----	----	----	----	----	----	----	----	----	----	----	----	----	----	----	----	----

NUMBER OF TRAILERS (ODD NUMBER)

ΔX NUMBER OF DOWNSTREAM STATIONS

NUMBER OF BLADES (MAX 6)

1	2	3	4	5	6	7	8	9	10	11	12	13	14	15	16	17	18	19	20	21	22	23	24	25	26	27	28	29	30	31	32	33	34	35	36	37	38	39	40	41	42	43	44	45	46	47	48	49	50
---	---	---	---	---	---	---	---	---	----	----	----	----	----	----	----	----	----	----	----	----	----	----	----	----	----	----	----	----	----	----	----	----	----	----	----	----	----	----	----	----	----	----	----	----	----	----	----	----	----

TOTAL NUMBER OF CONTROL POINTS ON BLADE (MAX 10)

CONTROL POINT SPACES (AT WHICH SPACES DO YOU WANT THE INDUCED VELOCITY ?) (MAX 10)

1	2	3	4	5	6	7	8	9	10	11	12	13	14	15	16	17	18	19	20	21	22	23	24	25	26	27	28	29	30	31	32	33	34	35	36	37	38	39	40	41	42	43	44	45	46	47	48	49	50
---	---	---	---	---	---	---	---	---	----	----	----	----	----	----	----	----	----	----	----	----	----	----	----	----	----	----	----	----	----	----	----	----	----	----	----	----	----	----	----	----	----	----	----	----	----	----	----	----	----

FIG. A8

[illegible]

FIG. A9

NOT REPRODUCIBLE

```

1010 Y=VAMP+VAVU(NTRL,HTL)=CUTSPSE+DTPSP/2./DTPSPSE
1011 V=YAMP+VIVU(NTRL,HTL)=CUTSPA+CUTSP/2./DTPSPA
1012 V=YAMP+VAVU(NTRL,HTL)=CUTSPA+CUTSP/2./DTPSPA
1013 GO TO 818
1014 CONTINUE
1015 IF (HTL=INTL+MEMO) 816,825,826
1016 IF (HTL=INTL+MEMO) 817,826,826
1017 Y=VAMP+VAVU(NTRL,HTL)=CUTSPA+CUTSP/2./DTPSPA
1018 V=YAMP+VIVU(NTRL,HTL)=CUTSPA+CUTSP/2./DTPSPA
1019 V=YAMP+VAVU(NTRL,HTL)=CUTSPA+CUTSP/2./DTPSPA
1020 GO TO 818
1021 CONTINUE
1022 IF (HTL=INTL+MEMO) 820,829,828
1023 IF (HTL=INTL+MEMO) 820,829,828
1024 Y=VAMP+VAVU(NTRL,HTL)=CUTSPA+CUTSP/2./DTPSPA
1025 V=YAMP+VIVU(NTRL,HTL)=CUTSPA+CUTSP/2./DTPSPA
1026 V=YAMP+VAVU(NTRL,HTL)=CUTSPA+CUTSP/2./DTPSPA
1027 GO TO 818
1028 Y=VAMP+VAVU(NTRL,HTL)=CUTSPA+CUTSP/2./DTPSPA
1029 V=YAMP+VIVU(NTRL,HTL)=CUTSPA+CUTSP/2./DTPSPA
1030 V=YAMP+VAVU(NTRL,HTL)=CUTSPA+CUTSP/2./DTPSPA
1031 VEL(HTL,1)=VEL(HTL,1)+V
1032 VEL(HTL,2)=VEL(HTL,2)+V
1033 VEL(HTL,3)=VEL(HTL,3)+V
1034 VEL(HTL,4)=VEL(HTL,4)+V
1035 VEL(HTL,5)=VEL(HTL,5)+V
1036 VEL(HTL,6)=VEL(HTL,6)+V
1037 VEL(HTL,7)=VEL(HTL,7)+V
1038 VEL(HTL,8)=VEL(HTL,8)+V
1039 VEL(HTL,9)=VEL(HTL,9)+V
1040 VEL(HTL,10)=VEL(HTL,10)+V
1041 VEL(HTL,11)=VEL(HTL,11)+V
1042 VEL(HTL,12)=VEL(HTL,12)+V
1043 VEL(HTL,13)=VEL(HTL,13)+V
1044 VEL(HTL,14)=VEL(HTL,14)+V
1045 VEL(HTL,15)=VEL(HTL,15)+V
1046 VEL(HTL,16)=VEL(HTL,16)+V
1047 VEL(HTL,17)=VEL(HTL,17)+V
1048 VEL(HTL,18)=VEL(HTL,18)+V
1049 VEL(HTL,19)=VEL(HTL,19)+V
1050 VEL(HTL,20)=VEL(HTL,20)+V
1051 VEL(HTL,21)=VEL(HTL,21)+V
1052 VEL(HTL,22)=VEL(HTL,22)+V
1053 VEL(HTL,23)=VEL(HTL,23)+V
1054 VEL(HTL,24)=VEL(HTL,24)+V
1055 VEL(HTL,25)=VEL(HTL,25)+V
1056 VEL(HTL,26)=VEL(HTL,26)+V
1057 VEL(HTL,27)=VEL(HTL,27)+V
1058 VEL(HTL,28)=VEL(HTL,28)+V
1059 VEL(HTL,29)=VEL(HTL,29)+V
1060 VEL(HTL,30)=VEL(HTL,30)+V
1061 VEL(HTL,31)=VEL(HTL,31)+V
1062 VEL(HTL,32)=VEL(HTL,32)+V
1063 VEL(HTL,33)=VEL(HTL,33)+V
1064 VEL(HTL,34)=VEL(HTL,34)+V
1065 VEL(HTL,35)=VEL(HTL,35)+V
1066 VEL(HTL,36)=VEL(HTL,36)+V
1067 VEL(HTL,37)=VEL(HTL,37)+V
1068 VEL(HTL,38)=VEL(HTL,38)+V
1069 VEL(HTL,39)=VEL(HTL,39)+V
1070 VEL(HTL,40)=VEL(HTL,40)+V
1071 VEL(HTL,41)=VEL(HTL,41)+V
1072 VEL(HTL,42)=VEL(HTL,42)+V
1073 VEL(HTL,43)=VEL(HTL,43)+V
1074 VEL(HTL,44)=VEL(HTL,44)+V
1075 VEL(HTL,45)=VEL(HTL,45)+V
1076 VEL(HTL,46)=VEL(HTL,46)+V
1077 VEL(HTL,47)=VEL(HTL,47)+V
1078 VEL(HTL,48)=VEL(HTL,48)+V
1079 VEL(HTL,49)=VEL(HTL,49)+V
1080 VEL(HTL,50)=VEL(HTL,50)+V
1081 VEL(HTL,51)=VEL(HTL,51)+V
1082 VEL(HTL,52)=VEL(HTL,52)+V
1083 VEL(HTL,53)=VEL(HTL,53)+V
1084 VEL(HTL,54)=VEL(HTL,54)+V
1085 VEL(HTL,55)=VEL(HTL,55)+V
1086 VEL(HTL,56)=VEL(HTL,56)+V
1087 VEL(HTL,57)=VEL(HTL,57)+V
1088 VEL(HTL,58)=VEL(HTL,58)+V
1089 VEL(HTL,59)=VEL(HTL,59)+V
1090 VEL(HTL,60)=VEL(HTL,60)+V
1091 VEL(HTL,61)=VEL(HTL,61)+V
1092 VEL(HTL,62)=VEL(HTL,62)+V
1093 VEL(HTL,63)=VEL(HTL,63)+V
1094 VEL(HTL,64)=VEL(HTL,64)+V
1095 VEL(HTL,65)=VEL(HTL,65)+V
1096 VEL(HTL,66)=VEL(HTL,66)+V
1097 VEL(HTL,67)=VEL(HTL,67)+V
1098 VEL(HTL,68)=VEL(HTL,68)+V
1099 VEL(HTL,69)=VEL(HTL,69)+V
1100 VEL(HTL,70)=VEL(HTL,70)+V
1101 VEL(HTL,71)=VEL(HTL,71)+V
1102 VEL(HTL,72)=VEL(HTL,72)+V
1103 VEL(HTL,73)=VEL(HTL,73)+V
1104 VEL(HTL,74)=VEL(HTL,74)+V
1105 VEL(HTL,75)=VEL(HTL,75)+V
1106 VEL(HTL,76)=VEL(HTL,76)+V
1107 VEL(HTL,77)=VEL(HTL,77)+V
1108 VEL(HTL,78)=VEL(HTL,78)+V
1109 VEL(HTL,79)=VEL(HTL,79)+V
1110 VEL(HTL,80)=VEL(HTL,80)+V
1111 VEL(HTL,81)=VEL(HTL,81)+V
1112 VEL(HTL,82)=VEL(HTL,82)+V
1113 VEL(HTL,83)=VEL(HTL,83)+V
1114 VEL(HTL,84)=VEL(HTL,84)+V
1115 VEL(HTL,85)=VEL(HTL,85)+V
1116 VEL(HTL,86)=VEL(HTL,86)+V
1117 VEL(HTL,87)=VEL(HTL,87)+V
1118 VEL(HTL,88)=VEL(HTL,88)+V
1119 VEL(HTL,89)=VEL(HTL,89)+V
1120 VEL(HTL,90)=VEL(HTL,90)+V
1121 VEL(HTL,91)=VEL(HTL,91)+V
1122 VEL(HTL,92)=VEL(HTL,92)+V
1123 VEL(HTL,93)=VEL(HTL,93)+V
1124 VEL(HTL,94)=VEL(HTL,94)+V
1125 VEL(HTL,95)=VEL(HTL,95)+V
1126 VEL(HTL,96)=VEL(HTL,96)+V
1127 VEL(HTL,97)=VEL(HTL,97)+V
1128 VEL(HTL,98)=VEL(HTL,98)+V
1129 VEL(HTL,99)=VEL(HTL,99)+V
1130 VEL(HTL,100)=VEL(HTL,100)+V
1131 VEL(HTL,101)=VEL(HTL,101)+V
1132 VEL(HTL,102)=VEL(HTL,102)+V
1133 VEL(HTL,103)=VEL(HTL,103)+V
1134 VEL(HTL,104)=VEL(HTL,104)+V
1135 VEL(HTL,105)=VEL(HTL,105)+V
1136 VEL(HTL,106)=VEL(HTL,106)+V
1137 VEL(HTL,107)=VEL(HTL,107)+V
1138 VEL(HTL,108)=VEL(HTL,108)+V
1139 VEL(HTL,109)=VEL(HTL,109)+V
1140 VEL(HTL,110)=VEL(HTL,110)+V
1141 VEL(HTL,111)=VEL(HTL,111)+V
1142 VEL(HTL,112)=VEL(HTL,112)+V
1143 VEL(HTL,113)=VEL(HTL,113)+V
1144 VEL(HTL,114)=VEL(HTL,114)+V
1145 VEL(HTL,115)=VEL(HTL,115)+V
1146 VEL(HTL,116)=VEL(HTL,116)+V
1147 VEL(HTL,117)=VEL(HTL,117)+V
1148 VEL(HTL,118)=VEL(HTL,118)+V
1149 VEL(HTL,119)=VEL(HTL,119)+V
1150 VEL(HTL,120)=VEL(HTL,120)+V
1151 VEL(HTL,121)=VEL(HTL,121)+V
1152 VEL(HTL,122)=VEL(HTL,122)+V
1153 VEL(HTL,123)=VEL(HTL,123)+V
1154 VEL(HTL,124)=VEL(HTL,124)+V
1155 VEL(HTL,125)=VEL(HTL,125)+V
1156 VEL(HTL,126)=VEL(HTL,126)+V
1157 VEL(HTL,127)=VEL(HTL,127)+V
1158 VEL(HTL,128)=VEL(HTL,128)+V
1159 VEL(HTL,129)=VEL(HTL,129)+V
1160 VEL(HTL,130)=VEL(HTL,130)+V
1161 VEL(HTL,131)=VEL(HTL,131)+V
1162 VEL(HTL,132)=VEL(HTL,132)+V
1163 VEL(HTL,133)=VEL(HTL,133)+V
1164 VEL(HTL,134)=VEL(HTL,134)+V
1165 VEL(HTL,135)=VEL(HTL,135)+V
1166 VEL(HTL,136)=VEL(HTL,136)+V
1167 VEL(HTL,137)=VEL(HTL,137)+V
1168 VEL(HTL,138)=VEL(HTL,138)+V
1169 VEL(HTL,139)=VEL(HTL,139)+V
1170 VEL(HTL,140)=VEL(HTL,140)+V
1171 VEL(HTL,141)=VEL(HTL,141)+V
1172 VEL(HTL,142)=VEL(HTL,142)+V
1173 VEL(HTL,143)=VEL(HTL,143)+V
1174 VEL(HTL,144)=VEL(HTL,144)+V
1175 VEL(HTL,145)=VEL(HTL,145)+V
1176 VEL(HTL,146)=VEL(HTL,146)+V
1177 VEL(HTL,147)=VEL(HTL,147)+V
1178 VEL(HTL,148)=VEL(HTL,148)+V
1179 VEL(HTL,149)=VEL(HTL,149)+V
1180 VEL(HTL,150)=VEL(HTL,150)+V
1181 VEL(HTL,151)=VEL(HTL,151)+V
1182 VEL(HTL,152)=VEL(HTL,152)+V
1183 VEL(HTL,153)=VEL(HTL,153)+V
1184 VEL(HTL,154)=VEL(HTL,154)+V
1185 VEL(HTL,155)=VEL(HTL,155)+V
1186 VEL(HTL,156)=VEL(HTL,156)+V
1187 VEL(HTL,157)=VEL(HTL,157)+V
1188 VEL(HTL,158)=VEL(
```

FIG. A9 (CONT.)

NOT REPRODUCIBLE

```

SUBROUTINE INVEL(I)
COMMON VAUV(50,50),VTUV(50,50),VRUV(50,50)
COMMON TH(50),GIA(10),RPHUP,GLRV(50),PI,X(50,2),Y(50,2),Z(50,2)
COMMON KBTOT,RCAUS(10),UAUB(50,10),UTUB(50,10),URUB(50,10),NOTRL
DIMENSION COEX(5),WEIGHT(5),R(50),COSKN(10),SINKN(10)
KT=KBTOT
DO 1000 NTRL=1,NOTRL
1000 R(NTRL)=Y(NTRL,1)/RPHUP
DO 12 NTRL=1,NOTRL
  UAUB(NTRL,M)=0.
  UTUB(NTRL,M)=0.
  URUB(NTRL,M)=0.
12  CONTINUE
DO 11 I=1,9
  DELTA=GIA(I+1)-GIA(I)
  COEX(1)=.046910*DELTA
  COEX(2)=.230765*DELTA
  COEX(3)=.5*DELTA
  COEX(4)=.769235*DELTA
  COEX(5)=.953090*DELTA
  WEIGHT(1)=.059232*DELTA*2.
  WEIGHT(5)=WEIGHT(1)
  WEIGHT(2)=.119657*DELTA*2.
  WEIGHT(4)=WEIGHT(2)
  WEIGHT(3)=.142222*DELTA*2.
DO 11 L=1,5
  GNU=GIA(I)+COEX(L)
  COSY=COS(GNU)
  SINY=SIN(GNU)
DO 11 K=2,KT
  COSKN(K)=COS(.2+.3.14159/FLOAT(KT)*FLOAT(K-1))
  SINKN(K)=SIN(.2+.3.14159/FLOAT(KT)*FLOAT(K-1))
  COSIKN=COSY+COSKN(K)-SINY*SINKN(K)
  SINKN=SINY+COSKN(K)+COSY*SINKN(K)
  VXI=GLRV(I)*GNU
  RZV=RCAUS(I)/RPHUP
DO 11 JCP=1,NOTRL
  BUG=SQRT((VXI+VXI+R(JCP)**2 -RZV*RZV-2.*R(JCP)*RZV+COSIKN)
1**3)
  BUG=WEIGHT(L)/BUG
  EXGNU=VXI+RZV
  UAUB(JCP,M)=UAUB(JCP,M)+(RZV*RZV-RZV*R(JCP)+COSIKN)*BUG
  UTUB(JCP,M)=UTUB(JCP,M)+(R(JCP)*GLRV(I)-RZV*GLRV(I)+COSIKN-EXGNU)*
1BUG
  URUB(JCP,M)=URUB(JCP,M)+(GLRV(I)*RZV+SINKN-EXGNU+COSIKN)*BUG
11 CONTINUE
RETURN
END
SUBROUTINE INDUCT
COMMON VAUV(50,50),VTUV(50,50),VRUV(50,50)
COMMON TH(50),GIA(10),RPHUP,GLRV(50),PI,X(50,2),Y(50,2),Z(50,2)
COMMON KBTOT,RCAUS(10),UAUB(50,10),UTUB(50,10),URUB(50,10),NOTRL
DIMENSION COEX(5),WEIGHT(5),R(50)
DO 1000 NTRL=1,NOTRL
1000 R(NTRL)=SQRT(Y(NTRL,1)+Z(NTRL,1)+Z(NTRL,1))/RPHUP
DO 11 NTRL=1,NOTRL
DO 11 MTL=1,NOTRL
  VAUV(NTRL,MTL)=0.
  VTUV(NTRL,MTL)=0.
  VRUV(NTRL,MTL)=0.
IF(NTRL-MTRL) 1001, 11, 1001
1001 CONTINUE
ANG=TH(NTRL)-TH(MTRL)
DO 11 I=1,9
  DELTA=GIA(I+1)-GIA(I)
  COEX(1)=.046910*DELTA
  COEX(2)=.230765*DELTA
  COEX(3)=.5*DELTA
  COEX(4)=.769235*DELTA
  COEX(5)=.953090*DELTA
  WEIGHT(1)=.059232*DELTA*2.
  WEIGHT(5)=WEIGHT(1)
  WEIGHT(2)=.119657*DELTA*2.
  WEIGHT(4)=WEIGHT(2)
  WEIGHT(3)=.142222*DELTA*2.
DO 11 L=1,5
  GNU=GIA(I)+COEX(L)
  COSY=COS(GNU)
  SINY=SIN(GNU)
  COSKN=COS(ANG)
  SINKN=SIN(ANG)
  COSIKN=COSY+COSKN-SINY*SINKN
  SINKN=SINY+COSKN+COSY*SINKN
  VXI=GLRV(I)*GNU
  RZV=R(IT,IL)
  BUG=SQRT((VXI+VXI+R(NTRL)*R(MTRL)+RZV*RZV-2.*R(NTRL)*RZV+COSIKN)
1**3)
  BUG=WEIGHT(L)/BUG
  EXGNU=VXI+RZV
  VAUV(NTRL,MTL)=VAUV(NTRL,MTL)+(RZV*RZV-RZV*R(NTRL)+COSIKN)*BUG
  M=MTL
  VTUV(NTRL,MTL)=VTUV(NTRL,MTL)+(R(NTRL)*GLRV(MTL)-RZV*GLRV(M)*
1COSIKN-EXGNU+SINKN)*BUG
  VRUV(NTRL,MTL)=VRUV(NTRL,MTL)+(GLRV(NTRL)*RZV+SINKN-EXGNU+COSIK
1N)*BUG
11 CONTINUE
RETURN
END

```

R 19.216+6.750

Figure A 10

NOT REPRODUCIBLE

BOUNDARY LAYER PROGRAMS

These programs are listed in the MAD language purely for the sake of completeness. They were written by Professor Jerome Milgram for calculations involving seperated flow on yacht sails. See Ref. (11) of the main text. The listings appear in Figure (A11)

[illegible][illegible]

```

4 2034.1
00010 01.000 00.300 250.0 00.600 01.600
00020 0.000 0.650 0.320 0.100 0.025 -0.050 -0.003 -0.052 0.040 0.155 0.202
0.015-0.350

leaves fat cv qlse
W 1050.7

```

WYC = 1.582500F 06
WTH = 1.022500F 06, WOL = 7.682801F 06,
CF = 2.320500F-03, WTHA = 6.035000F-03,

ALP = 083305, (LTAR = 7.000000E-03)
EXIT CALLED, PM MAY 91 TAPED.
0.060, 033

100000 OF
M 1033.5
FRTVCTW,
Z ZETA CF Y 974 L

3700	0002	0023	1,4157	9606,4636	0573
4000	0030	0026	1,6060	9150,6300	0529
5100	0059	0026	1,3773	9601,6713	0596
5800	0059	0026	1,3889	9385,3620	0663
6500	0050	0025	1,3807	9552,4727	0710
7200	0050	0026	1,5275	9607,5096	0665
7900	0056	0023	1,6131	10026,0116	0627
8600	0076	0032	1,6210	11208,0813	0608

1.0100 .0003 .0010 1.5202 12070.2601 -.0462
1.0000 .0100 .0017 1.7717 13372.0004 -.1368
EXIT COLLECT, PM MAY 22 1968.
9 7.568+.343

100000000
M 2037.1
EXECUTION

X	Y	Z	W	V
1.3760	0.0001	0.0025	1.3559	0.0075
1.4000	0.0050	0.0026	1.3541	0.0073
1.4240	0.0100	0.0026	1.3500	0.0074
1.4480	0.0150	0.0026	1.3474	0.0090
1.4720	0.0200	0.0026	1.3452	0.0071
1.4960	0.0250	0.0026	1.3405	0.0060
1.5200	0.0300	0.0026	1.3376	0.0064
1.5440	0.0350	0.0026	1.3353	0.0076

1.0000	1.0000	1.0000	1.0000	1.0000	1.0000
1.0000	1.0000	1.0000	1.0000	1.0000	1.0000
1.0000	1.0000	1.0000	1.0000	1.0000	1.0000
EXIT CALLED. PM MAY BE TAKEN.					
9,383,783					

```

00010 P# RAD 04/24 2207.2
00020 DIMENSION TIME(10),R(10),P,=000,0100,0100,1100,1100,06100(222)
00030 V% =0100+1,1,12
00040 INTERPOL 10
00050 DIMENSION W(10),Z(10),J(22)
00060 INTERPOL 10,=P,=J,=Z
00070 INTERPOL P# FROM RAD (10)=C(10+1,2)/C(10+1,3) P,=C(10+1,3)
00080 INTERPOL P# FROM RAD (10)=C(10+1,3)/C(10+1,3) P,=C(10+1,3)
00090 INTERPOL P# FROM RAD (10)=C(10+1,3)/C(10+1,3) P,=C(10+1,3)
00100 1
00110 INTERP=FUNCTION I(1)
00120 I=1
00130 P#UNT TO MPV,
00140 P#UNT TO MPV,
00150 P#UNT TO MPV,
00160 P#UNT TO MPV,
00170 P#UNT TO MPV,
00180 P#UNT TO MPV,
00190 P#UNT TO MPV,
00200 P#UNT TO MPV,
00210 P#UNT TO MPV,
00220 P#UNT TO MPV,
00230 P#UNT TO MPV,
00240 P#UNT TO MPV,
00250 P#UNT TO MPV,
00260 P#UNT TO MPV,
00270 P#UNT TO MPV,
00280 P#UNT TO MPV,
00290 P#UNT TO MPV,
00300 P#UNT TO MPV,
00310 P#UNT TO MPV,
00320 P#UNT TO MPV,
00330 P#UNT TO MPV,
00340 P#UNT TO MPV,
00350 P#UNT TO MPV,
00360 P#UNT TO MPV,
00370 P#UNT TO MPV,
00380 P#UNT TO MPV,
00390 P#UNT TO MPV,
00400 P#UNT TO MPV,
00410 P#UNT TO MPV,
00420 P#UNT TO MPV,
00430 P#UNT TO MPV,
00440 P#UNT TO MPV,
00450 P#UNT TO MPV,
00460 P#UNT TO MPV,
00470 P#UNT TO MPV,
00480 P#UNT TO MPV,
00490 P#UNT TO MPV,
00500 P#UNT TO MPV,
00510 P#UNT TO MPV,
00520 P#UNT TO MPV,
00530 P#UNT TO MPV,
00540 P#UNT TO MPV,
00550 P#UNT TO MPV,
00560 P#UNT TO MPV,
00570 P#UNT TO MPV,
00580 P#UNT TO MPV,
00590 P#UNT TO MPV,
00600 P#UNT TO MPV,
00610 P#UNT TO MPV,
00620 P#UNT TO MPV,
00630 P#UNT TO MPV,
00640 P#UNT TO MPV,
00650 P#UNT TO MPV,
00660 P#UNT TO MPV,
00670 P#UNT TO MPV,
00680 P#UNT TO MPV,
00690 P#UNT TO MPV,
00700 P#UNT TO MPV,
00710 P#UNT TO MPV,
00720 P#UNT TO MPV,
00730 P#UNT TO MPV,
00740 P#UNT TO MPV,
00750 P#UNT TO MPV,
00760 P#UNT TO MPV,
00770 P#UNT TO MPV,
00780 P#UNT TO MPV,
00790 P#UNT TO MPV,
00800 P#UNT TO MPV,
00810 P#UNT TO MPV,
00820 P#UNT TO MPV,
00830 P#UNT TO MPV,
00840 P#UNT TO MPV,
00850 P#UNT TO MPV,
00860 P#UNT TO MPV,
00870 P#UNT TO MPV,
00880 P#UNT TO MPV,
00890 P#UNT TO MPV,
00900 P#UNT TO MPV,
00910 P#UNT TO MPV,
00920 P#UNT TO MPV,
00930 P#UNT TO MPV,
00940 P#UNT TO MPV,
00950 P#UNT TO MPV,
00960 P#UNT TO MPV,
00970 P#UNT TO MPV,
00980 P#UNT TO MPV,
00990 P#UNT TO MPV,
01000 P#UNT TO MPV,

```

W 2157 6
CY MAD 04/26 A 17.7
00010 [EXTERNAL FUNCTION (C,R)]

```

00020      ENDT TO CV.
00030      A=0
00040      1:1 TH1, FOR I=1, L, 1, C, 2
00050      TH1      A=A+(I-1)*C(1,1)
00060      FUNCTION RETURN A
00070      INTEGER I
00080      C="
R 0009 JIB

```

```

W 2159.1
GLQ MAD 04/24 2159.2

PTR000001  SETNAME FUNCTION (A,Z,IC,NA,ALPHA,ELI,EL)
PTR000002  SETAY TO GLQ.
PTR000003  N0100+1
PTR000004  ELI

```

MTR00005 TMSUUGH Q00005, Func J=1,1,G,MH,AND E ME,1
 Q00003 I(1)=0
 MTR00007 I=1
 MTR00008 TMSUUGH Q00000, Func K=2,1,K,G,MH,AND E ME,1
 MTR00009 I(1)=1
 MTR00010 TMSUUGH Q00005, Func J=1,1,G,MH,AND E ME,1
 MTR00011 WAREHEV I,AA(1,K)=E1,G,0, TRANSFER TO Q00006
 MTR00012 TRANSFER TO Q00005
 Q00004 P=2,AA(1,K)=E1,G,0, P-23

[illegible]

```

MTR00022 JMSREVEN (,ABS (X(1,X))-E7),G,0, TRANSFER TO Q0000
MTR00023 TRANSFER TO Q0000
MTR00024 Q0000 IL(X)=1
MTR00025 I=I+1
MTR00026 Q0000 CONTINUE
MTR00027 X(I)=--1 0
MTR00028 I=I+1
MTR00029 THROUGH Q0000, FOR I=3,1,1 G M,AND I,RE 1

```

```

PTR00030 Q20009 X(1)=0
PTR00031 TRIMM00 Q20010, FUN J=1,J,C,M,ANG,J NE 1
PTR00032 WHENEVEN (1(113)),G,B, TRANSFER To Q20011
PTR00033 TRANSFER To Q20010
PTR00034 Q20011 S=0
PTR00035 L(1)=1
PTR00036 L(1(113)
PTR00037 TRIMM00 Q20012, FUN K=1,1,K G MI AMU,K NE LL
PTR00038 GOTO Q20011

```

```

P1TH00010  Q0010  X(I)=5/A(I,1)
P1TH00010  Q0010  I=I+1
P1TH00010  Q0010  WH(NEVEN I(I:NM))=0., TRANSFER TO Q0013
P1TH00010  Q0010  TRANSFER TO Q0010
P1TH00010  Q0013  ALPHA=0
P1TH00010  Q0013  TRANSFER TO Q0015
P1TH00010  Q0014  I=I(I:NM)
P1TH00010  Q0014  (PHANA(I,MM)

```

```

MTR00007 Q20015 FUNCTION RETURN
MTR00008 INTEGER MM,M,LL,J,PL,I
MTR00009 INTEGER E,I1,N1
MTR00050 Q20001 END OF FUNCTION
N 2,253=1 166 ,

```

BOUNDARY LAYER SOURCE

PROGRAMS IN MAD AND SA
RESULTS FOR THE RUDDER
AT AN ANGLE OF ATTACK

AT 6° ANGLE OF ATTACK A
25 FT./SEC WATER VELOC

REPRODUCTION

FIG.A11 BOUNDARY LAYER SOURCE
PROGRAMS IN MAD AND SAMPLE
RESULTS FOR THE RUDDER MODEL
AT 6° ANGLE OF ATTACK AND
25 FT/SEC WATER VELOCITY

NOT REPRODUCIBLE

BIOGRAPHICAL NOTES

The author was born in 1937, in the city of Annapolis, Maryland. He received his Bachelor of Science degree in 1959 in Physics, from the Massachusetts Institute of Technology. Following graduation he studied Naval Architecture at the T.H. te Delft in the Netherlands for three years. He was then an Engineer in the Vibrations and Sound Laboratory of the Boston Naval Shipyard for two years. He received his Master of Science degree in September 1964 from M.I.T. He is at present an instructor in the Department of Naval Architecture at M.I.T.

Unclassified
Security Classification

DOCUMENT CONTROL DATA - R & D		
<i>(Security classification of title, body of abstract and indexing annotation must be entered when the overall report is classified)</i>		
1 ORIGINATING ACTIVITY (Corporate author) Massachusetts Institute of Technology, Department of Naval Architecture and Marine Engineering, Cambridge, Massachusetts 02139		2a. REPORT SECURITY CLASSIFICATION Unclassified 2b. GROUP
3 REPORT TITLE VORTEX INTERACTIONS IN A PROPELLER WAKE		
4 DESCRIPTIVE NOTES (Type of report and inclusive dates) Annual		
5 AUTHOR(S) (First name, middle initial, last name) Damon E. Cummings		
6 REPORT DATE June 1968	7a. TOTAL NO. OF PAGES 91	7b. NO. OF REFS 18
8a. CONTRACT OR GRANT NO Nonr - 1841(63) b. PROJECT NO SR 009 01 01 c. d.	9a. ORIGINATOR'S REPORT NUMBER(S) 68-12 9b. OTHER REPORT NO(S) (Any other numbers that may be assigned this report)	
10 DISTRIBUTION STATEMENT This document is subject to special export controls and each transmittal to foreign governments or foreign nationals may be made only with prior ap- proval of the Head, Hydromechanics Laboratory, Naval Ship Research and Development Center, Washington, D. C. 20007		
11 SUPPLEMENTARY NOTES	12 SPONSORING MILITARY ACTIVITY Naval Ship Research & Development Center Washington, D. C. 20007	
13 ABSTRACT This report concerns the kinematics of the motion of trailing vortex sheets in the wake of a propeller and the dynamics of the tip vortex. The problem is solved numerically for a lifting line wing model and the results applied to propeller theory. Special consideration is given to the subjects of tip vortex cavitation, changes in loading on a blade due to rollup of the trailing vortex sheet, and the trajectory of the tip vortex. Experimental confirmation was obtained for the pressure at which cavitation appeared and the motion of the vortex sheet through testing a hydrofoil in the M. I. T. Propeller Tunnel.		

14

KEY WORDS

LINK A

LINK B

LINK C

ROLE

WT

ROLE

WT

ROLE

WT

Propeller

Wake

Vortex

Vortex Sheet

Wing Theory